UNIVERSITY OF CALIFORNIA,
IRVINE

Intra-body Communications for Body Area Networks

DISSERTATION

submitted in partial satisfaction of the requirements
for the degree of

DOCTOR OF PHILOSOPHY

in Electrical Engineering and Computer Science

by

Ahmed Eissa Fathy Khorshid

Dissertation Committee:
Professor Ahmed Eltawil, Chair
Professor Fadi Kurdahi
Professor Michael Green

2019

DEDICATION

To

My parents, grandparents, my brother and his family
and my friends

Table of Contents

Page

LIST OF FIGURES

LIST OF TABLES

ACKNOWLEDGMENTS

I would like to express the deepest gratitude and appreciation to my committee chair, Professor Ahmed Eltawil. Over the six years of my PhD program, Professor Ahmed provided me with guidance, support, motivation and above all the entrepreneurial spirit. Tackling a new and exciting project wouldn't have been possible without his continuous support, patience and guidance. It has been a thrilling and exciting scientific journey, where I was able to learn so many skills and gain hands on experience, none of which would have been possible without his support and effort. Without his guidance and persistent help this dissertation would not have been possible.

I would like to thank my committee member, Professor Fadi Kurdahi, for his guidance and support as well, where we worked closely with us and gave us helpful feedback throughout the different phases of the project. I also would like to thank Professor Michael Green, my committee member, for his support, guidance and helpful feedback.

In addition, I would like to thank Professor G. P. Li, Professor Mark Bachman and Sarkis Babikian at the Micro Integrated Devices and Systems Laboratory, University of California, Irvine for their help and guidance concerning preparing the experimental samples and the measurement setup.

A special thanks to Ibrahim Nasser I Alquaydheb, my colleague at the lab and the IBC research group at the Electrical Engineering and Computer Science, University of California, Irvine. I was blessed to have him working side by side with me on this interesting project. Without his effort and support, many of the results presented in this dissertation wouldn't have been possible.

In addition, a thank you to all my colleague and friends whom I met throughout this journey; Ahmed Ibrahim, Islam Rabie, Marwen Zourgi, Sherif Shakib, Sergie, Mohamed Nada, Tarek, Khairy, Wael, Sayed, Amira, Selima, Walid Ali and many other wonderful people

And of course, I am grateful to my family who always believed in me and supported me at all times. To my parents, I dedicate this work to you, and I hope I will make you proud of me, as I am always proud of you. Thanks to my brother Abdel Rahman, his wife Shaimaa, and their son Youssef for their support and encouragement.

I want to also thank the University of California, Irvine and all the great people working on campus.

I am also grateful for all the funding entities; UCI, Broadcom Foundation, and the National institute of justice, without which, this work wouldn't have been possible.

The research in this dissertation was mainly supported by the Broadcom Foundation Fellowship and the U.S. National Institute of Justice under 2016-R2-CX-0014.

CURRICULUM VITAE

Ahmed Eissa Fathy Khorshid

2010	Bachelor of Science, Cairo University
2010 - 2013	Teaching Assistant, Cairo University
2013	Master of Science in Electronics, Cairo University
2013 - 2018	Graduate Student Researcher and Teaching Assistant, University of California, Irvine
2016 – 2019	National Institute of Justice Graduate Research Fellow
2019	Ph.D. in Electrical Engineering and Computer Science University of California, Irvine

PUBLICATIONS

- **A. E. Khorshid**, *I. N. Alquaydheb, A. M. Eltawil and F. J. Kurdahi, " IBCFAP: Intra-body Communications Five-Layers Arm Phantom Model" Submitted to IEEE Access*
- **A. E. Khorshid**, I. N. Alquaydheb, A. M. Eltawil and F. J. Kurdahi, *"Physical Multi-Layer Phantoms for Intra-Body Communications," in IEEE Access, vol. 6, pp. 42812-42821, 2018.*
- Mohammed E. Fouda, **A. E. Khorshid**, *I. N. Alquaydheb, A. M. Eltawil and F. J. Kurdahi "Extracting the Cole-Cole Model Parameters of Tissue-mimicking Materials", BioCAS 2018.*
- **A. E. Khorshid** and A. M. Eltawil *"Wearable Intra-body Communication (IBC) Sensors for Body Area Networks" Pittcon 2018, Orlando, February,2018.*

- Ibrahim, N. Alquaydheb, **A. E. Khorshid**, , A. M. Eltawil, "Analysis and Estimation of Intra-body Communications Path Loss for Galvanic Coupling", *12th International Conference on Body Area Networks, Dalian, China, Sep.,2017*
- **A. E. Khorshid**, Ibrahim, N. Alquaydheb, A. M. Eltawil, "Electrode Impedance Modeling For Channel Characterization for Intra-body Communication", *12th International Conference on Body Area Networks, Dalian, China, Sep.,2017*
- **A. E. Khorshid**, A. M. Eltawil and Fadi Kurdahi, "On the Optimum data Carrier for Intra-body Communication Applications", *11th International Conference on Body Area Networks, Turin, Italy, Dec.,2016*
- **A. E. Khorshid**, A. M. Eltawil, Fadi Kurdahi, "Intra-Body Communications Model Driven by the Human's Body Biological Features", *Communications, Inference, And Computing In Molecular And Biological Systems Workshop, University of Southern California, Dec, 2015.*
- **A. E. Khorshid**, A. M. Eltawil, Fadi Kurdahi, "Intra-body Communication Model Based on Variable Biological Parameters", *2015 49th Asilomar Conference on Signals, Systems and Computers*, Pacific Grove, CA, 2015, pp. 948-951.

ABSTRACT OF THE DISSERTATION

Intrabody Communications for Body Area Networks

By

Ahmed Eissa Fathy Khorshid

Doctor of Philosophy in Electrical Engineering and Computer Science

University of California, Irvine, 2019

Professor Ahmed Eltawil, Chair

Mobile health has recently expanded to include wearable devices as a part of the vision of a holistic approach to wellness in general and health care services in particular. Once wearables become ubiquitous, they can provide healthy users, patients and doctors with an accurate reflection of the state of their body. This information will ultimately lead to better preventative medical practices and a truly personalized medical approach. Driven by the vision of a cable-free biomedical monitoring system, new wireless technologies that focus on sensor applications have been promoted as the next biomedical revolution, promising a significant improvement in the quality of health-care services. However, a major barrier to adoption of wearable technologies is the size and power requirements of wireless sensors which are typically dominated by the Radio Frequency (RF) section of the associated transceivers. There is a need to have a new class of devices that are small in area and exhibit ultra-low power consumption. An attractive solution to such emerging vision is the use of intra-body communication (IBC) systems where data transmission is achieved through the body rather than through air. Sensors and actuators can then inter-communicate through body and be relayed to a centralized wireless hub that could be a

smart watch for instance. This technique would ultimately lead to body area networks (BANs) that operate at extremely low power, with minimal foot print by replacing expensive, power consuming Radio Frequency front ends, for each individual node with simpler interfaces.

In this work, we study and explore the characteristics, nature, specifications and potential of the IBC technology. We introduce novel approaches to accurately model this new channel, through simulation techniques as well as physical ones, in form of physical phantoms, to understand and model the channel behavior and relation between the system's different components. This work aims at providing a platform for the design of body area networks that adopt IBC as means of connection between the network's nodes. Finally, possible applications that uniquely utilize such technology are introduced, verifying its potential to boost the healthcare field.

Chapter 1

Introduction & Literature Survey

1.1 Background

Human resources are undoubtedly considered to be the most crucial and valuable asset in any system, consequently, ensuring the personal safety and efficiency is a major concern. Monitoring the performance of vital body functions (body temperature, blood pressure, heart beat, electrocardiogram, stress profile) for patients, personal that undergo harsh environments as firefighters, policemen and workers in mines, is thus a necessity for their safety, and has to be conducted without any hindering to their efficiency on field. Even for healthy individuals, monitoring one's vitals is a necessity nowadays to maintain a certain healthy lifestyle, ensure adherence with a specific diet or even to just monitor any abnormalities in the bodies performance or activity. The solution for such need seems to residue in personal telemetry which, supported by the progress achieved in the field of mobile health, has recently expanded to include wearable devices as a part of the vision of a holistic approach to wellness in general and health care services in particular.

Driven by the vision of a cable-free biomedical monitoring system, new wireless technologies that focus on sensor applications have been promoted as the next biomedical revolution, promising a significant improvement in the quality of monitoring the physical and mental condition of the personal. Moving from the cable era, where monitoring the individual's vitals were tied by both time and space constraints, the next era, known as Wireless Body Area Networks (WBAN), proved to possess unprecedented potential for wide range of applications

that is not only limited to the health care field right now, but is extended to various other sectors that became able to harness the information obtained by the biosensors, about the body's condition, behavior, physiological status, or even posture for adapting different environments for the individuals' needs or satisfaction. These applications range from simple health monitoring portals, to custom lifestyle applications, special diet programs, wellness and fitness courses, entertainment fields like video games and applications based on Augmented reality and virtual reality headsets, to security based applications (biometric identity), stress profile monitoring, driver's behavior monitoring and many other applications that are emerging nowadays building upon this new wave of wireless and IoT (Internet of Things) networks and systems. Yet, as ca be inferred from the previous mentioned applications, designing a wireless body area network for biomedical and lifestyle applications faces multiple key challenges that must be taken in consideration:

- *Safety* first and foremost, the basic concern of building body area networks is monitoring and maintaining a healthy life for the human being, thus adhering to the health safety regulations (output signal levels, frequency range of operation, power levels, heat dissipation, interference with the bio-signals ...etc.) is a necessity.
- *Security*, since body area networks will be transmitting highly sensitive and confidential data, that is directly related to an individual's body status and physical and mental condition, and sometimes can be considered as a biometric identity to that personal as well, securing such data is an important constraint that should be considered
- Accuracy; some of these senor networks will be responsible for gathering sensitive data that determines the personal certain condition, like the stress profile of on duty personnel in the field as policemen and firefighters, upon which a decision by the person in charge

will be taken, thus it should be guaranteed that the correct sensors are placed at the correct position on the body and correctly calibrated as well.

- *Battery lifetime:* in other words, the power consumption of the whole network in general and of each sensor node specifically, which is necessary for determining the reliability of the networks, especially for applications like implanted sensors, where changing the battery over short time cycle cannot be an option.
- *Sensor node footprint:* area of the senor node, which includes the area of the senor itself, supporting signal processing circuits, communication modules and the battery as well.

Numerous applications are currently being designed and implemented using wireless body sensors networks as their backbone. At the core of these networks, are a number of essential sensors that monitor the basic physiological bio-signals. A summary of these basic signals, with the minimum data rate required to correctly, accurately and continuously monitor and transmit these signals on a real time bases is represented in Table 1.1. As can be seen from the table, due to the nature of bio-signals that oscillate at low frequencies which do not exceed 42 Hz [1-2], the required bit rate to transmit bio-signals is in the order of few kb/s. To fulfill such requirements, innovative wireless solutions have been adopted from the telecommunications and the networks fields for such purpose, and are standardized by IEEE Task Groups as the IEEE 802.15.6 [3]. Table 1.2 reviews and compares the properties of the major wireless solutions adopted for wireless body area networks, such as Bluetooth, ZigBee, ANT, Sensium and Zarlink technologies.

Bluetooth standard offers sufficient bit rate and low cost with the option of ultra-low power if using the low-power Bluetooth technique; Yet, all the other listed topologies incorporate lower power consumption with different data rates. ZigBee lower average power consumption is

Table 1.1. Requirements for Bio-signals Data Rate and Latency

Biomedical Signal	Data rate	Latency
Heart Rate	80 -800 bps	< 1s
Blood Pressure	80 – 800 bps	< 1s
Respiration	50 -120 bps	< 300 ms
Accelerometer	< 100 bps	< 300 ms
ECG	4 Kbps per channel	< 250 ms per channel
EMG	64 Kbps per channel	< 15.6 ms per channel
EEG	3 Kbps	< 350 ms per channel

suitable for WBAN bio-signal sensors due to the low-duty-cycle of required devices. However, low data rate limits ZigBee priority over other standards. ANT and Sensium are proprietary standards that are optimized for WBAN health care and lifestyle applications. ANT features higher data rate compared to Sensium and it enables user trade-off between data rate and power consumption. Nevertheless, Sensium adopts ultra-lower power consumption. In contrast to all of the previous four technologies which is deployable for only wearable body sensor, Zarlink has developed a wireless implanted transceiver modeled as ZL70101. This system utilizes extremely low transmission power consumption which is suitable for implanted sensors due to the need for less frequent battery replacement.

Bluetooth, ZigBee, ANT and Sensium technologies operate at the overcrowded industrial, scientific, and medical (ISM) band, ranging from 902MHz-928MHz and 2400MHz-2500MHz, with a frequency spectrum centered at 868 MHz, 915 MHz for Sensium and at 2.4 GHz for the other standards resulting in coexistence, interference and severe performance degradation problems which is a real concern for critical continuous monitoring medical applications.

Table 1.2: Characteristics summary of wireless technologies for BAN [4].

	Spectrum	Channels	Data rate	Peak power
Bluetooth	2.4 GHz	classic-79 low energy-3	classic (1-3 Mb/s) low energy(1 Mb/s)	classic (45mA@3.3V) low energy(28mA@3.3V)
ZigBee	2.4 GHz	16	250 kb/s	16.5 mA@1.8V
ANT	2.4 GHz	125	1 Mb/s	22 mA@3.3V
Sensium	868 MHz, 915MHz	16	50 kb/s	3 mA@1.2V
Zarlink (ZL70101)	402-405 MHz, 433-434 MHz	10	200-800 kb/s	5 mA@3.3V

As demonstrated in Figure 1.1, together with the associated data from tables 1.1 & 1.2, it is clear that although the current available wireless technologies did help revolutionize the health care solutions, enabling telehealth and other numerous applications, there is still a huge margin for improvement. This is mainly due to the fact that most of these solutions were lent by the telecommunications field, yet not designed specifically for body area networks. These solutions provide higher data rates than needed for most bio-signals, and at the expense of higher and unnecessary power consumption, where it is in fact the lower left corner in Figure 1.1 is where

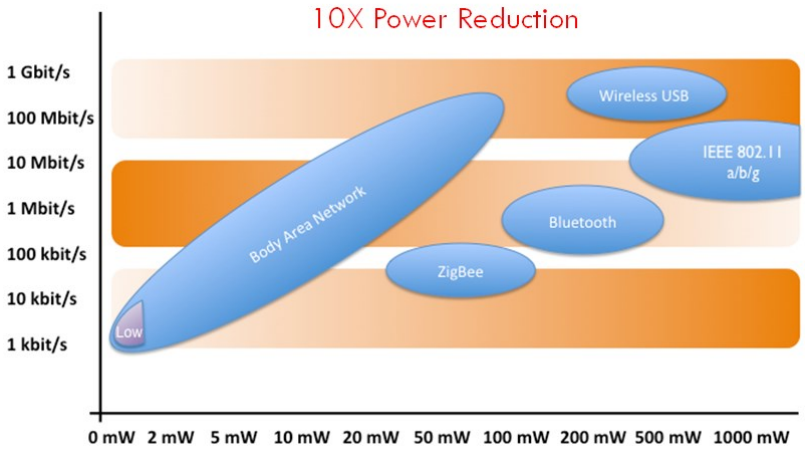

Figure 1.1: Power consumption and data rates for currently available wireless solutions, showing the need for a novel and more efficient solution that satisfies the needs for body area networks [5]

the optimum design point for boy area networks system should be. A major reason for such inefficiency of the current wearable technologies is the size and power requirements of wireless sensors which are typically dominated by the RF section of the associated transceivers. Clearly there is a need to have a new class of devices that are wirelessly networked, small in area and exhibit ultra-low power consumption thus having the ability to perform distributed monitoring in a seamless manner. An attractive solution to such emerging vision is the use of Intra-body Communication (IBC) systems where data transmission is achieved through the *body* rather than through air. Sensors and actuators can then inter-communicate through the body and be relayed to a centralized wireless hub that could be a smart watch for instance. This technique would ultimately lead to body area networks (BANs) that operate at extremely low power, with minimal foot print by replacing expensive, power consuming Radio Frequency (RF) front ends, for each individual node with simpler interfaces. Furthermore, while the body operates as a channel for the communicating nodes, it is relatively protected from the higher levels of interference expected when broadcasting via the air. From a security prospective, intra-body communications poses an important advantage over traditional wireless solution since the communication between the sensors/actuators, the processing units and the gateway would be confined to the human body only, providing higher level of security. Unlike in the wireless sensor case, where the safety of the personal would be at risk in case the transmitted data is anticipated by any hostile entity.

1.2 Intra-Body Communications (IBC)

IBC is a novel merging technology, aiming at designing smart, secured and efficient body area networks. Through coupling the signal into the human body, the signal propagates through the body, that acts as a secure transmission medium, between the transmitter and receiver nodes being sensors, actuator, relays or just a wireless gateway. Such novel technology has the potential of eliminating the whole RF chain, thus minimizing the area of the senor node and the operating power significantly. IBC can thus be the technology that would enable body area networks to operate at the far lower left corner in Figure 1.1, where novel sensor networks would be solely designed to satisfy the needs and constraints of boy area networks. IBC uses the human body as a communication channel/medium to facilitate data exchange and transmission between wearable-wearable, implanted- wearable and implanted-implanted sensors and actuators or to be exported to an external medical monitor for further processing, monitoring and medical assessment, as shown in Figure 1.2.

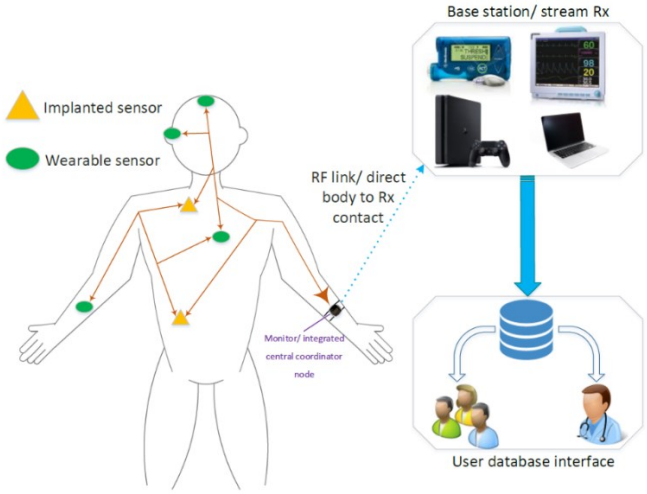

Figure 1.2: An example for an IBC network where communications occur between wearable sensors, between wearables and implants, between sensors and a wireless gateway, like a smart watch, to transmit the data to the outside world for further processing and monitoring [6].

To achieve so, there are two main techniques for implementing the IBC technology, namely through; electrostatic (capacitive) coupling or galvanic coupling.

1.2.1 Electro-static (Capacitive) Near-field Coupling

Capacitive or electrostatic coupling is historically the first historically introduced approach for constructing IBC systems, as introduced by Zimmerman in [7]. In this approach, the signal electrodes at both the transmitter and the receiver nodes are connected to the skin, while the ground/reference (GND) electrodes at both nodes are left exposed to air. This way, a closed circuit is formed, where the forward path is through the human body, while the return path is through the ground, and thus communication is established, as shown in Figure 1.3.

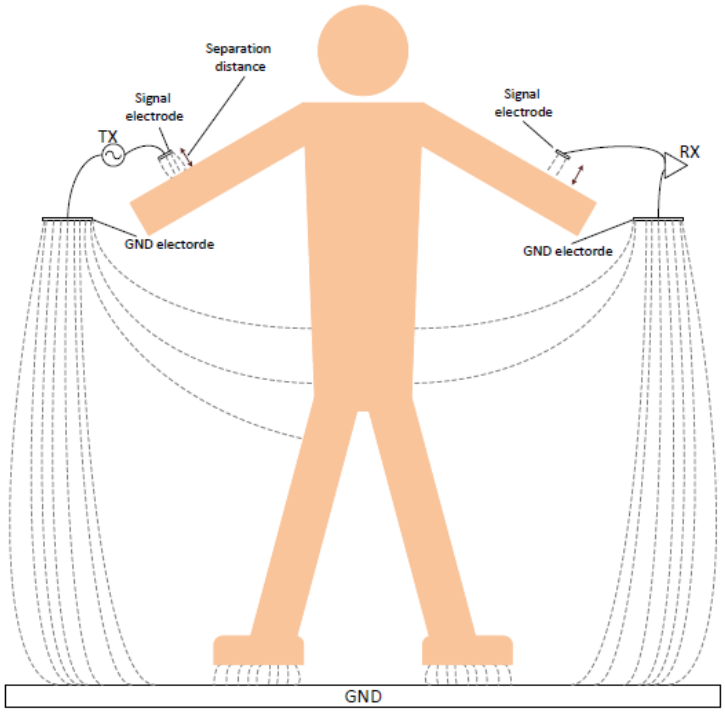

Figure 1.3: Capacitive/Near field coupling, where the signal electrodes are attached directly or at a proximity with the skin, to form the forward path, while the ground electrodes are left floating in the air to form the return path through the air and ground.

The transmitting and receiving signal electrode can be placed directly on the human body or in close proximity to the body, still closing the circuit loop through capacitive/near field coupling. Such approach facilities near-field IBC. In spite of the system simplicity, the main drawback is the return path that goes through the air and ground. Such fact makes the simple susceptible to external interference, and may impose further restrictions to ensure the security of the transmitted data.

1.2.2 Galvanic Coupling

Introduced later [8], in galvanic coupling both electrodes at both the communicating nodes are placed in contact with the skin. The signal is thus totally coupled into the body at the transmitter side to be picked up at the receiver side, where a large portion of the injected current is mutually co-located between the transmitting electrodes, yet a small traveling current initiates body confined electromagnetic propagation that results in potential difference between receiving electrodes, as shown in Figure 1.4, and is mainly responsible for data transfer between both nodes. A major advantage for galvanic coupling is that the whole signal is confined into the body, thus more resilient to external interference and much more secure than the first approach, as taping into the signal is a much harder task with this approach, thus securing a safe data exchange. For this reason, among others that will be introduced throughout the dissertation, this approach will be our choice of implementation for the IBC technology, as it possesses the potential to overcome most of the challenges that faces currently available solutions for wireless body area networks, as will be discussed throughout the chapters of this dissertation.

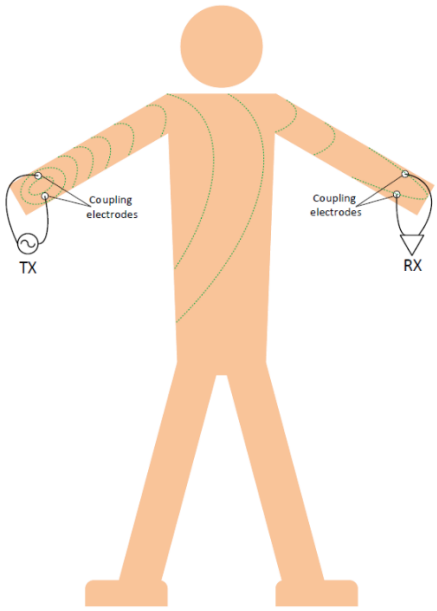

Figure 1.4: Galvanic coupling approach, where both electrodes for both nodes are directly connected to the skin, thus the whole signal is confined into the body, providing a secure and reliable communication channel

1.3 Prior Work

In the rest of this chapter, we will review the major milestones in the history of Intra-body communications, the basic attempts to model the human body as a communication channel, and simple prototype systems that were built using this new technology. We will also be able to point out the pros and cons of each of the above mentioned techniques, so that designer can select the approach that is more appropriate for the application at hand. More literature survey will also be introduced throughout the chapters of this dissertation, according to the topic/work that is being investigated.

1.3.1 Zimmerman & Personal Area Networks (PANs)

As mentioned earlier, the first Intra-Body Communication system was first introduced by Zimmerman in 1995 [7]. The interest emerged out of a research conducted by MIT Media lab on using electric field sensing to determine object's position. Consequently, the motivation to interconnect wearable and carry-on devices with low powered, cheaper and smaller in size system hardware drove the author to investigate the validity of electrostatic coupling to transfer information which is known as capacitive coupling. By calculating the internal resistance of the human body and comparing electrode to body impedances, the human body is approximated as a perfect conductor. To derive a human channel model, all electric fields that result from electrostatic coupling were identified. Every capacitive coupling is calculated as pure reactive impedance to define the lumped-circuit electrical model. A coil is connected in parallel with the body to determine body to environment capacitance by measuring the resonance frequency. A lock-in amplifier is utilized to measure electrode capacitance. The coupling electrodes' size and shape is defined by the chosen wearable or portable object; For example, wrist watch, shoes and credit cards. The hardware components of suggested system consist of analog circuitry controlled by micro-controller with all components implemented on a single CMOS integrated circuit. Half-duplex transceiver is preferred over full-duplex transceiver in order to avoid receiver electrostatic field saturation. On-off keying (OOK) and direct sequence spread spectrum (DSSP) modulation techniques are investigated on the same implemented hardware system. Although DSSP reported higher received signal, OOK was the optimal modulation method due to the complexity of phase detection in the case of DSSP. The suggested PAN system showed a bit rate of 2400 bit per second. This is also considered as the first trial for implementing an IBC system using the electrostatic (Near-field) approach

1.3.2 Capacitive Coupling Trials

Upon the transceiver system presented by Zimmerman, *Partridge et al.* used FSK modulation to replace OOK modulation technique in order to increase the overall performance of the physical and encoding layers [9]. The carrier frequency was set to 180kHz and 140kHz to ensure avoiding the body antenna effect. The transmitting voltage of 20V was selected. The transmitting electrodes and circuit were placed on a cardboard box which represents a wearable device with capacitive coupling electrodes. When the subject touches one of these electrodes, a return path is formed between the grounding environment and to one of the receiving electrodes that are attached to the subject. Different electrodes positioning has been investigated which showed that shoe position recorded the highest signal strength. The transceiver system implemented a data rate of 38.4kbps.

1.3.3 Galvanic Coupling Trials

Handa et al. in 1997 introduced the galvanic coupling implementation for IBC [8]. The main objective of their work was to investigate the transmission gain of very low-power health monitoring systems by attaching both transmitting and receiving electrodes and coupling the required signal directly into the human body which later one became known as the galvanic coupling approach. The bio-signal of interest was an ECG signal. Pulse-width modulator with a sampling frequency of 900Hz and carrier frequency of 70KHz was utilized by the detector to couple the modulated signal with power of 8μW to the relay transmitter. The transmitted signal through the body is detected by the micro data recorder or relay transmitter initially by amplifying the signal, filtering and demodulating it. Finally, prior stage is followed by FM modulation for wireless radio wave propagation. The final result of transmission system shows

the detected ECG without any significant distortion which is very promising to pursuit for further research in this coupling approach.

In [10], *Oberle et al*. chose the galvanic approach to implement a low-power biomedical communication system. A simplified engineering model has been derived with respect to the human tissue's dielectric characteristics. The coupled alternating current is in the range of μA. The transceiver communication system utilized continuous phase frequency shift keying (CPFSK) modulation with encoding frequencies of 51.2kHz and 61.4kHz which provided a data rate of 4.8kbps.

Hachisuka et al. used a function generator connected to Ag/AgCl electrodes that are attached to a human arm and an oscilloscope to detect the galvanic coupled signal, where they were able to determine the basic transmission characteristics of the human body [11]. The transmission results confirmed that the frequency of 10MHz has the highest transmission gain. To determine the electrode's contact impedance, a simple circuit model was proposed. It had been shown that regardless of the electrode metal material, the obtained impedance had small value fluctuation. Moreover, a phantom solution has been fabricated to replace the need for bio-signal experimentation which provided nearly the same gain as in human measurements at 10MHz. By using FM and FSK modulations, the authors observed a robust human channel communication against surrounding noisy devices with data rate of 9600bps. Further research by the authors however proved that two-electrode arrangement or electrostatic coupling is superior to the galvanic coupling [12].

Wegmueller et al. thoroughly investigated galvanic coupling approach throughout his work [13]. The Finite element method (FEM) alongside with in vivo measurements from 20 subjects has been conducted to estimate the human channel attenuation. The presented final results of FEM

and experimental measurements demonstrate gain value agreement at various frequencies that evaluate the effect of electrodes' size of both TR and electrodes transmission distance. The size of transmitting electrodes is proportional to the coupling gain. On the other hand, the muscle tissue resistivity and electrodes distance is inversely proportional to the gain. Different electrodes placing on the thorax area yields location independent gain data with channel capacity of 130kbps and 30kHz channel band- width. Further conducted research by the group implemented an enhanced system which improved the thorax channel capacity to 0.87Mbps [14]. Nevertheless, higher data rate of 1.23Mbps is observed along the upper arm channel.

1.3.4 Alternative & Mixed Trials

Lindsey et al. in 1998 [15] proposed a transceiver system for an implantable device that includes a function generator with a fixed voltage of 3.25V rms, a current limiting resistor to vary the value of input current into 1mA, 2mA and 3mA rms and couple it through a galvanic approach using Ag-AgCl electrodes. Measurements have been conducted on a cadaver tissue. The transmission results shown by the oscilloscope prove that injected current is proportional to transmission gain as well to the inter-electrodes separation. However, transceiver electrodes separation distance and signal frequency is inversely proportional to the transmission gain.

In [16], *Fujii et al*. focused on capturing the influence of transmitter ground electrode on surrounding and penetrating electric field which is the result of electrodes capacitive coupling. The transmitter components which includes electrodes and circuit board are modeled as perfect conductor sheets to simplify power calculations after deriving the circuit model and to enable the use of FDTD calculations. The human arm model has been selected and modeled as a rectangular parallelepiped with dielectric properties of muscle tissue. For simpler equivalent circuit derivation, common transmission line laws are imported. A sine wave with 3V amplitude and

10MHz frequency is fed to the transmitting electrode. With both GND configurations, attached and not attached transmitting electrode ground, the first setup showed full electric field distribution along the arm due to electric field penetrating the arm. On the other hand, the lateral configuration showed an electric field with less intensity resulting from the increase in reactive value of the human input impedance.

Shinagawa et al. later replaced the common signal detection technique that utilizes a regular oscilloscope probe with an electro-optic (EO) probe [17]. The electro-optic sensor consists of both transverse and longitudinal type for sensing all electric field orientations. In addition, this sensor offers low electric field intensity detection due to the very high input impedance and ultra wide detection band. Two personal digital assistants (PDA) are connected to the transceiver system to transmit an information and verify receiving it correctly. All components are battery powered and suspended in the air to mimic an actual transmitting situation. A coupling voltage of 25V is assigned to the transmitting circuit; However, less than 100mV is induced on the human body. Finally, by sending a connection confirmation command, the authors established a half-duplex communication in accordance with IEEE 802.3 with data rate of 10Mbp.

A comprehensive experimental measurement for both coupling approaches was presented by Callejon et al. to explore a suitable operating frequency range and to determine the influence of electrodes' types, channel length and grounding strategy [18]. The experimental setup of galvanic coupling included a signal generator, oscilloscope, coupling electrodes and baluns to eliminate the effect of internal ground of signal source and detector. A spectrum analyzer has been used in the capacitive setup to transmit and detect the coupled signal where the rest of experiment components are the same as the galvanic setup. Over a 100 experimental measurements have been conducted. An optimum operating frequency range between 20-60kHz has been determined

for the galvanic method and between 60-70MHz for the capacitive approach where the measurements were performed over several days. In addition, the authors concluded that the material of the electrodes did not have a significant influence on the channel performance; However, the capacitive approach measurements showed sensitivity to grounding electrode type. Also, they deducted that as the inter-electrode spacing of TX and RX increases, the transmission gain enhances for the galvanic status.

1.3.5 Channel Modeling & Modulation Techniques

Yong Song et al. had derived a transfer function that is able to capture the geometrical and dielectric properties of the human channels [19]. All the human main body tissues had been simplified into multiple concentric cylinders to construct a circuit model where each cylinder represent a human tissue with frequency dependent permittivity and conductivity values. and a diameter of 50mm is assigned to the largest cylinder of the arm with specific diameter for each tissue and set in proportion for other human parts. The measurement and simulation attenuation profiles of all presented human channels showed data agreement with a constant error which had been neutralized using a correction factor defined as K.

Swaminathan et al. derived a tissue equivalent model with the same impedances distribution as shown by [19]; In addition, the authors considered the impedance of the path between each human tissue [20]. Finite element method has been utilized to verify the equivalent model which indicated data agreement for multiple transmission paths that are represented in terms of wearable to wearable, wearable to implant and implant to implant. The muscle to muscle path showed the highest SNR and stable readings compared to the other paths. Transceiver and inter-electrode separation have been investigated which support the results of all prior mentioned

authors in this chapter. Finally, experimental measurement has been conducted on a porcine meat to validate the readings of the equivalent model which showed a small readings variation.

Ruiz et al. investigated a new transmission frequency range; 1MHz-2.5GHz, in terms of received signal power magnitude [21]. In addition to setting an environmental ground, a signal electrode is isolated vertically from a reference electrode (GND) which is connected to the ground of a network analyzer for both TX and RX electrodes where two setups of GND electrode touching the skin or not touching are included. The network analyzer is used to display the received signal. The acquired data from the network analyzer verify that as the distance of transmission and the signal frequency increase, the detected signal magnitude decreases. A signal generator that is able to generate and modulate a radio signal in order to propagate it thorough the human body and a wireless communication analyzer that is capable to detect, demodulate and plot the received signal are implemented to evaluate the performance of digital modulation technique using intra-body channels. MSK, BPSK, QPSK, 8PSK and 16QAM were the digital modulation schemes of transmission with symbol rate of 100ksps to 5Msps. By contacting the signal electrode to the human body, which is referred by the authors as intra-body channel, along the modulation methods showed superior performance comparing to the other setup, which is referred to as air propagation, where MSK modulation reported the best performance, but 16QAM the farthest symbols to the reference constellation points of the constellation diagram when the symbol rate is 100ksps and transmission distance is 60cm. By increasing the transmission distance and symbol rate, BPSK provided the best performance. By using Error vector magnitude (EVM), the authors were able to quantify the difference between the ideal and measured signal. The EVM measurements provided that BPSK modulation with symbol rate of 2.5Msps could be used for transmission distance below 155cm to achieve high detection

accuracy and good modulation quality. Also, it provided 5Msps for distance of 20cm for BPSK and MSK modulations. More research by the authors aimed to derive a statistical channel model of intra-body propagation characteristics relying on the best fitting probability function where multiple families of probability distribution such as T-location scale, extreme value, normal, logistic and non-parametric are chosen based on their shape [22]. The same experimental setup had been applied; however, walking and static body situation has been tested to investigate its effect on human channel performance. The normal distribution showed the best fitting along all specified electrodes' placement. Finally, the authors were able to define a general linear statistical model for a reasonable range of transceiver distance.

1.4 Summary & Challenges

As seen in the prior work presented in the previous section, IBC is a promising technology that can offer major opportunities to various fields like healthcare, wellness, fitness, sports, emergency monitoring, entertainment and others. Table 1.3 shows a brief summary for the major contributions in this field. Table 1.4 summarizes the main differences between the basic two approaches as well; the galvanic and the capacitive coupling techniques, from a systems and implementation point of view, as observed from the presented prior art. However, there is still much research and standardization is needed to accurately and fully define the aspects of this new technology and how to best harness its potential. First major challenge is to fully understand this new communication channel, the human body, and accurately derive a channel model that can fully characterize the body as a transmission medium, to be used in later stages as systems and circuits design. As seen earlier, different approaches have been adopted to study this novel channel, where each of these approaches vary even for the same coupling method. Each of the previously presented prior work presented certain metrics for characterizing the channel, certain

Table 1.3. Summary for IBC System Trials [6]

	Coupling	Frequency Range	Modulation	Data Rate
Zimmer	Capacitive	100-500 kHz	OOK	2.4kbps
Handa	Galvanic	10-100kHz	PWM	0.9 kbps
Lindsey	Galvanic	2-160kHz	FM	-
Partridge	Capacitive	140-180kHz	FSK	38.4kbps
Oberele	Galvanic	--	CPFSK	4.8 kbps
Fuji	Capacitive	10-100MHz	OOK	9.6 kbps
Hachisuka	Capacitive	10k-50GHz	FSK	10 Mbps
Shinagawa	Capacitive	--	-	
Wegmueller	Galvanic	10k-1MHz 1k-10MHz	FSk, BPSK	128,255 kbps
Ruiz	Capacitive	10k-1MHz 1k-10MHz	BPSK, MSK	100- 2500 Kbps
Song	Galvanic	100k-5MHz	--	--
Callejon	Galvanic/ Capacitive	10k-2MHz 1M-100MHz	--	--
Swaminathan	Galvanic	100k-1MHz	--	--

Table 1.4. Comparison between Capacitive and Galvanic Coupling techniques

	Galvanic Coupling	Capacitive Coupling
Topology	Both the signal and ground electrodes are in contact with the skin (body	The signal electrodes are in contact, or close proximity, to the body, while the GND electrodes are floating in the air
Induced Signal Intensity	Amplitude of the injected alternating current controls the intensity of induced signal	Electrical potential difference controls the intensity of induced signal
Interference and the surrounding environment	Robust against these factors as the signal is confined into the body	Sensitive to them
Supported Data Rates	Low	High
Frequency range of Operation	Low, < 50 MHz	High, > 50 MHz

proposed range for the operating frequency, as well as specific optimum frequency for optimizing the power budget. Unfortunately, there is still no solid standard values for these parameters, in spite of the effort exerted by the community and the regulation authorities and task groups, like the IEEE. Similarly, the setup and location of electrodes, as well as their impact of the system performance, are still debatable as well. The authors in [13], [15], and [18-19] showed the influence of transmission distance that separates the electrodes wherein the last two examined the inter-electrodes spacing effect of transmission.

Simulation techniques have been extensively used in modeling the channel, from simple circuit models [19] to the Finite Element Methods [13] were all considered, where usually the gain/ attenuation profile (gain/attenuation of the channel versus frequency) is reported. Experimental setups were also considered as in [9], [13], [18-19] and [21] for data validation. Yet testing on human subjects, especially for a novel emerging technology as IBC, impose various restrictions and safety issues. Thus, there is a necessity for a more reliable testing platform, that is more reliable and accurate compared with computer models, yet doesn't involve human subjects for safety reason. As a tradeoff, the research in [15] shows the use of a cadaver to conduct measurements. The authors in [11] and [17] followed simpler approach by using a polymeric material and polyvinyl chloride, respectively. The author in [20] utilized porcine tissue to conduct the experimental measurements. However, these models are not accurate enough, nor do they capture the different factors responsible for mimicking the signal propagation and diffusion throughout the various body tissues, thus there is still a need for more accurate testing platforms for IBC.

1.5 Dissertation Contribution

The basic contributions presented in this dissertation can be summarized as follows:

- Study, present and summarize prior work in the IBC fields, current challenges and opportunities, as well as possible applications
- Explore and compare between the different possible data carriers to be used as means for data transmission over this novel channel – the body
- Accurately model the channel characteristics and behavior over the targeted frequency range of operation, model the different basic components of the IBC system, as well as the biological aspects and parameters of the body that impacts the channel performance and characteristics, and conclude such findings in a circuit representation for that model.
- Develop a 3D Finite Element Method (FEM) model to represent other factors and parameters, such as the field distribution
- Perform and present an in depth study for the electrodes' contact impedance, being the gateway between the electronics domain and the biological one, compare between different modeling approaches, study the effect of different design parameters on these modeling techniques, decide on the most comprehensive modeling technique, include it into the final developed IBC model, and study the impact of the electrode-related parameter on the overall channel performance.
- Design, fabricate and test the first multi-layer tissue mimicking materials' phantoms, designed specifically for IBC applications, providing a novel and unique physical platform for IBC technology testing – a platform that is provided for the first time with such accuracy in this field, to the author's knowledge.

- Carryout experimental testing on real subjects, to study the IBC channel characteristics for different scenarios ad for different sensors' location on the body, then statistical modeling approaches were studied and compared to better represent the channel behavior and dynamics with respect to both the time and frequency domains.
- Develop a software platform that combines the knowledge developed throughout this research work, for the design of distributed body senor networks that utilizes the IBC technology as means of communications between the network's different nodes. Stress profile analysis application is demonstrated as a use case.
- Develop applications based on the IBC technology in the security field, where machine learning algorithms are used to process the experimental data collected throughout this project and successfully to demonstrate the use of IBC channel characteristics as a biometric identity, where data collected from subjects were used for both identification and authorization (verification) applications, with outstanding accuracy, exceeding 98%

1.6 Dissertation Outline

In Chapter 2, we start exploring the IBC channel by investigating the most appropriate data carrier for IBC applications that would secure the pros of IBC technique over other solutions.

In Chapter 3, after deciding on the optimum data carrier for IBC, the human body as a communication channel is accurately modeled using different modeling techniques to study the relation between the different blocks of the IBC system and the impact of all on the performance of the IBC channel.

Chapter 4 focuses on modeling a crucial component in the IBC system, the electrodes, their impedance, relation with other IBC components and their influence on the overall system performance.

Chapter 5 introduces the implementation of a multilayer arm phantom model to serve as a reliable and accurate test platform for body area networks in general and IBC applications specifically.

Chapter 6 shows the experimental results performed on real subjects, where the channel performance is thoroughly investigated. We also introduce two novel applications that are developed using the IBC technology; namely a software design platform for distributed body sensor networks, and using the IBC channel characteristics as a biometric identity for security applications.

Chapter 7 includes the conclusion and future work.

References

[1] The Physics Factbook. Frequency of A Beating Heart. https://hypertextbook.com/facts/1998/ArsheAhmed.shtml, 2013 (Accessed: 2017- 09- 08).

[2] WHAT ARE BRAINWAVES? http://www.brainworksneurotherapy.com/what-are-brainwaves, 2013 (Accessed: 2017- 09- 08).

[3] Riccardo Cavallari, Flavia Martelli, Ramona Rosini, Chiara Buratti, and Roberto Verdone. A survey on wireless body area networks: Technologies and design challenges. IEEE Communications Surveys & Tutorials, 16(3):1635-1657, 2014.

[4] Maulin Patel and Jianfeng Wang. Applications, challenges, and prospective in emerging body area networking technologies. IEEE Wireless communications, 17(1), 2010.

[5] IEEE 802.15 TG6 http://www.ieee802.org/15/pub/TG6.html (Accessed: 2019- 10- 04).

[6] Ibrahim Alquaydheb; "Human Channel Modeling and Optimization for Intra-body Communication." Master Thesis, UC Irvine, 2018.

[7] Thoams Guthrie Zimmerman. Personal area networks: near-field intrabody communication. IBM systems Journal, 35(3.4):609-617, 1996.

[8] Takashi Handa, Shuichi Shoji, Shinichi Ike, Sunao Takeda, and Tetsushi Sekiguchi. A very low-power consumption wireless ecg monitoring system using body as a signal transmission medium. In Solid State Sensors and Actuators, 1997. TRANSDUCERS'97 Chicago., 1997 International Conference on, volume 2, pages 1003-1006. IEEE, 1997.

[9] Kurt Partridge, Bradley Dahlquist, Alireza Veiseh, Annie Cain, Ann Foreman, Joseph Goldberg, and Gaetano Borriello. Empirical measurements of intrabody communication performance under varied physical con_gurations. In Proceedings of the 14th annual ACM symposium on User interface software and technology, pages 183-190. ACM, 2001.

[10] Michael Oberle. Low power systems-on-chip for biomedical applications. PhD Dissertation, 2002.

[11] Keisuke Hachisuka, Azusa Nakata, Teruhito Takeda, Yusuke Terauchi, Kenji Shiba, Ken Sasaki, Hiroshi Hosaka, and Kiyoshi Itao. Development and performance analysis of an intra-body communication device. In TRANSDUCERS, Solid-State Sensors, Actuators and Microsystems, 12th International Conference on, 2003, volume 2, pages 1722-1725. IEEE, 2003.

[12] Keisuke Hachisuka, Yusuke Terauchi, Yoshinori Kishi, Ken Sasaki, Terunao Hirota, Hiroshi Hosaka, Katsuyuki Fujii, Masaharu Takahashi, and Koichi Ito. Simplified circuit modeling and fabrication of intrabody communication devices. Sensors and actuators A: physical, 130:322-330, 2006.

[13]Marc Simon Wegmueller, Andreas Kuhn, Juerg Froehlich, Michael Oberle, Norbert Felber, Niels Kuster, and Wolfgang Fichtner. An attempt to model the human body as a communication channel. IEEE transactions on Biomedical Engineering, 54(10):1851-1857, 2007.

[14] Marc Simon Wegmueller, Michael Oberle, Norbert Felber, Niels Kuster, and Wolfgang Fichtner. Signal transmission by galvanic coupling through the human body. IEEE Transactions on Instrumentation and Measurement, 59(4):963-969, 2010.

[15] Derek P Lindsey, Eric L McKee, Maury L Hull, and Stephen M Howell. A new technique for transmission of signals from implantable transducers. IEEE transactions on biomedical engineering, 45(5):614-619, 1998.

[16] Katsuyuki Fujii, Koichi Ito, and Shigeru Tajima. Signal propagation of wearable computer using human body as transmission channel. In Proceedings of the International Symposium on Antennas and Propagation ISAP-02, pages 512-515, 2002.

[17] Mitsuru Shinagawa, Masaaki Fukumoto, Katsuyuki Ochiai, and Hakaru Kyuragi. A near-field-sensing transceiver for intrabody communication based on the electrooptic elect. IEEE Transactions on instrumentation and measurement, 53(6):1533-1538, 2004.

[18] Maria Amparo Callejon, David Naranjo-Hernandez, Javier Reina-Tosina, and Laura M Roa. A comprehensive study into intrabody communication measurements. IEEE Transactions on Instrumentation and Measurement, 62(9):2446-2455, 2013.

[19] Yong Song, Qun Hao, Kai Zhang, Ming Wang, Yifang Chu, and Bangzhi Kang. The simulation method of the galvanic coupling intrabody communication with different signal transmission paths. IEEE Transactions on Instrumentation and Measurement,
60(4):1257-1266, 2011.

[20] Meenupriya Swaminathan, Ferran Simon Cabrera, Joan Sebastia Pujol, Ufuk Muncuk, Gunar Schirner, and Kaushik R Chowdhury. Multi-path model and sensitivity analysis for galvanic coupled intra-body communication through layered tissue. IEEE transactions on biomedical circuits and systems, 10(2):339-351, 2016.

[21] Jordi Agud Ruiz and Shigeru Shimamoto. Experimental evaluation of body channel response and digital modulation schemes for intra-body communications. In Communications, 2006. ICC'06. IEEE International Conference on, volume 1, pages 349-354. IEEE, 2006.

[22] Jordi Agud Ruiz and Shigeru Shimamoto. Statistical modeling of intra-body propagation channel. In Wireless Communications and Networking Conference, 2007. WCNC 2007. IEEE, pages 2063-2068. IEEE, 2007.

Chapter 2

Intrabody Communications Data Carrier

2.1 Introduction

First step to building an efficient IBC system is determining the optimum data carrier for this novel technology. In this chapter, a comparison of the main potential means of data carriers for IBC, namely using electro-magnetic waves, ultrasonic waves and magnetic coupling is presented where the pros and cons of each approach are discussed.

2.2 Electromagnetic (EM) Waves

The first and most traditional approach for data transmission is EM waves. EM waves is the favorable data carrier for wireless communications in general, especially when the propagating medium is air or space. For IBC, EM waves were also adopted in the majority of the prior art as the data carrier of choice. As shown in the previous chapter, use of EM waves in intra-body communications can be categorized into two main types; capacitive coupling (near field coupling method) and galvanic coupling. In capacitive coupling, only the signal electrodes of the transmitter and the receiver are attached to the body while the ground (GND) electrodes are left floating in the air. The conductive body forms the forward path while the signal loop is closed through the capacitive return path between the transmitter and the receiver GND electrodes. The second approach, which depends on the galvanic coupling principle, uses a pair of electrodes for both the transmitter and the receiver to propagate the electromagnetic wave. The signal is applied over two coupler electrodes and received by two detector electrodes. An attractive feature of the

galvanic coupling approach is that the signal is totally confined to the body, unlike capacitive coupling where the signal return path is established through the air. Galvanic coupled signals experience minimal interference from other electronic devices, enabling robust and secure data exchanges.

2.2 Magnetic Human Body Communications

A new approach was recently proposed in [1] where resonant magnetic coupling was suggested to be used as an alternative physical layer for BAN. In this approach, coils wrapped around anatomy (arm, leg, head ...etc.) are used to generate magnetic base signals at the transmitter side and receive them (pick them up) at the receiver end, as shown in Figure 2.1. The main motivation is that the permeability of human tissues is similar to air which enables the magnetic fields to travel more freely through the human body. Unfortunately, this approach suffers from a number of drawbacks. The fact that the permeability of human tissues is similar to air makes it more difficult to confine the signal within the human body, thus part of the signal will be lost in the air. This means that the network power leakage will be high which cause two main drawbacks:

- Increase the power budget to operate the whole network
- Threatens the security of the transmitted data, as part of it is being leaked into the surrounding medium, thus IBC losses one of its main advantages over wireless solutions

Moreover, it is not possible to separate the electric and magnetic fields for an EM wave as long as the displacement current ratio to the conduction one is considerable. The ratio is plotted for different body tissues, as shown in Figure 2.2, showing that in the Mega-Hertz frequency range it

is not possible to assume that both fields are independent. Such results imply that data transmission cannot be attributed to the magnetic field only, but to the electric field as well since

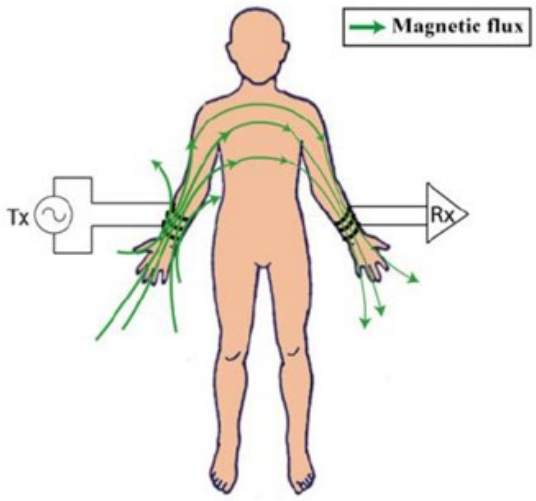

Figure 2.1: Using magnetic fields as the data carrier solution for IBC, where coils wrapped around the arm are used to generate magnetic base signals at the transmitter side and pick them up at the receiver end [1]

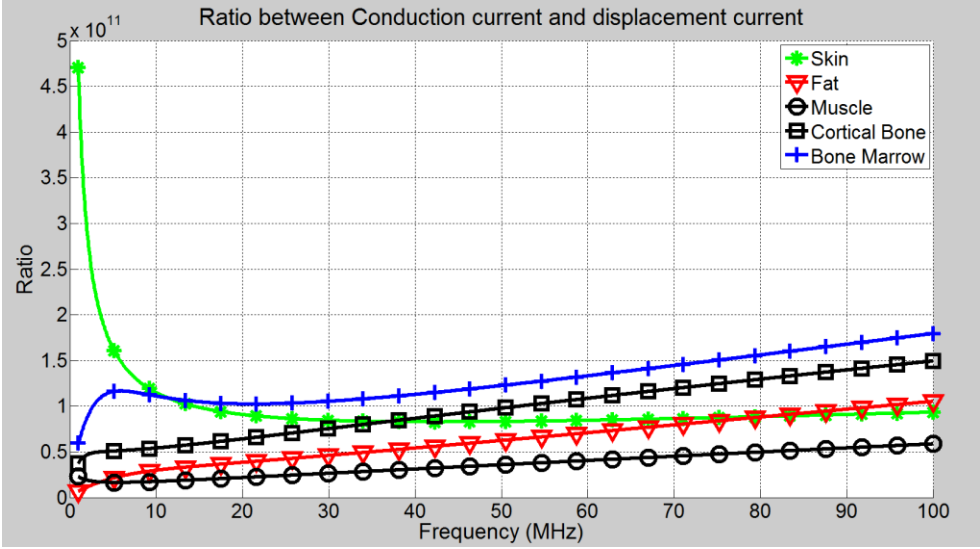

Figure 2.2: Ratio between displacement and conduction currents in different body tissues, showing that the displacement current values are large enough thus electric and magnetic fields cannot be assumed to be independent of each other in this frequency range.

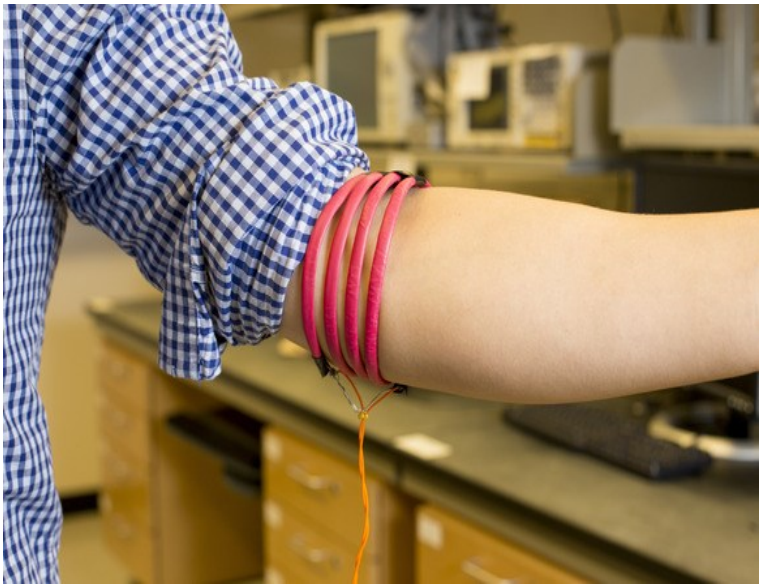

Figure 2.3: For each communicating node that will use the magnetic fields only approach as means for data carrier, a wrapped coil is need [203], where each node becomes really bulky in size, inconvenient and not efficient compared with wireless solutions in this case.

they cannot be separated at the frequencies of interest while propagating through human tissue. Moreover, the need to wrap a coil around the body wherever we need to setup a communication node limits the use of such approach, as shown in Figure 2.3, making it inconvenient especially if multiple nodes are considered, as each node becomes really bulky in size, which again, strips IBC technology of one of its important advantages over convenient wireless solutions, which is its potential to be significantly compact in size, thus convenient for body area networks applications.

2.3 Ultrasonic Waves

Acoustic waves are mostly used for underwater communications since they possess better propagation properties in water as compared to RF waves. Since more than 65% of the human

body consists of water, ultrasonic waves (acoustic waves at the non-audible frequency range; above 20 KHz) was thought to have good potential as a means of communication for BAN. Research then followed [2-3] to investigate the efficiency of using ultrasonic waves in BANs, mainly to communicate between implantable devices, since ultrasonic waves propagate very poorly through air. This approach suffered from some drawbacks as well. A major drawback is the acoustic bio-effects, among which are heating and cavitation [4]. As ultrasonic waves propagate through the body tissues, a portion of the wave energy is absorbed and converted to heat, leading to an increase of these tissues' temperature, especially when wave intensity is increased, leading to undesirable biological effect. The other serious biological effect is cavitation. Ultrasonic waves are associated with pressure variations, causing bubbles in the propagation medium, body tissues in our case, to expand and contract. As this pressure variation activity increases, bubbles may collapse leading to tissue damage, a concern that has to be seriously considered when dealing with ultrasonic waves' propagation on a periodic, repeated manner. However, the impact of these two bio-effects can still be minimized through techniques of impulsive transmissions with low power and pressure levels, as ways of keeping the acoustic intensities to which the tissues are exposed to within the safety limits [5].

2.4 Electromagnetic V.S. Ultrasonic Waves

From the above, it became obvious that electromagnetic waves and ultrasonic waves are more convenient as data carriers for IBC and BANs applications in general. Yet, to decide which of them is the optimum data carrier for IBC, more in depth comparison will be shown between the two mediums, taking into consideration the biological properties of the human body, within the frequency range for intra-body communications; from low KHz up to 100 MHz's. The main to consider, being key factors for any system design, are attenuation (gain) and the delay profiles.

This comparison is also based on the assumption that health safety issues were already considered and both solutions are being implemented and operated in a manner that would adhere to the health safety regulations mentioned earlier [6-7].

2.4.1 Attenuation

Human tissue is considered to be a lossy medium where ultrasonic waves are dissipated in the form of heat. Attenuation of acoustic waves is caused mainly due to the absorption of the pressure energy by the medium in which the wave is propagating. Such attenuation is dependent on the type of the tissue as well as the frequency of operation. In general, attenuation for acoustic waves follows the relation:

$$\alpha = af^b$$

Where α is the attenuation in (Decibels/ (centimeter*Mega-hertz)), f is the frequency, a and b are constants that depend on the acoustic properties of each tissue. Figures 2.4 and 2.5 clarify the attenuation properties of the main human tissue types (skin, fat, muscle, cortical bone and bone marrow) to the propagation of both ultrasonic and EM waves. For ultrasound attenuation profiles versus frequency, the constants a and b are calculated from previous work in literature [8-10] using curve fitting techniques. As for EM attenuation, it was calculated according to the following equation:

$$\alpha = \frac{w}{2}\sqrt{\mu\,\varepsilon(w)}\tan(\delta(w))$$

Where α is the attenuation (dB/cm), w frequency (rad/s), μ permeability, $\varepsilon(w)$ frequency dependent permittivity and $\tan(\delta(w))$ is the loss tangent, and these electrical properties were all calculated for each tissue [11].

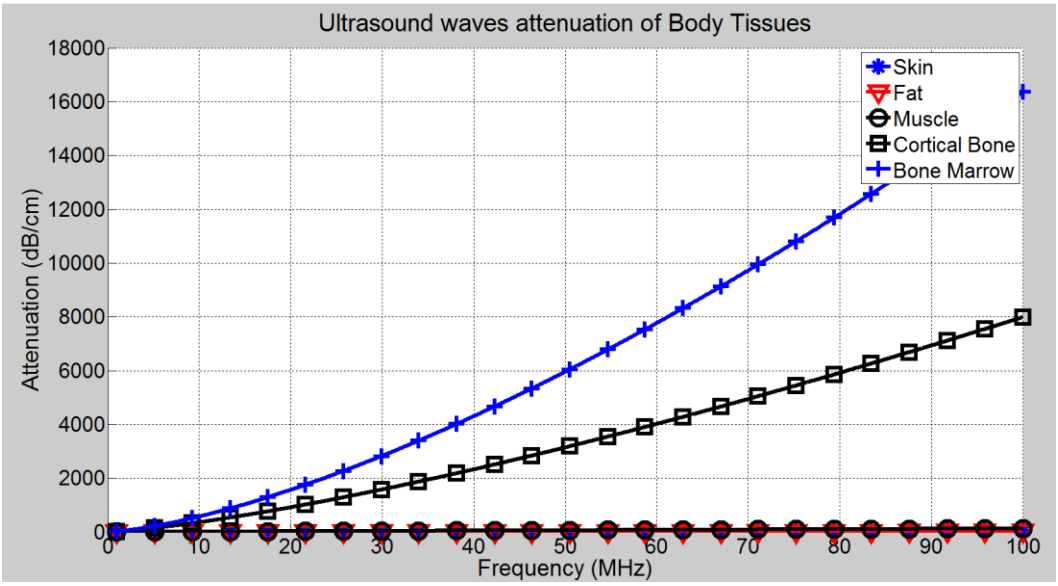

(a)

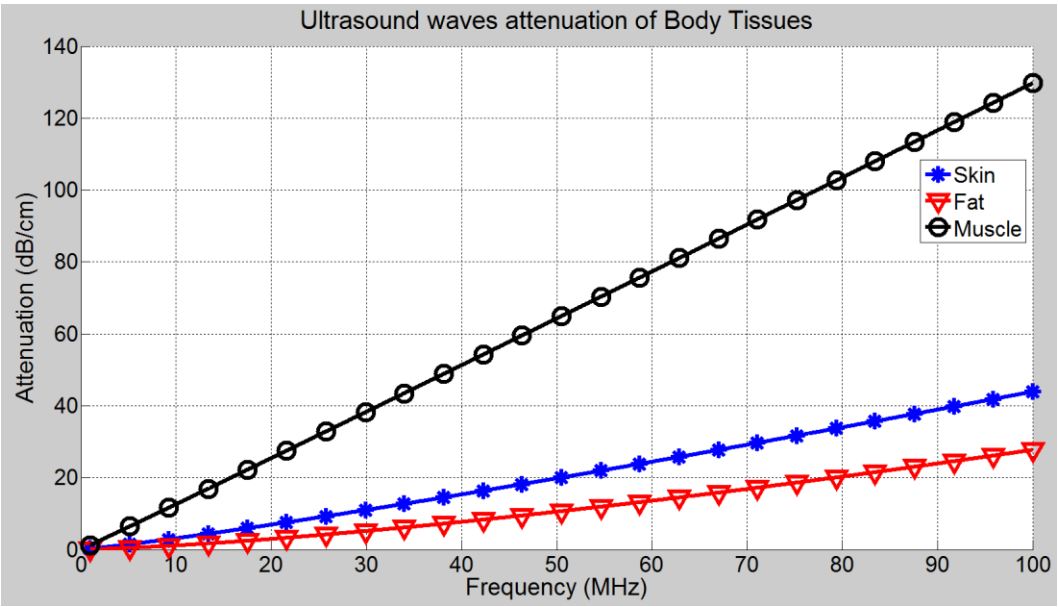

(b)

Figure 2.4 (a)Attenuation that Ultrasonic waves experience when propagating through each of the main five tissues of the human body, (b) zoomed in version to show attenuation for skin, fat and muscle tissues.

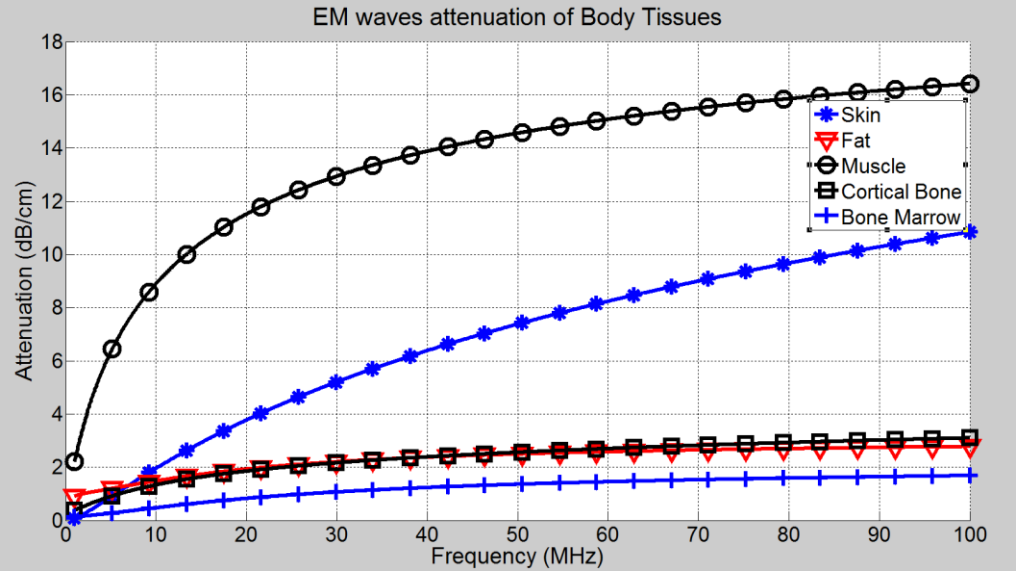

Figure 2.5 Attenuation that EM waves experience when propagating through each of the main five tissues of the human body.

From Figures 2.4 & 2.5, it can be shown that according to the attenuation profiles for the human body tissues, ultrasonic waves experience more attenuation, in the form of heat dissipation, compared with EM waves within the targeted frequency range for BAN. This means that adopting EM waves as the data carrier of choice would yield a smaller power budget, as less power is need to transmit a signal between two IBC nodes in case EM waves are used, when compared to the ultrasonic solution.

2.4.2 Delay

Another important aspect is the propagation delay; i.e. how fast these waves can travel through the body tissues. Ultrasonic waves are known to travel at very low speeds in the human body [12]; ranging between 1450 m/s in fat to 4080 m/s in bone. Such low speed introduces a significant delay at the receiver node which is directly translated into severe multi-path reflection problems. That drawback requires complicated system topologies and extra hardware at each

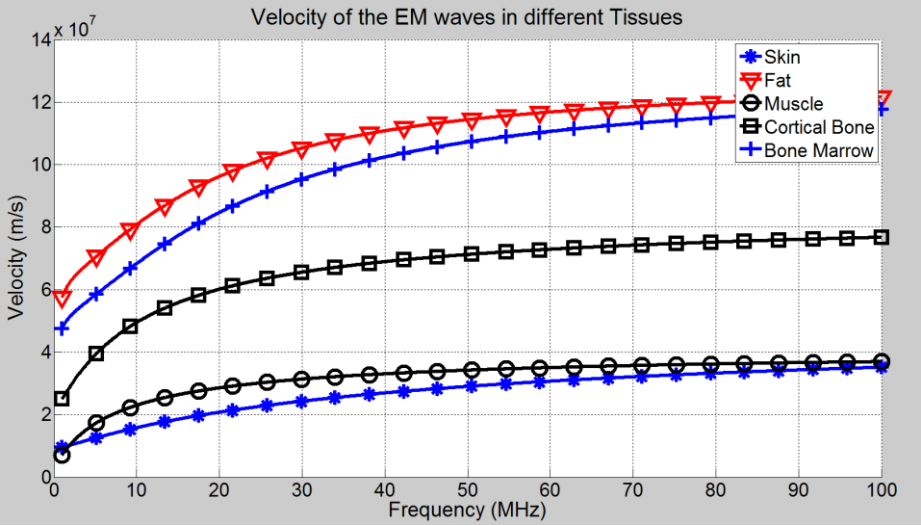

Figure 2.6 Propagation speed of EM waves in different body tissues.

node, leading to more complicated power hungry systems. Such a problem is much less pronounced in the case of EM waves' propagation. Velocity of EM waves' propagation within the different body tissues are shown in Figure 2.6. With such high propagation speeds, delay problems can be considered to be much less severe to deal with, especially with short distance communications as in the case of BANs, when EM waves are used as data carriers as opposed to Ultrasonic waves.

2.5 Conclusion

From the previous comparison, it is clear that EM waves are advantageous over other mediums for data transmission through the human body. It was shown that EM waves possess better properties, that can support BAN requirements, versus ultrasonic waves as EM waves experience much less attenuation and delay when traveling through the body. Such facts are crucial for system designers, as although ultrasonic circuits may appear simple in general, the hardware that would be required to compensate for the loss caused by ultrasonic waves' propagation in body tissues would add extra hardware and power compensation, making it a less attractive solution

when compare with EM waves. The magnetic field communication option showed a couple of drawbacks, namely:

- Power leakage to the surrounding medium
- Hard to implement from a scientific point of view, at the specific frequency range of interest for IBC, due to the inability to separate the magnetic fields from the electric ones within that frequency range.
- The need for a wrapped coil at each node makes it bulky and inconvenient

On the other hand, EM waves possess the following advantages:

- Shows better tissue-related propagation properties (attenuation and delay) when compared to the ultrasonic solution
- Simple system, with smaller area and power footprint
- Much easier to integrate with currently available wearable systems and platforms, thus has the advantage of compatibility as well.

For all of the above, it is concluded that Electro-Magnetic waves are indeed the optimum data carrier for IBC applications in the specified frequency range of interest (100 KHz till 100 MHz). Findings in this chapter are published in [13]. Next step is modeling the propagation of this data carrier through the human body as a communication channel.

References

[1] Park, J. and Mercier, P.P. 2015. Magnetic human body communication. In *2015 37th Annual International Conference of the IEEE Engineering in Medicine and Biology Society (EMBC) (Aug. 2015),* 1841-1844.

[2] Galluccio, L., Melodia, T., Palazzo, S., & Santagati, G. E. 2012. Challenges and implications of using ultrasonic

communications in intra-body area networks. In *9th Annual Conference Wireless On-demand Network Systems and Services (WONS), (Jan. 2012)*. 182-189.

[3] Davilis, Y., Kalis, A., & Ifantis, A. 2010. On the use of ultrasonic waves as a communications medium in biosensor networks. *IEEE Transactions on Information Technology in Biomedicine,* 14(3), 650-656.

[4] Santagati, G.E. and Melodia, T. 2013. Opto-ultrasonic communications in wireless body area nanonetworks. In *2013 Asilomar Conference on Signals, Systems and Computers* (Nov. 2013), 1066-1070.

[5] Miller, D.L. 2008. Safety assurance in obstetrical ultrasound. In *Seminars in Ultrasound, CT and MRI*, 29, 2 (April 2008), 156-164. WB Saunders.

[6] International Commission on Non-Ionizing Radiation Protection (ICNIRP), Guidelines for limiting exposure to time-varying electric, magnetic, and electromagnetic fields (up to300GHz), 1997.

[7] IEEE C95.1-2005, IEEE Standard for Safety Levels with Respect to Human Exposure to Radio Frequency Electromagnetic Fields, 3 kHz to 300 GHz, The Institute of Electrical and Electronics Engineers Inc., New York , 2006.

[8] Shore, D., Woods, M. O., & Miles, C. A. 1986. Attenuation of ultrasound in post rigor bovine skeletal muscle. *Ultrasonics*, *24*(2), 81-87.

[9] Pichardo, S., Sin, V. W., & Hynynen, K. 2011. Multi-frequency characterization of the speed of sound and attenuation coefficient for longitudinal transmission of freshly excised human skulls. *Physics in medicine and biology, 56, 1 (2011)*, 219.

[10] Moran, C. M., Bush, N. L. and Bamber, J. C. 1995. Ultrasonic propagation properties of excised human skin. *Ultrasound in medicine & biology* 21, no. 9 (1995), 1177-1190.

[11] Gabriely, S., Lau, R. W. and Gabriel, C. 1996. The dielectric properties of biological tissues: II. Measurements in the frequency range 10 Hz to 20 GHz. Phys. Med. Biol., 41, 11 (Nov. 1996), 2251–2269.

[12] Thurston, Robert, N., and Allan, D. Pierce, eds. 1999. *Ultrasonic Instruments and Devices I*. Academic Press.\

[13] Khorshid, A.E., Eltawil, A.M. and Kurdahi, F., 2016, December. On the optimum data carrier for intra-body communication applications. In *Proceedings of the 11th EAI International Conference on Body Area Networks* (pp. 137-140). ICST (Institute for Computer Sciences, Social-Informatics and Telecommunications Engineering).

Chapter 3

Human Channel Modeling

3.1 Introduction

As shown in chapter 2, Electromagnetic (EM) waves are the most efficient means for data transmission for applications adopting intra-body communications technology. Intra-body communications using EM waves can be categorized as mentioned earlier into into two main types; capacitive coupling (near field coupling method) and galvanic coupling. In capacitive coupling, only the signal electrodes of the transmitter and the receiver are attached to the body while the ground (GND) electrodes are left floating in the air. The conductive body forms the forward path while the signal loop is closed through the capacitive return path between the transmitter and the receiver GND electrodes. The second approach, which depends on the galvanic coupling principle, uses a pair of electrodes for both the transmitter and the receiver to propagate the electromagnetic wave. The signal is applied over two coupler electrodes and received by two detector electrodes. The coupler establishes a modulated electrical field, which is sensed by the detector. An attractive feature of the galvanic coupling approach is that the signal is totally confined to the body, unlike capacitive coupling where the signal return path is established through the air. Galvanic coupled signals experience minimal interference from other electronic devices, enabling robust and secure data exchanges. Having identified the appropriate data carrier, our next step is modeling the propagation of this data carrier through the human body, form a telecommunication, systems and circuits aspects, to take one step closer to the realization of practical intra-boy communications systems' implementation. Numerous research

efforts exist that address modeling the body as a communication channel. In this chapter, we present a model for intra body communications using galvanic coupling. In the proposed model, biological parameters are assumed to be variable, taking into consideration the impact of important factors; such as age and weight, on these parameters and thus on the overall attenuation profile. For the proof of concept, a model for the arm was considered. The basic concepts for the model and how such biological factors were taken into considerations are explained. Simulation results are then plotted and compared with published experimental results, showing high accuracy in identifying the optimum frequency for signal transmission for intra-body communications systems. Sensitivity of the model parameters, as well as the transmitter and receiver nodes' components are investigated as well, for a more accurate understanding of the system design requirements and constraints.

3.2 Basic Model Blocks

As shown in Figure 3.1, the basic blocks for any general intra-body communication channel model are:

- Transmitter node; source of information being it a sensor that collects physiological data and or just a relay for improving the signal quality and account for the path loss
- Receiver node; can be an actuator, a processing unit or even a gateway node, that transmits the data collected by the local body area network to the outside world
- Electrodes; the interface between the circuits/systems domain and the biological/body domain, responsible for coupling the signal to and from the body
- The Body; the channel/medium through which the signal propagates from the transmitter node to the receiver node.

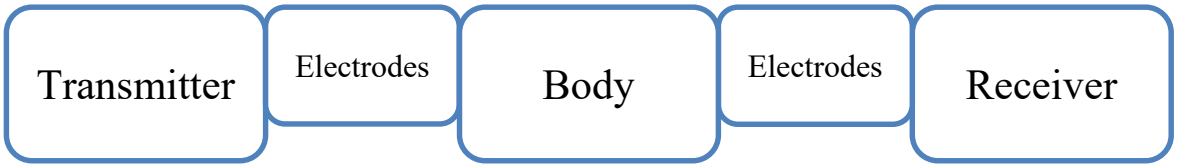

Figure 3.1: Basic blocks constituting any general intra-body communications system

The body is the corner block in the IBC system though, as its properties dictates the constraints and design requirements for all the other blocks. An accurate model for an IBC channel should thus be able to accurately represent the following:

- The nature of each block
- Basic parameters for each block
- Relation between the different model blocks
- Design variables and their effect on the model
- Sensitivity of the model to all of these parameters

Various approaches were adopted throughput the literature to fulfil these requirements in order to reach an accurate channel model for the IBC communication channel. Providing such model is a crucial step in order to be able to design systems and circuits that can efficiently utilize the IBC technology. The primary performance metric that is reported in literature for the comparison between different models and validation of these models against experimental results is the *gain/attenuation profile*. Simply, the gain/attenuation profile is an accurate map of the body, representing the amount of gain/attenuation (loss) that the signal will witness as it propagates through the body from one node to the other. The gain/attenuation profile is frequency specific and distance dependent too. The gain/attenuation profile is also function in many parameters that should all be taken into consideration in order to accurately model the signal propagation through the body, and match the model results as much as possible with the experimental/actual findings.

Among these parameters that should be taken into consideration are:

- *Transmitter:* output impedance of the transmitter, spacing between the electrodes of the transmitter mode
- *Receiver;* input impedance of the receiver, spacing between the electrodes of the receiver mode
- *Electrode*s; material they are fabricated from, whether a gel is used or not, dimensions of the electrode, position of the electrodes
- *Body:* electrical properties of the body tissues, the propagation path through the body, geometric features (thickness of each layer, height, mass, body frame, ...etc.), transmission distance (distance between the transmitter and the receiver).

Other performance metrics were also reported in the literature, as the electric field distribution, current density distribution and potential distribution, yet these metrics vary significantly from one simulation to the other and also are very challenging to measure experimentally, that's why in our study we will stick with the golden reference in reporting our results, which is the gain/attenuation channel profile.

Different models are used for modeling the IBC channel, the most common of which are: circuit models and finite element models (FEM). When both models are accurate enough, circuit models are more favorable as they are simpler to build, much faster to simulate and easy to integrate with the system/circuits design process. We started by building an accurate circuit model that takes as many parameters as possible into consideration. We then validated our model through comparing it to experimental results reported in the literature. Finally, we developed a FEM model as well to provide other performance metrics that may be required by the system designer,

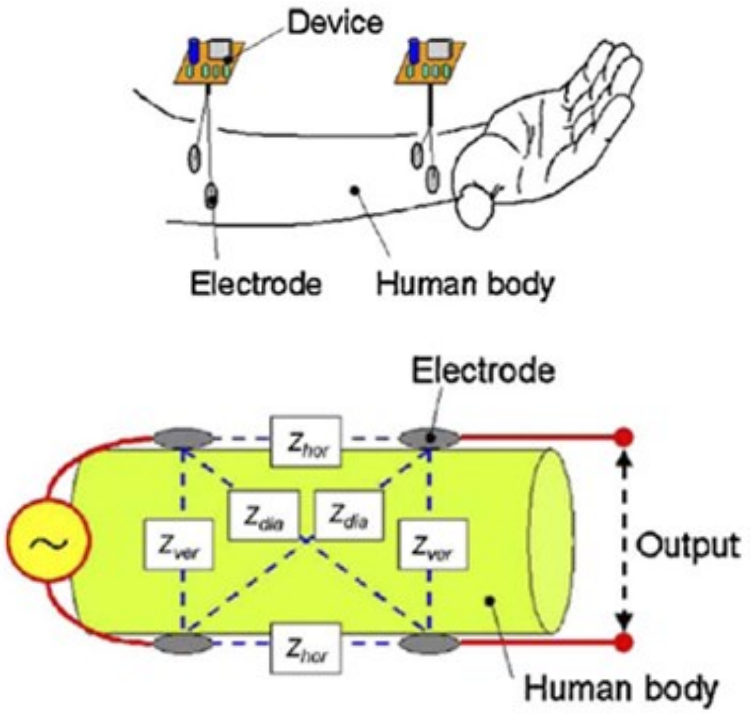

Figure 3.2: (a) Circuit model for the IBC system, showing how the signal propagates through the body, taking into account the transmitter and the receiver nodes but not accounting for the electrode impedance [2].

to compare between both the circuit model and the FEM model and finally to provide a platform of modeling tools for the IBC technology in general.

3.3 IBC Circuit Model

For IBC circuit models, RC networks are used to represent the basic system blocks explained earlier. First model was proposed by Zimmerman [1], where transverse and longitudinal impedances were proposed to represent the signal propagation through the body. Improved models then followed [2-4], taking the transmitter and receiver nodes into account as well, as shown in Figure 3.2. However, it was not until electrodes were taken into consideration [2], that circuit models started to provide an accurate and mature representation for the IBC system. In all of these models, the channel gain/attenuation profile versus frequency, and sometimes versus the

distance between the transmitter and receiver electrodes, are the main performance metrics reported. The gain/attenuation profile is computed through getting the transfer function expression that defines the relation between the input node of the system and the output terminal, in terms of the impedances modeling the different blocks of the system. Different impedances (as shown in Figure 3.2 for example) represent the different IBC system components as well as the signal propagation path (between the transmitter and the receiver nodes). These impedances are then computed through taking into consideration the biological, electrical and geometrical properties of the body. An accurate circuit model for galvanic IBC systems is proposed in [5], and is shown in Figure 3.3, where the signal transmission is represented by a four terminal circuit model. V_i represents the signal source at the transmitter, Z_c represents the coupling impedance between the electrode and the skin. The two transmitting electrodes are attached to the human skin at I_1 and I_2, while the receiving electrodes are attached to the human body at O_1 and O_2. Z_i represents the impedance between I_1 and I_2, thus can be considered as the input impedance of the human body. Z_{t1} and Z_{t2} are the transverse impedances of the transmission path, while Z_{b1} and Z_{b2} are the cross impedances of the transmission path in the human body. The output resistance of the transmitter is represented as R_O, while the input impedance of the receiver is represented by Z_{ceo}. The unit for all these impendences is Ohms (Ω). The transfer function is then derived for the relation between V_i and V_o (voltage across Z_{ceo}) which would give us the gain profile for the transmission through the human arm, in other words, how much of the signal V_i will be picked by the receiver. The transfer function of the model is then obtained where the final expression is:

$$H_A = \frac{V_0}{V_i} = \frac{Z_i Z_h}{Z_i Z_h + (2Z_c + R_O)(Z_i + Z_h)} * \frac{Z_{ceo}}{Z_{ceo} + 2Z_c} * H_h \qquad (3.1)$$

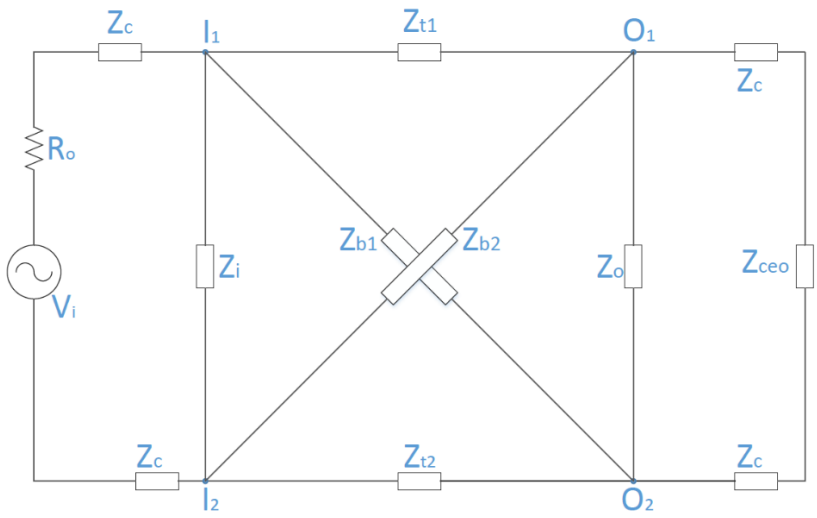

Figure 3.3. Full circuit model for the galvanic IBC system, V_i represents the signal source at the transmitter, Z_c represents the coupling impedance between the electrode and the skin. Z_{t1} and Z_{t2} are the transverse impedances of the transmission path, while Z_{b1} and Z_{b2} are the cross impedances of the transmission path in the human body. The output resistance of the transmitter is represented as R_O , while the input impedance of the receiver is represented by Z_{ceo}.

Where $$Z_h = \frac{Z_{t1}(Z_{t2}\, Z_{01}+Z_{b1}\, Z_{01})}{(Z_{t1}+Z_{b1}+Z_{01}-K_1 Z_{01})(Z_{01}-Z_{t2}H_h)} \quad (3.2)$$

$$Z_{01} = \frac{Z_o(2Z_c+Z_{ceo})}{(Z_o+2Z_c+Z_{ceo})} \quad (3.3)$$

$$K_1 = \frac{Z_{b2}\, Z_{t1}+Z_{b2}\, Z_{01}+Z_{b1}\, Z_{b2}+Z_{t1}\, Z_{01}}{Z_{b2}\, Z_{t1}+Z_{b2}\, Z_{01}+Z_{t1}\, Z_{t2}+Z_{t1}\, Z_{01}} \quad (3.4)$$

$$H_h = \frac{Z_{01}(K_1-1)}{Z_{b1}+K_1 Z_{12}} \quad (3.5)$$

The final gain in dB is then calculated as $$G = 20log_{10}H_A + K \quad (3.6)$$

Where K is a correction factor to account for uniform error across various frequency (calibration value obtained from experimental values). We will adopt this circuit model as the main circuit model representing the IBC channel, yet we applied novel, innovative and more accurate methods for modeling and calculating the impedances in these model.

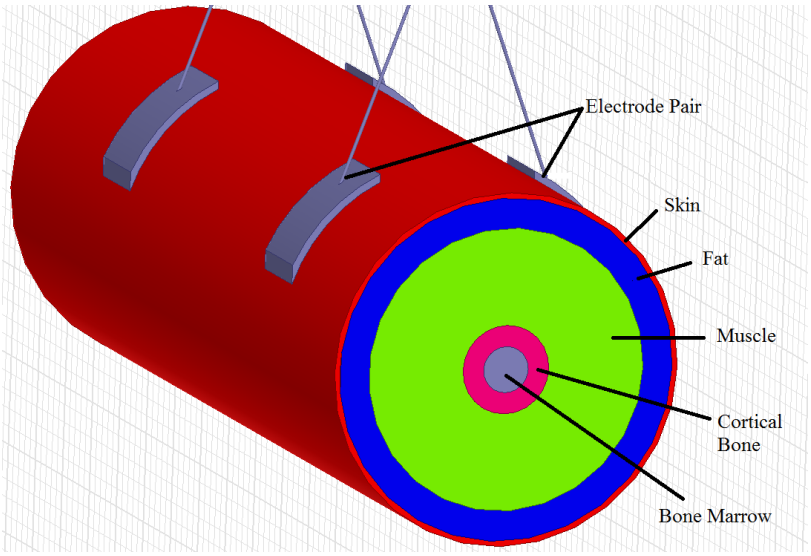

Figure 3.4: Arm model used in calculating the values of the circuit elements. The model consists of five concentric cylinders representing the main body layers; skin, fat, muscle, cortical bone and bone marrow.

Calculating these impedances in terms of the variables and parameters that represents the transmission properties of the IBC channel is a crucial step towards fully representing the IBC channel. The different circuit impedances constituting the model are calculated according to the electrical properties of the different body tissues (mainly the permittivity and conductivity), the geometrical aspects of the body organs, the electrodes' material and dimensions. To calculate the circuit impedances, an arm model is considered as shown in Figure 3.4, where the main tissue layers constituting the arm, namely; skin, fat, muscle, cortical bone and bone marrow, are represented as concentric cylinders. In order to obtain an accurate circuit model that can be sufficient for the next steps that would follow in the IBC system design-flow, more variables and channel dependent parameters need to be considered and accounted for the in the model as shown in the following sections.

3.3.1 Bio-Electrical Parameters

As explained in the previous chapter, the nature of the Electromagnetic signal propagation through the body is mainly shaped by tissue related bioelectric properties. Among the most important are the dielectric properties of the tissues, namely conductivity σ(w) and permittivity ε(w). The permittivity of a tissue is its resistivity to form an electric field through the tissue, in other words, its ability to store a unit charge under the influence of an electric field. On the other hand, the conductivity of the tissue is its ability to transport charge. Due to the heterogeneous property of the human tissue, both values of σ and ε of the tissue are frequency dependent, as shown in Figures 3.5 and 3.6. In these figures, the dielectric properties of each of the main five body tissue are plotted. These are experimental values that are reported in the literature [6-7] and are widely used as the standard values for body tissue dielectric properties. We will use these values in calculating the tissue-related impedances in our model as will be shown in the next sections.

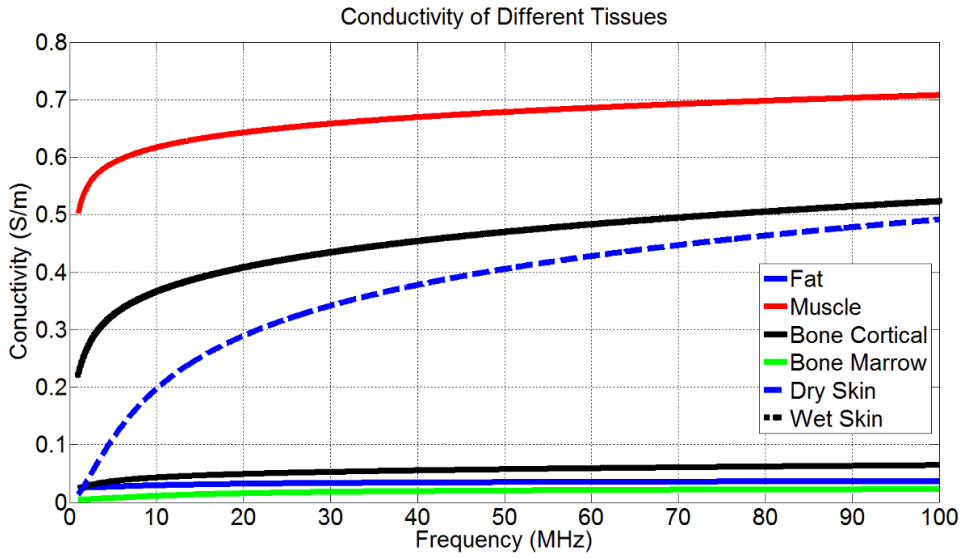

Figure 3.5. Conductivity of the main five tissues (skin, muscle, fat, cortical bone and bone marrow) using the experimental measurement values reported in [6-7].

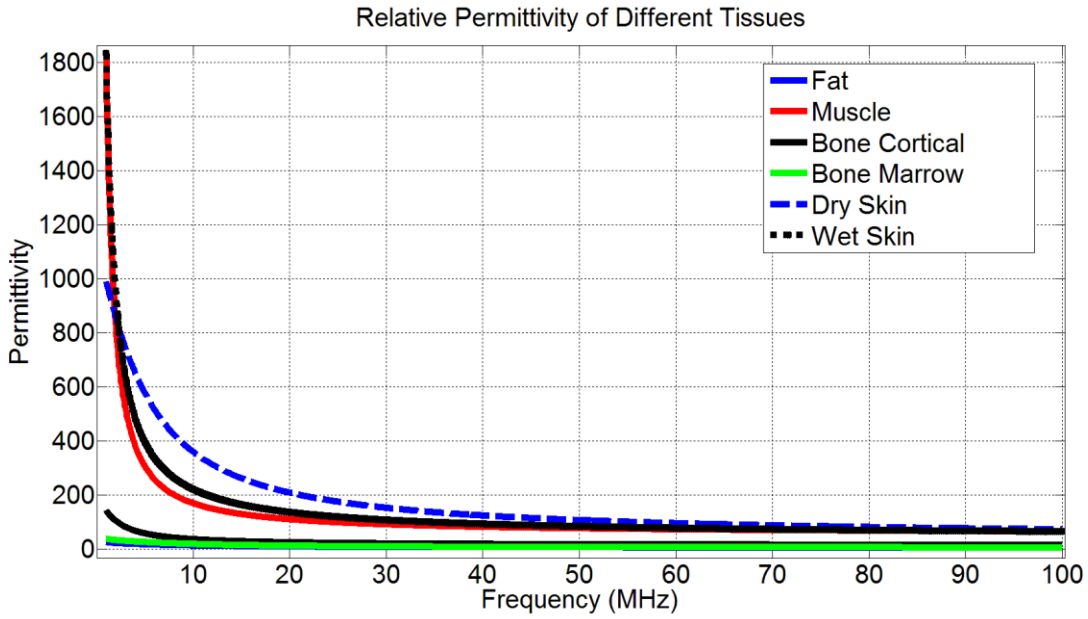

Figure 3.6. Relative permittivity of the main five tissues (skin, muscle, fat, cortical bone and bone marrow) using the experimental measurement values reported in [6-7].

3.3.2 Biological Properties

As mentioned earlier, in order to calculate the circuit impedances, an arm model is considered. as shown in Figure 3.4, where various layers are represented as concentric cylinders covering the main body tissues; skin, fat, muscle, cortical bone and bone marrow. In prior work [5], the thicknesses of the concentric cylinders were assumed to be calculated based on a constant ratio with respect to the arm radius, however, this does not capture the natural variation between individuals based on biological features such as age, weight (frame size) and gender. The model we propose assumes the layers' geometry to be variable, with values dependent on biological features. Various statistical studies were considered, relating the thickness of some of these layers to biological factors such as age, gender and weight. Curve fitting techniques were utilized to yield equations that represent such relations.

3.3.2.1 Skin

The effect of aging on the physical properties of skin was studied in [8]. The study was conducted over 39 individuals, males and females. Skin specimens were taken from two different sites on the body to represent both exposed and unexposed skin, thus including a wider range of skin properties. Findings of the study are summarized in Figure 3.7, which shows that on average women have thinner skin as compared to men. Furthermore, skin thickness reaches its peak at around 20 years of age and then steadily declines following a roughly linear progression with age. Simple curve fitting techniques were then used to render a linear approximation to describe the relation between age and skin thickness, formalized in (3.7),

$$Skin\ Thickness = \begin{cases} -0.0167882 * age + 1.9 & age \geq 20 \\ 0.04468 * age + 0.5793 & age < 20 \end{cases} \qquad (3.7)$$

where skin thickness is in mm, and age in years.

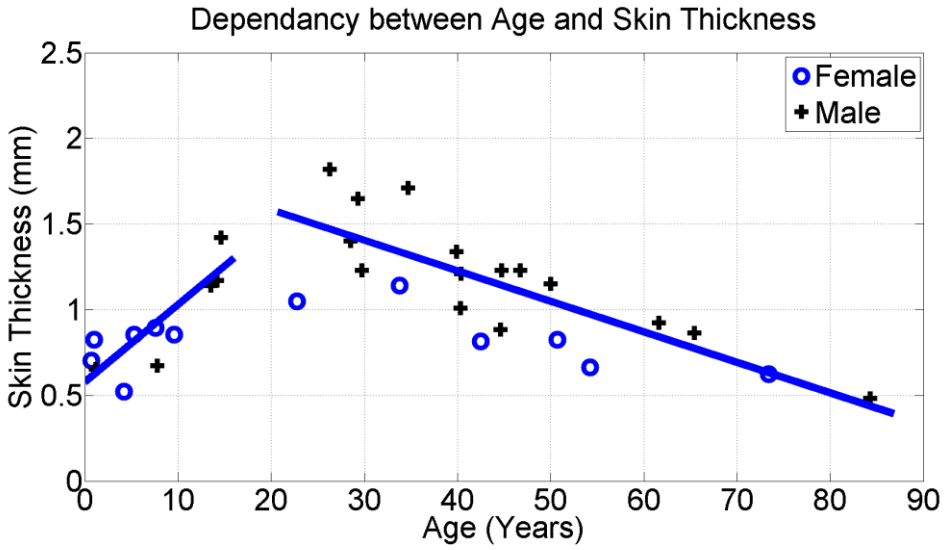

Figure 3.7: Findings from [8] where the skin thickness is plotted for different age groups. A linear approximation for the relation between age and skin thickness is proposed, represented by (3.7)

3.3.2.2 Bone

Cross sectional geometric properties of different bones with different size measures (body mass) are compared in [9]. Properties were measured across a population of 100 individuals approximately equally divided between males and females. Results of the survey are plotted in Figure 3.8, showing results pertaining only to the Humerus bone, as it is more related to the model under consideration (arm model). As discussed in the skin section, a linear approximation as expressed by (3.8) is proposed to capture the relation between the bone cross section and the body mass,

$$\ln(\text{bone cross sectional}) = 1.491 * (\ln(Body\ mass)) - 0.9358 \qquad (3.8)$$

where bone cross sectional area is in mm^2, and body mass in kg.

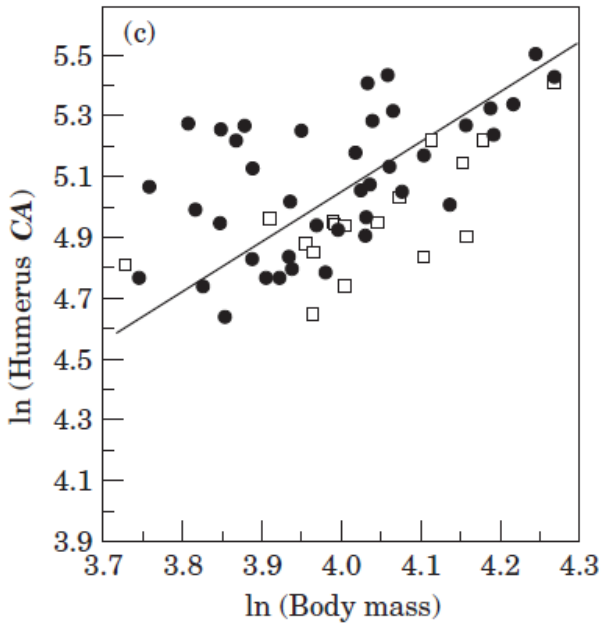

Figure 3.8: Cross sectional area of humerus bone relative to the size (body mass), results were measured on samples from New Mexico (open squares) and East Africa; Kenya and Uganda (closed circles) [9]. Linear approximation, relating both quantities, is presented in (3.8).

The thicknesses of the remaining layers are then calculated according to the arm radius, the previously proposed ratio between layer's thickness [5] and finally the recently calculated skin and bone thicknesses.

3.3.3 Geometrical Approximation

To calculate the input and output impedances of the human body (the impedance seen between each pair of electrodes), the signal path was assumed to be straight and vertical between both electrodes, as opposed to the curved cylindrical path that was assumed in [5]. Each layer is divided into smaller sectors, whose impedance is calculated according to its specific geometry (length and cross sectional area), and then assumed to be in parallel with other sectors in the

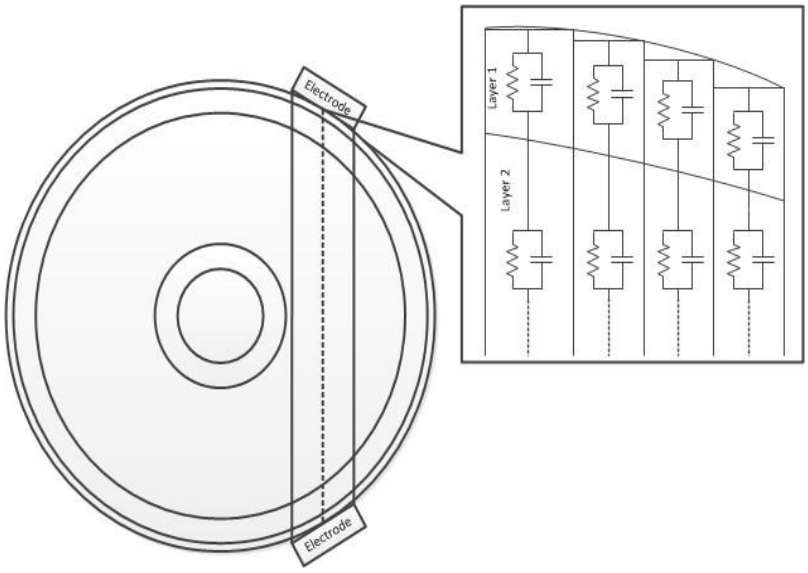

Figure 3.9: The proposed method for calculating the input and output impedances, where each layer is segmented into parallel smaller sections, each represented with a resistance and capacitance in parallel, then each layer's impedance is connected in series with the adjacent ones.

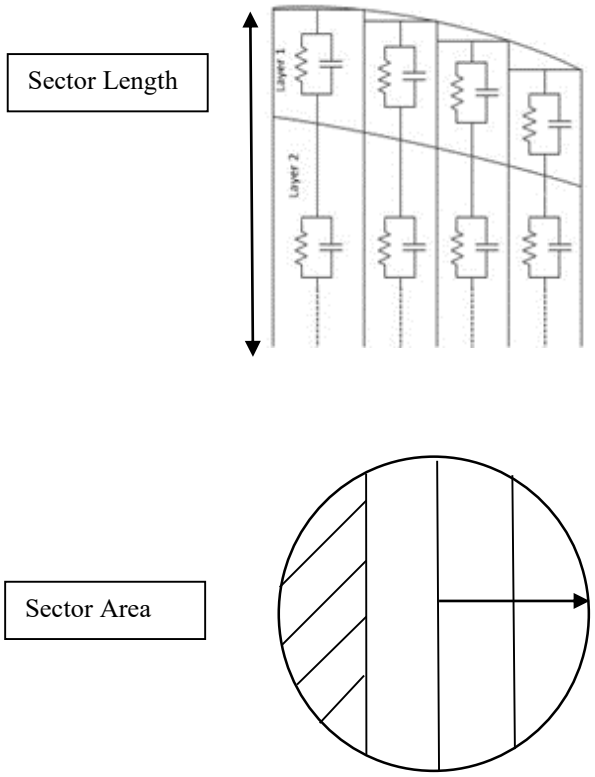

Figure 3.10: Side view (upper figure) and top view (bottom figure) for cylinder section approximation for the signal path between the two electrode of the same node, for calculating the input/output body impedance.

same layer, as shown in Figure 3.9 The total impedance is then the series summation of these impedances. To calculate the length and cross sectional area of each sector, a geometrical representation is shown in Figures 3.10, 3.11, 3.12 and 3.13. Figure 3.10 highlights an example for one of the sectors (hashed sector) that we are interested in calculating its geometrical dimensions across different layers, where both a side and a top view (view for the cylinder showing the signal path underneath the electrode, thus the circle displayed in the top view is a circle with radius equals to that of the electrode used) are displayed. To get the **area** shaded in Figure 3.10, we will use the geometrical representation shown in Figure 3.11.

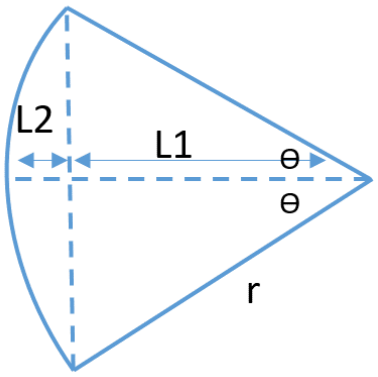

Figure 3.11: Calculating the cross sectional area for a mini-sector (seen from a top view), where r is the radius of the electrode, L1 is the distance from the center till the beginning of the sector of interest, L2 is the maximum depth for the section of interest and 2Θ is the angle enclosed by the 2 radii bounding the sector of interest.

Assuming the cylinder used to represent the path between the two electrodes is uniformly divided into n vertical sectors. Then from Figure 3.11, for the outermost sector (S1):

$$L2 = \frac{r}{n/2} \quad (3.9)$$

$$L1 = r - L2 = \frac{(\frac{n}{2}-1)r}{n/2} \quad (3.10)$$

$$\Theta = cos^{-1}(\frac{(\frac{n}{2}-1)r}{(\frac{n}{2})r}) \quad (3.11)$$

$$\text{Cross sectional area of the sector} = \pi r^2 * 2\Theta - 2 * \frac{1}{2} * \frac{(\frac{n}{2}-1)r}{\frac{n}{2}} * rsin(\Theta) \quad (3.12)$$

Where r is the radius of the electrode, L1 is the distance from the center till the beginning of the sector of interest, L2 is the maximum depth for the section of interest of the, and 2Θ is the angle enclosed by the 2 radii bounding the sector of interest. To get the area of the next sector (S2), repeat the same above steps but for the new L1 & L2, where L1 would be the distance between the center of the circle and the beginning of the new sector, and L2 would be the radius minus

this L1. The newly calculated area would be the total of both sectors (S1+S2) thus subtract the area of S1 from the calculated value to get the area of sector S2. Similarly, for sector 3 subtract the area of the previous two sectors (S1+S2) from the newly calculated area to get that of S3, and so on for the rest of the sectors.

The next step is to calculate the length of each sector (the depth of each sector of the virtual cylinder that represents the path between the two electrodes). We used the geometrical representation shown in Figure 3.12, where for a certain sector, its inner chord (L3) is determined by the angle Θ_1 and the outer chord (L4) is determined by Θ_2, where L3 and L4 can be calculated as follows:

$$\Theta_1 = \frac{Electrode\ Spacing + 4*r}{Arm\ radius} \quad (3.13)$$

$$L_3 = 2 * Arm\ Radius * \sin(\frac{\Theta_1}{2}) \quad (3.14)$$

$$\Theta_2 = \frac{Electrode\ Spacing}{Arm\ radius} \quad (3.15)$$

$$L_4 = 2 * Arm\ Radius * \sin(\frac{\Theta_2}{2}) \quad (3.16)$$

Where r is the radius of the electrode. Through getting the outer and inner length for each sector, the thickness of each layer enclosed by each sector is then determined and the impedance per unit sector is finally calculated, as represented in Figure 3.10, where for each sector in a certain layer l,

$$Y_l = \frac{1}{R_l} + jwC_l = \frac{\sigma_{lf} S_l}{L_l} + \frac{jw\epsilon_O \epsilon_{rlf} S_l}{L_l} \quad (3.17)$$

Where Y_l is the admittance of this unit sector, R_l is the parallel resistance, C_l is the parallel capacitance, w is the angular frequency, L is the length of the signal transmission path (length

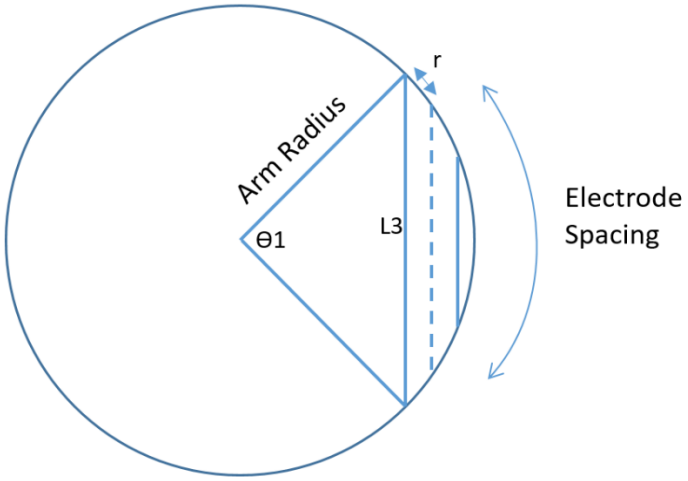

(a)

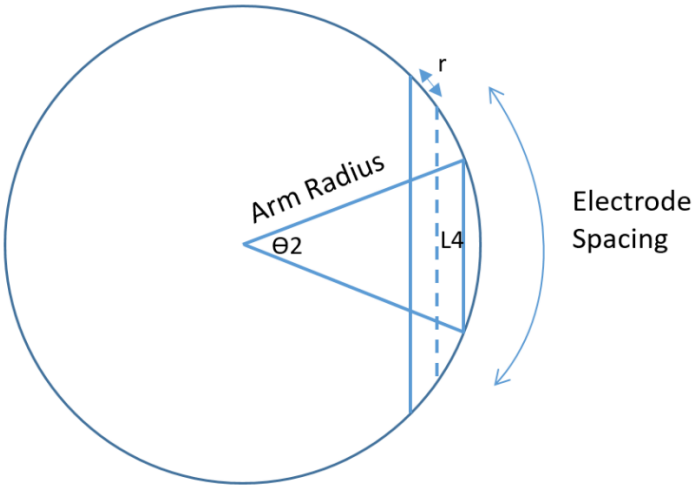

(b)

Figure 3.12: Calculating the length of each sector where in (a) the inner dimension is calculated and in (b) the outer dimension is determined.

of layer l in this sector), S_l is the cross sectional area of the sector, σ_{lf} and ϵ_{rlf} are the conductivity and relative permittivity corresponding to layer l at frequency f and ϵ_O is the permittivity of free space.

The cross impedances ($Zb1$ and $Zb2$) from Figure 3.3, representing the portion of the signal that flows from I_1 to O_2 as well as that from I_2 to O_1, were previously calculated from a circuit perspective as being the summation of the transverse impedance (Zt) and the input/output impedance (Zi /$Zout$) [5]. However, in the proposed model, we calculated the cross impedance based on a physical approach; following the same path as the transverse impedance but with a slightly longer signal path. The transverse impedance (Z_t) is calculated as follows:

$$Z_t = \frac{1}{\sum_l \frac{1}{Z_l}} = \frac{1}{\sum_l \left(\frac{1}{R_l} + jwC_l\right)} \qquad (3.18)$$

$$= \frac{L}{\sum_l (\sigma_{lf} S_l + jw\epsilon_O \epsilon_{rlf} S_l)} \ \Omega \qquad (3.19)$$

where Z_l is the impedance of the layer l, L is the length of the signal transmission path (between I_1 and O_1), S_l is the cross sectional area of layer l, w is the frequency, σ_{lf} and ϵ_{rlf} are the conductivity and relative permittivity corresponding to layer l at frequency f and ϵ_O is the permittivity of free space.

The path proposed to calculate $Zb1$ (from electrode I_1 to electrode O_2) is explained by (3.19-3.21), as represented in Figure 3.13

$$(I_1O_2)^2 = (I_1I_2)^2 + (I_2O_2)^2 \qquad (3.20)$$

$$I_1I_2 = Arm\ radius * \theta_{tx} \qquad (3.21)$$

$$I_2O_2 = L \qquad (3.22)$$

I_1I_2 is the distance between the two electrodes of the transmitter, I_2O_2 is the separation between the transmitter and the receiver electrode pairs and θ_{tx} is the angle between the transmitter electrode pair. Similar equations can be used for $Zb2$.

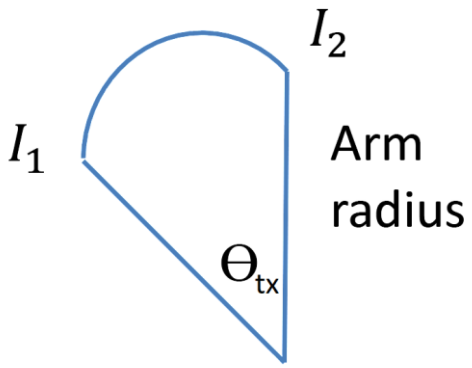

Figure 3.13: Geometry used in calculating the signal path between I_1, and O_2, showing the arm radius and the angle between each electrode pair (θ_{tx}).

Finally, to calculate the contact impedance Z_C, experimental values were measured for different electrodes at 100 KHz and 1 MHz in [4]. This set of data was used for parameter fitting where a linear relation was assumed for calculating the contact impedance parameters (R and C) in terms of frequency.

3.4 Simulation results

The gain profile, computed according to the circuit model described in this chapter, was then plotted as shown in Figure 3.14 Gain is plotted for three different body frames; 50, 70 and 90 kg. It can be observed that the gain increases sharply with the increase in frequency till it reaches the peak at 10.5 MHz, after which the gain decays slowly with frequency. Simulation results also showed that as the body frame (mass) increases, the gain of the channel decreases. Results are then compared with those using the conventional circuit model [5], where the layer thicknesses were assumed constant, and the input /output impedances, as well as, the cross impedances are calculated through the traditional method, as explained earlier. To validate our model, results are compared against experimental trials reported in [10], and plotted in Figure 3.15, where gain for transmission through air is compared to that through the body, showing much better performance

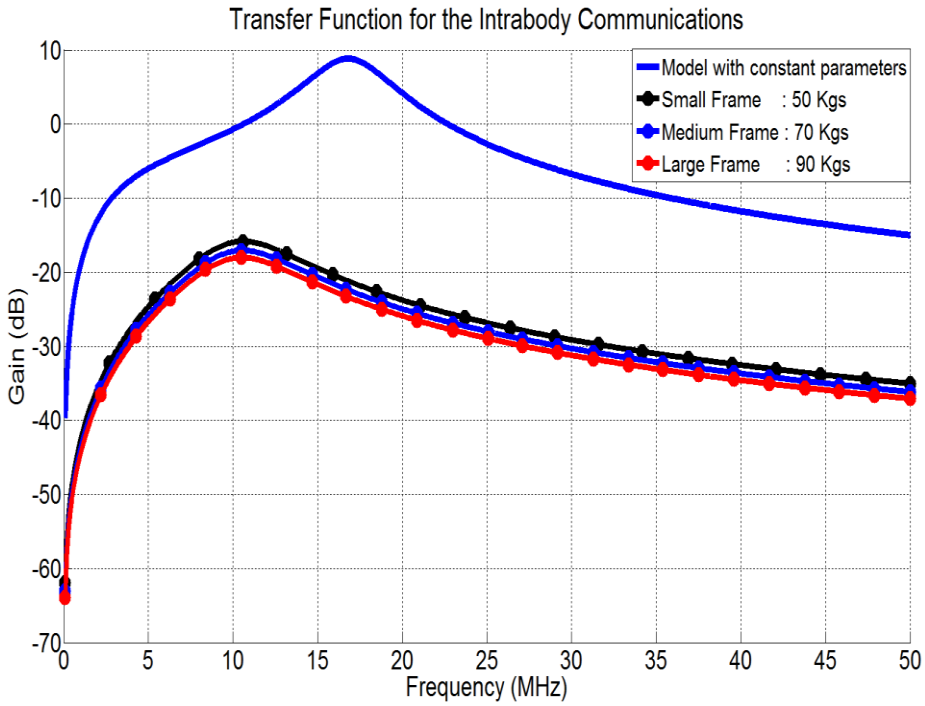

Figure. 3.14: Simulation results, where the Gain in dB is plotted from 100 KHz till 50 MHz, are plotted for three different body frames; small, medium and large. The results from our model are compared to those obtained from circuit model in which the biological parameters are assumed to be constant. The proposed model succeeds in determining the optimum frequency as well (10.5 MHz).

in favor of intra-body communications for frequencies up to 35 MHz. Experimental results show that the frequency at which gain was found to be maximum is around 10.7 MHz, which is very close to what our model predicted, with a percentage error much less than that in case of adopting traditional techniques to calculate the model parameters. Figure 3.16 presents the impact of aging versus the channel profile. Results show that as the age increases, the channel gain also increases (assuming constant mass), which is due mainly to the decrease in skin thickness.

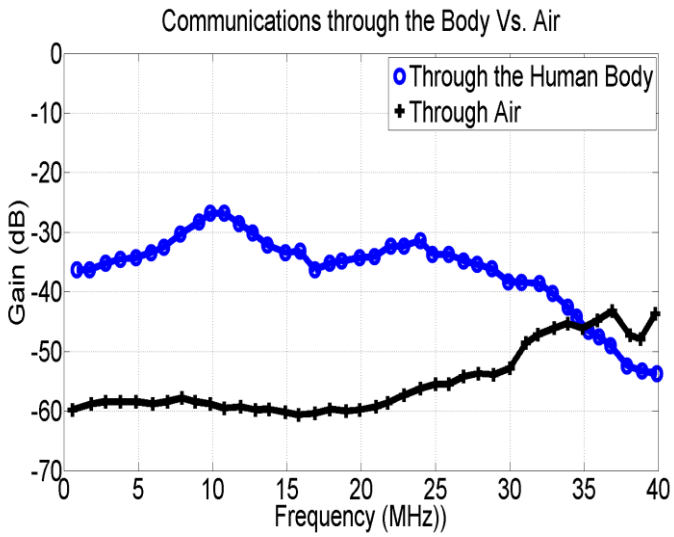

Figure 3.15: Experimental results from [11], showing good match with results from our proposed model.

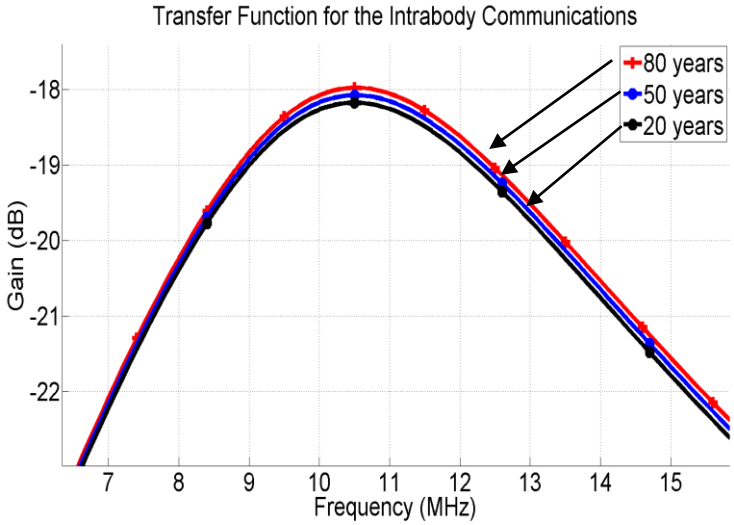

Figure. 3.16: Simulation results, showing the channel sensitivity to the individual's age, where gain is plotted for three different age groups; 20, 50 and 80 years old.

3.5 Finite Element Method

As mentioned in earlier, there are other methods used for modeling the path loss through the galvanic IBC channel. In this section, we will use the Finite Element Method (FEM) for modeling the gain/attenuation profile for galvanic IBC channels. Finite element method are common methods for the analysis of the human body channel, yet they are sometimes being avoided due to the lengthy simulation time resulting from the complex geometry and interconnections of the human body [2]. We carried out FEM simulation on a reduced order human model with focus on the human arm. An arm model is then designed with simple constructed details yet capable to capture essential electrical properties. A comparative study of the two approaches is presented and the channel gain profile plotted. We vary the complexity of the model and investigate the effect of that on the simulation results. ANSYS Electronics Desktop was used for accurate full wave electromagnetic simulation to find an estimation of the human channel path loss. The tool can solve for Electro-Magnetic (EM) fields every tetrahedron of the 3D meshed structure of the arm model for the transmitting and receiving electrodes. Finally, results are compared with those obtained from the circuit model.

3.5.1 FEM Models

Simple Arm Mode: A simplified 3D model of an arm model has been constructed, as show in Figure 3.17, through constructing five concentric cylinders representing the five main tissue layers; skin, fat, muscle, bone marrow and cortical bone. The dimensions of the cylinders mimic the average total thickness of the arm related to each tissue thickness [4]. The dielectric properties, which are described in terms of conductivity $\boldsymbol{\sigma}$ and relative permittivity $\boldsymbol{\epsilon}$, are the same as the experimental values used earlier [6-7].

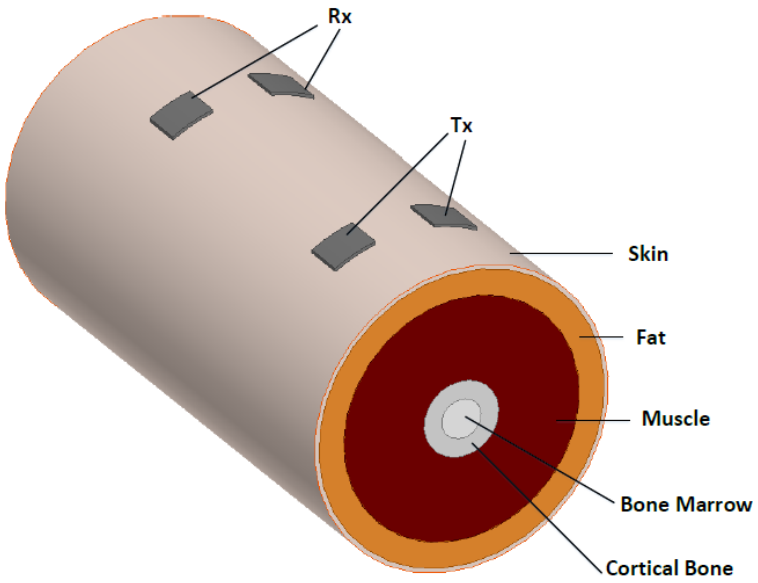

Figure. 3.17: Simple 3D arm model consisting of five concentric cylinders representing the five main tissue layers.

Full Body Model: The full FEM model was based on the model created by NEVA Electromagnetic group which was subsequently imported on ANSYS HFSS environment as shown in Figure 3.18 [11]. In addition to the five main layers of human body, blood streams or veins are included in the design of the arm model. Moreover, the detailed geometry of the internal and external structure of the imported model mimics the proportions, dimensions and geometry of an averaged human arm.

Although the detailed model results in higher accuracy, the simulation time is much longer than the required time in case of the concentric cylinders. Furthermore, in addition to the arm, the imported model includes over 25 tissues of other organs and human parts that complicate the meshing procedure of the targeted simulation by adding a high number of meshing elements to the simulation.

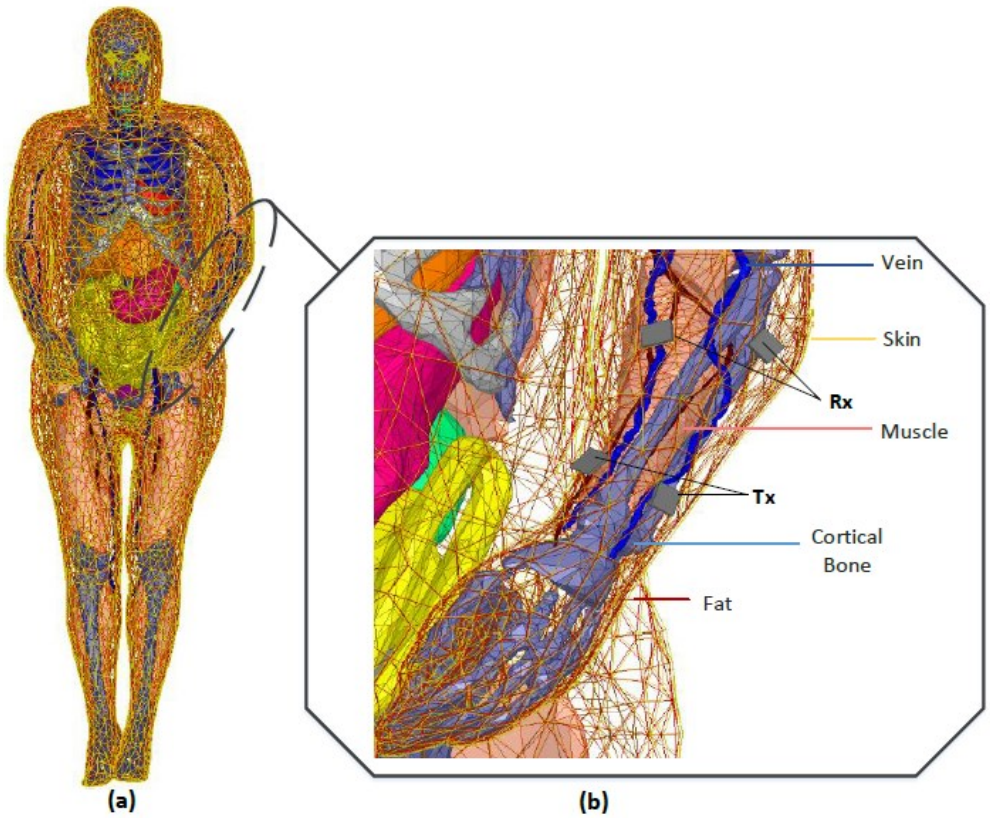

Figure 3.18: The full human model including with detailed geometry and anatomy where (a) is the human body and (b) is the human arm where the transmitter and receiver nodes are placed for the sake of comparison.

3.5.2 FEM Simulations

The transmitting and receiving electrodes dimensions of both models were 15x15 mm. Copper is used as the electrodes material. The transmission path length is 10 cm. The excitation of transmitting side is set to a lumped port which allows us to embed internal ports of excitation with an input impedance of 50 **Ω**. The current source of the exciting ports is set to 1 mA which conforms to the safety standards of the International Commission on non-ionizing radiation protection (ICNIRP) by controlling the power of exciting source [12]. Results between both FEM models are plotted in Figure 3.19. As shown in the figure, in spite of the simplicity of the concentric cylinders' 3D arm model, yet it is still accurate enough compared to the full body

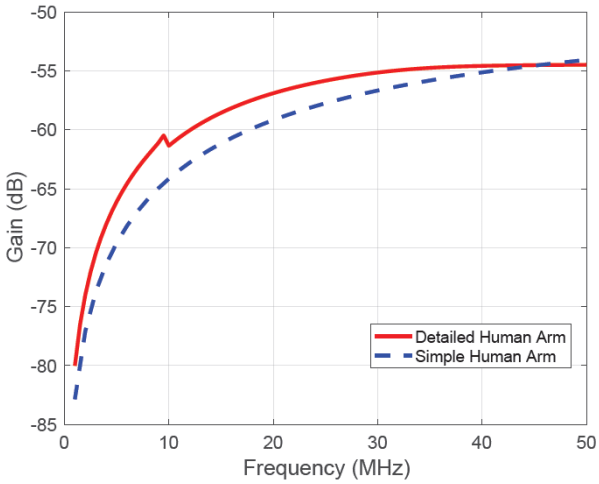

Figure 3.19: Simulation results of transmission gain including the full-order human arm model, solid line, and the concentric cylinders representing the human arm, dashed line.

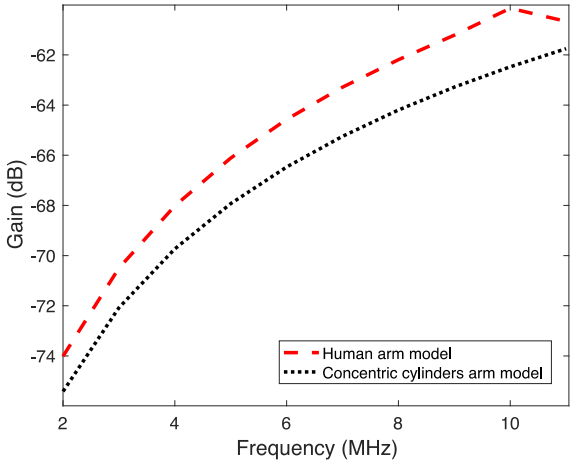

Figure 3.20: Simulation results of the gain profile for the two FEM models at low frequencies (<10 MHz)

model provided from NEVA. For low frequency IBC applications (<10 MHZ) we plotted the results in Figure 3.20, showing how still the accuracy of both models are still very close.

3.5.3 Current Density Distribution

One advantage for FEM simulations over circuit models is the ability to fully and accurately simulate and visualize the different fields and currents distributions in different layers, mediums

and spaces. In the galvanic coupling approach, the coupled electromagnetic signal exhibit dipole type field behavior [13]. This field can be represented in terms of current density vectors to show current paths along multiple tissues. Current paths are mainly composed of a primary path that flows between the transmitting electrodes and secondary path the results in potential difference between the receiving electrodes. The source electrode current exciting the primary and secondary flows is as follows

$$I = \iint_s J.ds = \iint_s \sigma.E.ds \qquad (3.23)$$

Where J (A/m^2)is the current density, s is the surface area of the transmitter electrode and E is the normal electric field intensity component between the contact area of the transmitting electrodes and the skin tissue. Current density distribution within the five main human layers is affected by the relative permittivity and conductivity of these tissues. The skin layer has higher σ than fat tissue. Due to this fact, current density distribution values in skin is higher than observed values in fat, which can be observed in Figures 3.21 and 3.22. Moreover, we can notice that the values of J along the muscle tissue are higher than along the fat layer, as shown in Figure 3.23. The conductivity of muscle tissue, which is the highest compared to the other layers, is the reason behind this observation as the primary current of coupled signal penetrates through the fat tissue located under the transmitter electrodes and easily transmitted along the muscle tissue. Finally, the current distribution has been plotted along bone marrow tissue to verify the impact of its low conductivity property as shown in Figure 3.24.

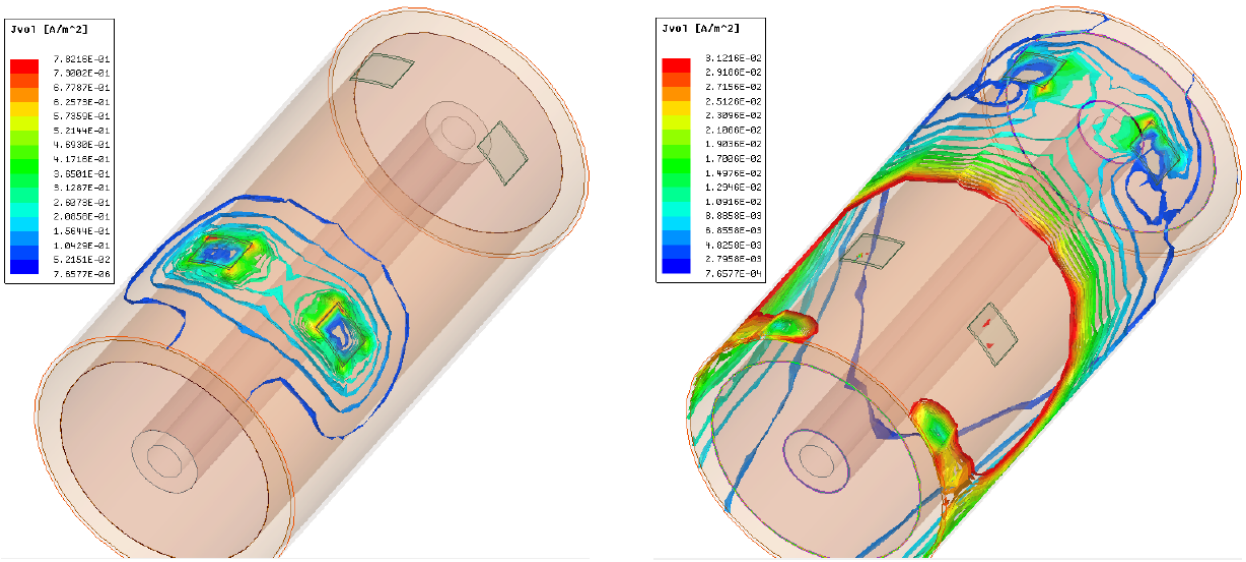

(a) Primary current distribution (b) Secondary current distribution

Figure 3.21: Skin tissue's current density distribution.

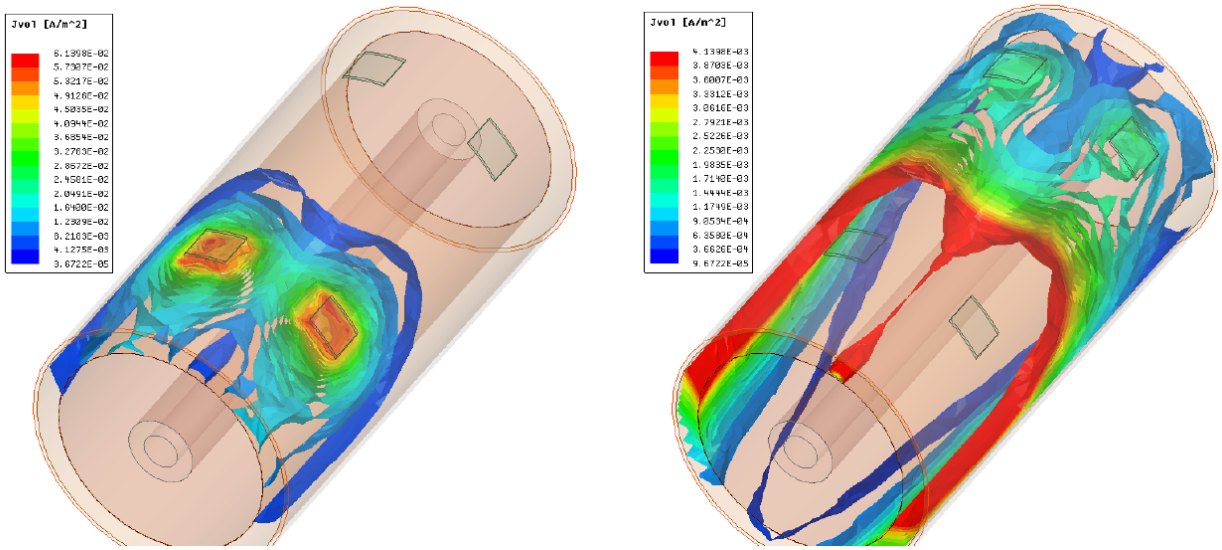

(a) Primary current distribution (b) Secondary current distribution

Figure 3.22: Fat tissue's current density distribution.

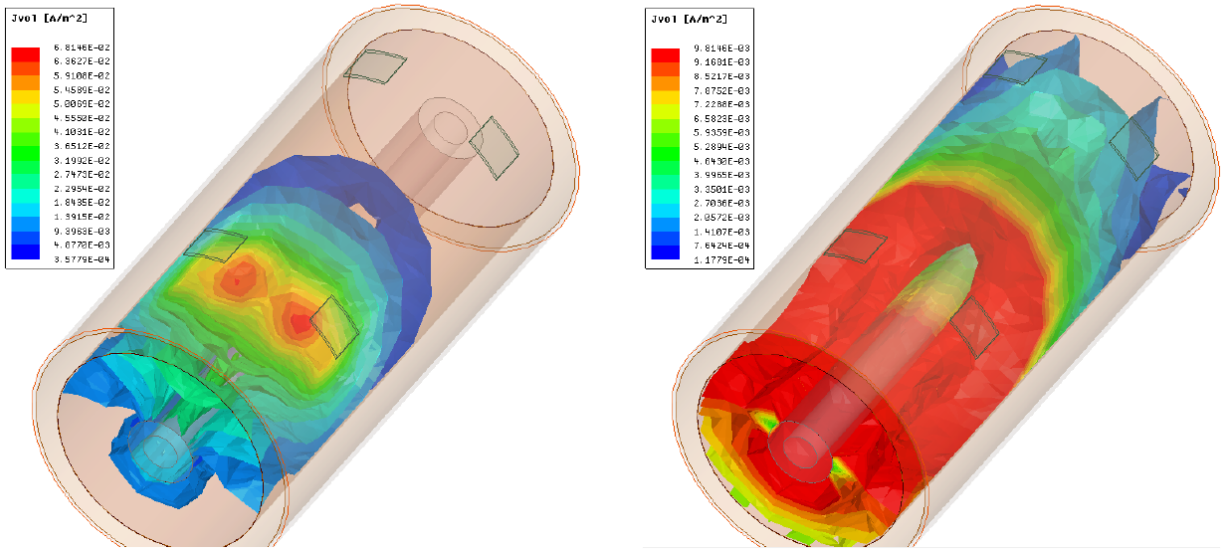

(a) Primary current distribution (b) Secondary current distribution

Figure 3.23: Muscle tissue's current density distribution.

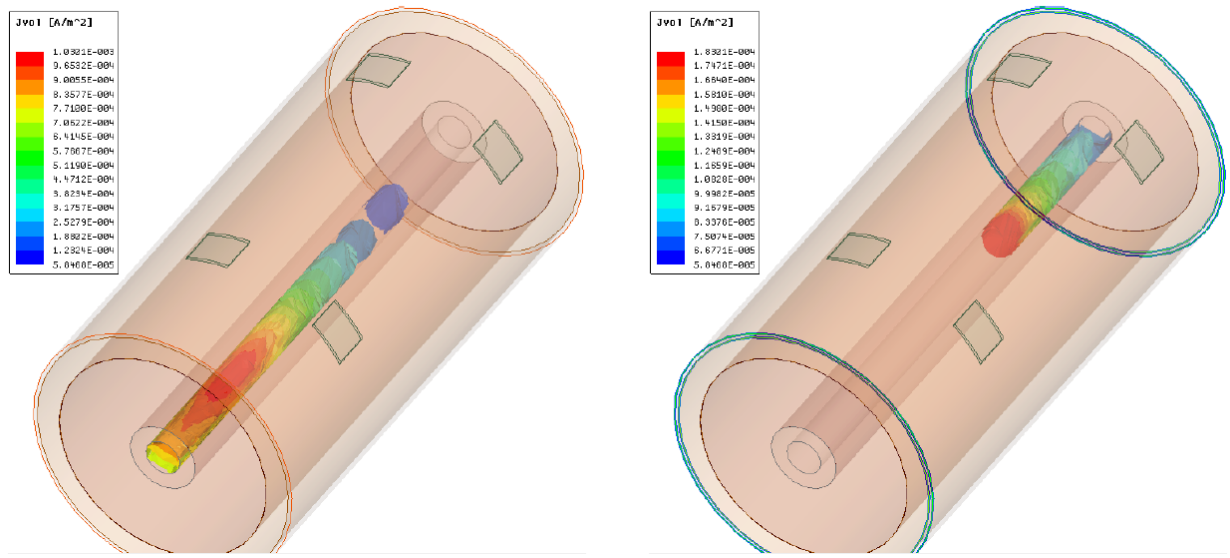

(a) Primary current distribution (b) Secondary current distribution

Figure 3.24: Bone Marrow tissue's current density distribution.

3.5.4 FEM Models & the Circuit Model

Next step is comparing the results we obtained, for the transmission gain, from the FEM simulations with those obtained from the circuit model ones. With using the appropriate correction factor, results are shown in Figure 3.25 for low frequency IBC applications. To examine the whole frequency range where IBC technologies have high potential, we plotted the results over an extended range (100 KHz till 100 MHz) between the FEM model results (the full body model) and the simplified circuit model, as shown in Figure 3.26. It is clear now how, in spite of its simplicity, the circuit model with all the different biological and electrical parameters taken into consideration, is accurate enough compared with a much complicated 3D FEM model. However, the circuit model possesses one extra advantage due to its simplicity, which is being much faster to simulate and get accurate results.

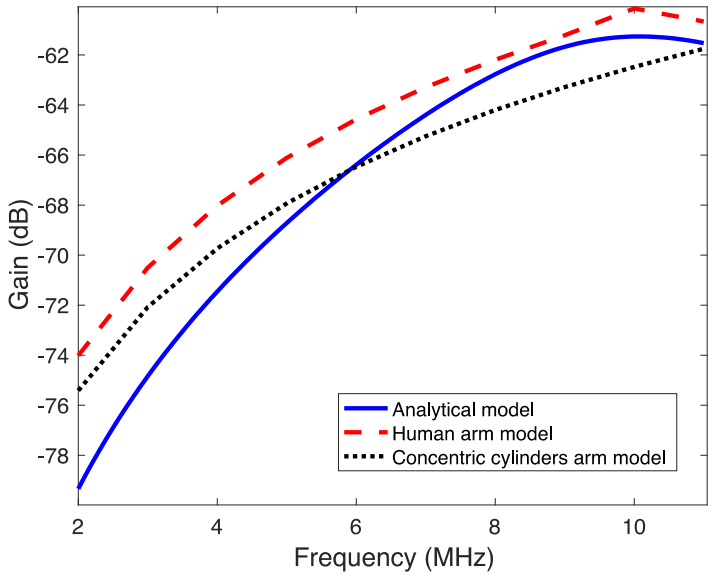

Figure 3.25: Simulation results for the circuit (analytical) model, the full body model and the concentric cylinders' arm model, for low frequency IBC applications (<10 MHz), showing a good match between all results.

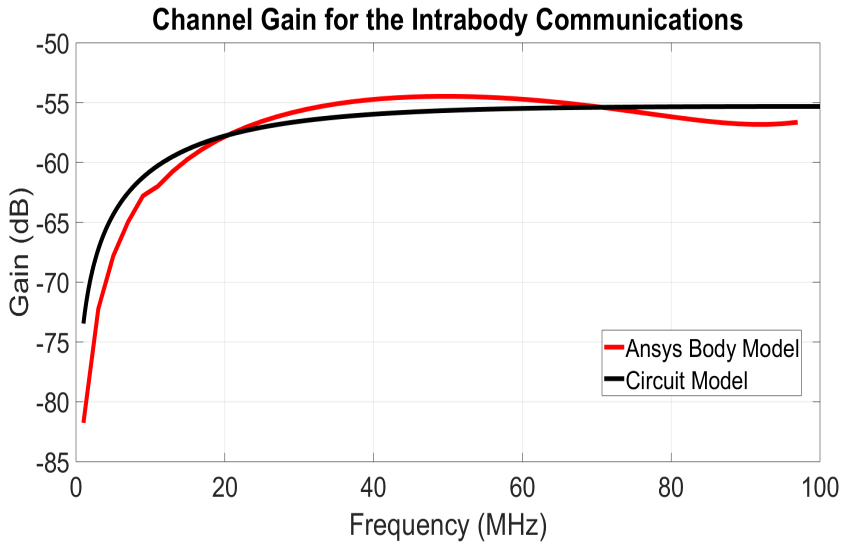

Figure. 3.26: Comparison between the gain profile for the galvanic IBC channel calculated once through the circuit model then using the FEM mode over an extended range of frequencies (100 KHz till 100 MHz) , showing how accurate the circuit model is.

For comparison, the simulations have been executed on a common computing setup. Simulations were performed using a quad core processor running at 2.3 GHz with 8 GB of RAM. Simulation time is calculated in terms of CPU time required to complete each simulation. Table 3.1 summarizes the estimated CPU time for each model simulation Clearly, the total CPU time of the detailed human arm FEM simulation is more than **48 times** the estimated time in case of the simplified circuit model.

Table 3.1: CPU time of the Circuit model, the arm of the full body model and the 3D concentric cylinders' arm model.

Model	**CPU time (hh:mm:ss)**
Circuit Model	(00:00:1.77)
FEM of cylindrical arm	(00:02:34)
FEM of human arm	(01:34:07)

3.6 Galvanic IBC Channel's Sensitivity to System Parameters

Having identified the main blocks for the galvanic IBC system model, and proven how accurate our channel circuit model is, in this section we will study and summarize the sensitivity of the galvanic IBC channel to the electrical, geometrical and biological parameters of the system, through observing the channel gain/attenuation profile using the circuit model over the extended frequency range of interest for IBC; 100 KHz to 100 MHz, to provide the system designers with the basic guidelines and tradeoffs that they need to be aware of when designing an efficient IBC system. We will study the sensitivity of the system to the remaining biological/electrical aspects of the communication channel; the body, that were not considered earlier then will consider the impact of the system design parameters; properties of the transmitter (TX) and receiver (RX) nodes. Effect of the electrodes will be discussed in more details in the next chapter.

3.6.1 Tissue's Electrical Properties

In the previous chapter, it was shown that electromagnetic waves possess better properties, that can support BAN requirements, versus ultrasonic waves as EM waves experience much less attenuation and delay when traveling through the body which is crucial for system designers. The basic human tissues' properties of concern are those of the complex dielectric properties; namely the permittivity and the conductivity. The first sensitivity analysis test performed was then on how the variation in these electrical properties would affect the IBC channel characteristics (gain). We studied the effect of varying the properties of each tissue solely in a range between -20 % to 20% of the average nominal values [6-7], and results are plotted in for skin and muscles in Figures 3.27 and 3.28. The error was also calculated (the deviation of the IBC channel gain from the nominal value) and summarized in Table 3.2, where the maximum error percentage is

Table 3.2. Maximum error percentages for the deviation in the IBC channel gain when varying the Electrical properties of the Tissues

Tissue	Conductivity				Permittivity			
	-20%	*-10%*	*10%*	*20%*	*-20%*	*-10%*	*10%*	*20%*
Skin	0.1013%	0.05008%	0.04923%	0.09785%	0.04311%	0.02162%	0.02162%	0.04311%
Fat	0.5278%	0.259%	0.2497%	0.4906%	0.03%	0.01506%	0.01525%	0.03069%
Muscle	2.194%	1.053%	0.9776%	1.891%	0.1624%	0.08082%	0.08011%	0.1595%
Cortical Bone	0.004617%	0.002302%	0.002302%	0.004617%	0.001275%	0.000637%	0.000637%	0.001275%
Bone Marrow	0.0014%	0.000697%	0.000697%	0.0014%	0.000524%	0.000262%	0.000262%	0.000524%

reported for each case. As can be shown, the IBC channel characteristics are much more sensitive to the conductivity of the tissues over the permittivity, since the conductivity mainly accounts for the signal transmission capability through a certain medium. From a tissue perspective, muscle, skin and fat layers tend to affect the characteristics of the IBC channel more than cortical bone and bone marrow, this is due to: a) the better conductive properties of the first three tissues, b) the fact that only a tiny portion of the signal will travel through the bones (since most of the signal is transmitted through the skin, then muscles.

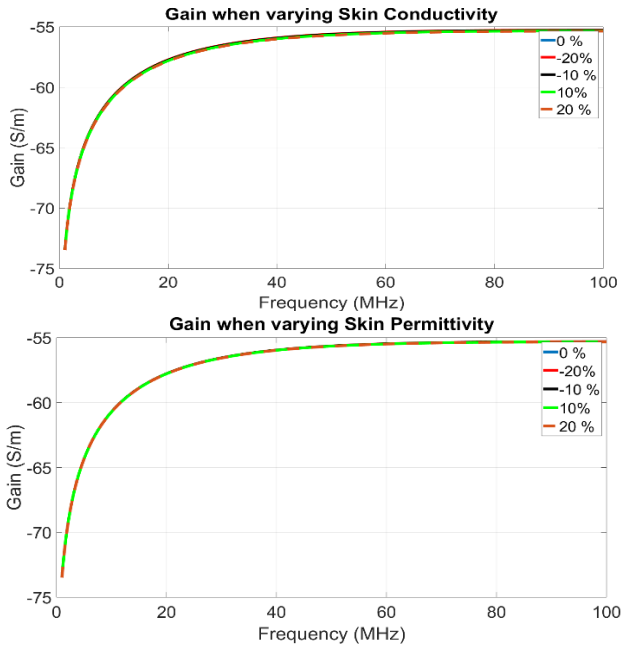

Figure 3.27: The variation in the IBC channel gain profile, when varying the conductivity and permittivity of skin tissue, within the range -20% to 20% from the nominal measured values [6-7].

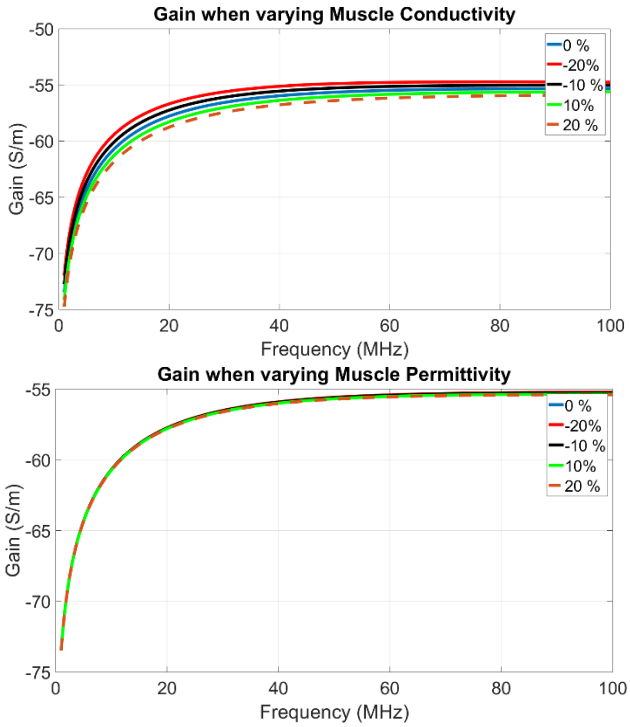

Figure 3.28: The variation in the IBC channel gain profile, when varying the conductivity and permittivity of the muscle tissue, within the range -20% to 20% from the nominal measured values [6-7].

3.6.2 Transmitter and Receiver Impedances

The final blocks in the IBC system are the transmitter and the receiver nodes. Since the channel characteristics are mostly affected by the relation between the impedances of the basic blocks of the system; an impedance matching issue for maximum power transfer between the electronics system and the body and vice versa, we will investigate the impact of the TX output impedance and the RX input impedance on the IBC channel. In Figure 3.29, we vary the magnitude of the RX input impedance between 100, 1K, 10 K, 100 K and 1M Ohms, and observe the channel gain. As expected, the gain of the channel improves as the RX input impedance value increases, as more signal power is delivered to the receiver node. However, after reaching a certain value (~10K in this case) the gain saturates, since the RX input resistance becomes much larger than

the system impedance, thus most of the power is transferred from the system (body and electrodes) to the RX anyway. On the TX side, the TX output impedance is our concern, since it partially determines the portion of the power that will be delivered from the source to the system. While 50 Ohms would be the nominal value that most devices/circuits try to design according to, for matching purposes, we included other values;10, 100, 500, 1K, 2K, 5K and 10K Ohms to study its impact on the gain of the channel, as shown in Figure 3.30. Clearly the gain improves as the value of the resistance drops, as less power is lost in the TX node; more transmitted to the system.

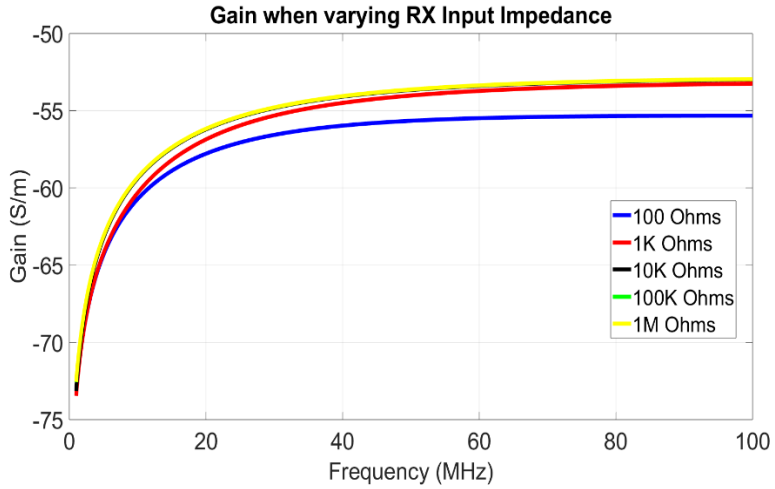

Figure 3.29: Gain when varying the value of the RX input impedance; 100, 1K, 10 K, 100 K and 1M Ohms.

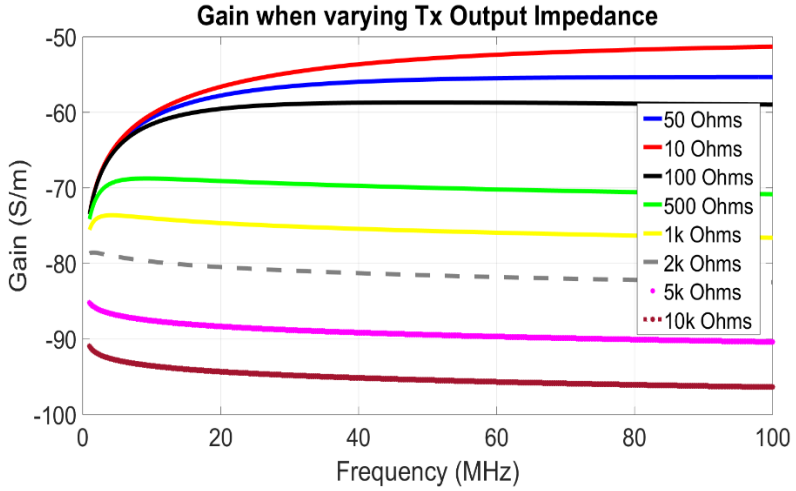

Figure 3.30: Gain when varying the value of the TX output resistance; 10, 100, 500, 1K, 2K, 5K and 10K Ohms.

3.7 Conclusion

In this chapter we presented a novel approach in modeling the human body as a communication channel for galvanic intra-body communications. A simple circuit model was adopted, where the different impedances in the model represents the whole system, starting with the output impedance of the transmitter, the contact impedances of the electrode, the body impedances representing the channel path and finally the input impedance of the receiver. The main novelty of this paper is in calculating the body impedances, so that it accurately models the features of the human body both physically (through the electrical properties of the tissues) and geometrically. Statistical studies were adopted to relate such geometrical aspects to practical parameters; namely age and body frame. More accurate approaches were also proposed in identifying the signal path through the body, thus imposing changes on the way some circuit elements are calculated. To validate the proposed model, results were compared with prior published experimental results, showing that the proposed model is able to capture the channel profile while accounting for variations due to difference between individuals. Sensitivity profile of the channel to age and body frame were also investigated, where gain was plotted for different values covering a reasonable range in which these two parameters are expected to change. We then compared the results with those obtained from simulation results using FEM on two different models; on the arm of a full body model and on a five concentric cylinder's arm model. The circuit model's accuracy proven to be very close to that of the FEM models over an extended frequency range (100 KHz till 100 MHz), yet with a much faster time execute, proving that it is the adequate model to be adopted in the later phases in the IBC system design flow. Finally, we used the corrected circuit model to study the sensitivity of the IBC channel to the system parameters. Findings in this chapter are published in [14-15].

References

[1] Thoams Guthrie Zimmerman. Personal area networks: near-field intrabody communication. IBM systems Journal, 35(3.4):609-617, 1996.

[2] Keisuke Hachisuka, Yusuke Terauchi, Yoshinori Kishi, Ken Sasaki, Terunao Hirota, Hiroshi Hosaka, Katsuyuki Fujii, Masaharu Takahashi, and Koichi Ito. Simplified circuit modeling and fabrication of intrabody communication devices. Sensors and actuators A: physical, 130:322 330, 2006.

[3] K. Fujii, M. Takahashi, and K. Ito, "Electric field distributions of wearable devices using the human body as a transmission channel," *IEEE Trans. Antennas Propag.,* vol. 55, no. 7, pp. 2080–2087, Jul. 2007.

[4] Marc Simon Wegmueller, Andreas Kuhn, Juerg Froehlich, Michael Oberle, Norbert Felber, Niels Kuster, and Wolfgang Fichtner. An attempt to model the human body as a communication channel. IEEE transactions on Biomedical Engineering, 54(10):1851-1857, 2007.

[5] Yong Song, Qun Hao, Kai Zhang, Ming Wang, Yifang Chu, and Bangzhi Kang. The simulation method of the galvanic coupling intrabody communication with different signal transmission paths. IEEE Transactions on Instrumentation and Measurement, 60(4):1257-1266, 2011.

[6] S. Gabriely, R. W. Lau, and C. Gabriel. The dielectric properties of biological tissues: II. Measurements in the frequency range 10 Hz to 20 GHz . Phys. Med. Biol., vol. 41, no. 11, pp. 2251–2269, Nov. 1996.

[7] S. Gabriely, R. W. Lau, and C. Gabriel, "The dielectric properties of biological tissues: III. Parametric models for the dielectric spectrum of tissues," Phys. Med. Biol., vol. 41, no. 11, pp. 2271–2293, Nov. 1996.

[8] Lee MMC, Physical and structural age changes in human skin. Anat Res 129:473-493, 1957

[9] Christopher B. Ruff, Body size, body shape, and long bone strength in modern humans,1999

[10] Keisuke Hachisuka, Teruhito Takeda, Yusuke Terauchi, Ken Sasaki, Hiroshi Hosaka, and Kiyoshi Itao. Intra-body data transmission for the personal area network. Microsystem Technologies, 11(8-10):1020-1027, 2005.

[11] NEVA Electromagnetics. https://www.nevaelectromagnetics.com/, 2009 (Accessed:2017- 09- 08).

[12] A Ahlbom, U Bergqvist, JH Bernhardt, JP Cesarini, M Grandolfo, M Hietanen, AF Mckinlay, MH Repacholi, David H Sliney, J Stolwijk, et al. Guidelines for limiting exposure to time-varying electric, magnetic, and electromagnetic fields (up to 300 GHz). Health physics, 74(4):494-521, 1998.

[13] Behailu Kibret, MirHojjat Seyedi, Daniel TH Lai, and Micheal Faulkner. Investigation of galvanic-coupled intrabody communication using the human body circuit model. IEEE journal of biomedical and health informatics, 18(4):1196-1206, 2014.

[14] Khorshid, Ahmed E., Ahmed M. Eltawil, and Fadi Kurdahi. Intra-body communication model based on variable biological parameters. In *2015 49th Asilomar Conference on Signals, Systems and Computers*, pp. 948-951. IEEE, 2015.

[15] Alquaydheb, Ibrahim N., Ahmed E. Khorshid, and Ahmed M. Eltawil. "Analysis and Estimation of Intra-body Communications Path Loss for Galvanic Coupling." In *Advances in Body Area Networks I*, pp. 267-277. Springer, Cham, 2019.

Chapter 4

Electrode Modeling

4.1 Introduction

A basic block in Intra-body communication systems is the electrode used. Electrodes are the main interface between the circuits/systems blocks and the human body (the channel), responsible for coupling the signal into the body at the transmitter side and picking it up at the receiver one. Accordingly, accurate modeling of the electrode impedance is crucial for IBC system performance estimation. In the previous chapter, we used values from experimental measurements to represent the contact impedance, yet that limits our modeling generality to the scenarios tested only. In this chapter, we present different approaches for modeling the electrode and electrode-body contact impedances. Each approach is thoroughly investigated and the channel model and overall gain characteristics for each case are presented. Different physical factors (material, size, spacing ...etc.) are also taken into consideration to study their impact on the overall attenuation profile. Finally, a study of the relation between the different impedances constituting the channel model, how electrode parameters affect them, how they change with respect to each other, and their role in shaping the final channel gain characteristics.

4.2 Electrode Impedance Modeling

A basic element in the human body communication channel is the electrode used at both the transmitter and the receiver sides. Modeling the electrode and electrode-body compact impedance has a significant impact on the overall channel model. Parameters as the electrode

size, material, shape, width, thickness …etc. should all be taken into account. Other factors that further determine the value of the electrode-contact impedance include the operating frequency, spacing between each of the electrode pairs (ex: separation between the two electrodes of the transmitter), location of the electrodes on the human body and finally the transmitted power level (operating voltage and induced current). Providing an accurate impedance model that would take in as many from the above-mentioned factors as possible is a complicated task. Several approaches had been considered for accurately modeling the electrode contact impedances. One approach is through measuring the impedance of the electrodes experimentally, as followed in [1], where the impedance measurement for different materials and different electrode areas, as well as different locations on the body were carried out at a number of frequencies. Collected data is then used to calibrate the circuit model. In [2], a set of measured impedances was also used to try to generate a simple equation that relates electrode impedance to the operating frequency and electrode size, using curve fitting techniques. Yet another approach is to use 3D Finite Element Models (FEM) [3], where more complex human body models are proposed, taking into consideration more biological features and factors, to accurately model the signal path through and around the human body. Although such models accurately solve the EM wave simulations, providing more insight on how the signal travels in various body tissues, diffusion of power into deeper tissues, power dissipation through the human limbs, and other vital information for the channel modeling, it still fails in accurately modeling the electrode-body contact impedance. The main reason for that is failing to represent the physical/biological interactions at the electrode interface; the ionization of the electrode/gel, movement of the ions and the interaction at the interface.

The same shortcomings apply to simplified circuit models used to represent IBC channel models [2] [4-6]. Although some of these models were able to accurately take into account the electrodes properties, it still suffered from drawbacks when it comes to the electrode-body impedance modeling, since in most cases very simple models were assumed, limiting the fidelity of the model when representing electrode-body interface. In [7], a new method was proposed for a better representation for the electrodes impedance, where a hybrid approach (circuit model, FEM technique and experimental measurements) was adopted for modeling the IBC channel. The proposed simulation model uses measurement-derived S-parameters for modeling the electrode-body contact impedances and uses lumped circuit models to describe the electrode properties. Although this approach provided more accurate results, it still had some limitations. Mainly, the measurement-derived S-parameters are very unique to the measurement setup/conditions, including; the electrodes material and dimensions, subjects participating in the measurement and the operating frequency. If any of those parameters are changed, a new set of measurements will be needed, which would be a tedious process with expected variations due to the measurement setup conditions. Clearly there is still a need for an approach that would accurately model the electrode and electrode-contact impedances, taking into account the different factors and electrode properties, yet is not case specific (takes into account the electrodes material, size, spacing, operating frequency ...etc.).

Electrodes are responsible for connecting electronic systems to the human body through transducing ionic currents from the human body into electric currents and vice versa. Chemical reactions (oxidation-reduction) at the interface between the metal electrode and the electrolyte gel solution, as well as that between the electrolyte and the skin are responsible for carrying out this process, through the transfer of the charges between the electrons in the metal and the ions in

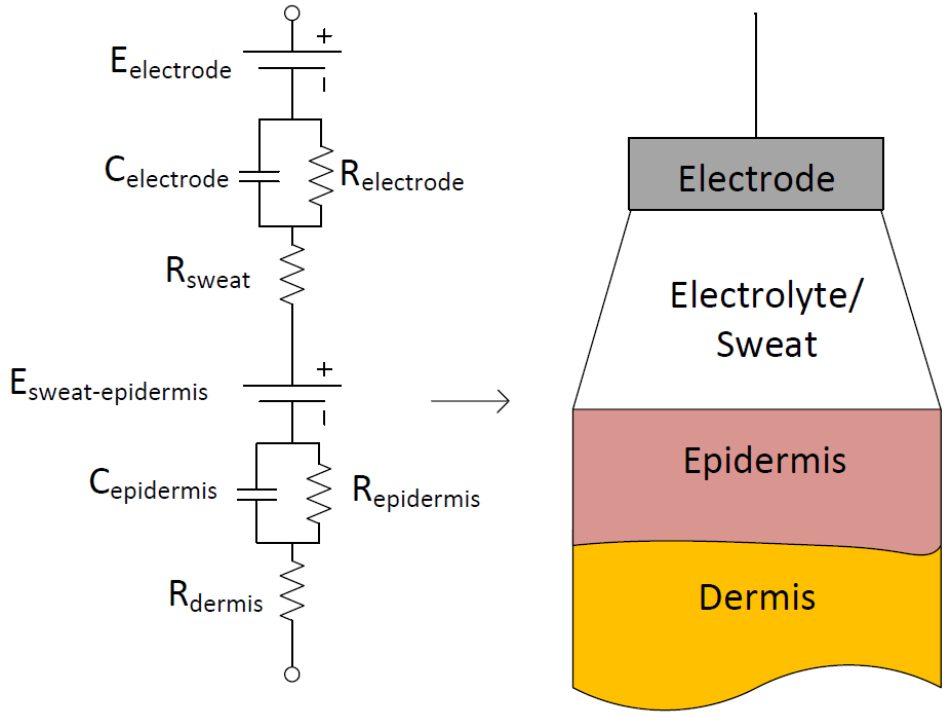

Figure 4.1: The electrical representation of the skin-electrode interface, showing the electrode, electrolyte, the skin layers impedances and the potential developed at the interfaces due to the chemical reactions.

the electrolyte solution/the human body building up a potential difference at the interface [8]. Modeling this interaction is the main concern in this paper. The complexity of this process resides in the fact that it is a function of variable parameters such as the metal of the electrodes, the electrolyte, electrodes' dimensions, quality of the electrode attachment to the skin and the skin electrode interface which may vary from one person to the other. The basic electrical representation for the skin electrode interface [8] is shown in Figure 4.1. It shows the electrode, electrolyte, skin layers, and the potential differences developed at the interfaces; $E_{electrode}$ representing the potential difference at the electrode electrolyte interface and $E_{sweat\text{-}epidermis}$ representing that at the electrolyte skin interface. Model parameters are highly subjective, due to the complexity of subject dependent voltage sources, capacitances and ohmic resistances.

A number of circuit modeling representations (with varying degrees of fidelity) have been proposed to capture the parameters shown in Figure 4.1. The following section, compares three common models (under the same assumptions) to illustrate the variability in channel gain profile that can be attributed to electrode-body interface modeling.

4.2 Single Order Model

For simplicity, an alternative electrical representation [8] for the electrode skin interface is shown in Figure 4.2. R_1 and C_1 represent the impedance associated with the electrode-electrolyte interface and the polarization at that interface, R_2 is the series resistance associated with interfacial effect as well as the resistance of the electrode material, and E is the potential developed at the interface due to the chemical interaction between electrons/ions. This simplified model is commonly used in circuit models for channel representation in the IBC field. The amplitude of the electrode-interface impedance using the single order model is plotted in Figure 4.3 over the frequency range of interest for galvanic coupling (100 KHz till 50 MHz). In order to generate the impedance shown in the Figure, curve fitting was used to find appropriate R, C values based on the experimental frequency dependent values of R, C presented in [1].

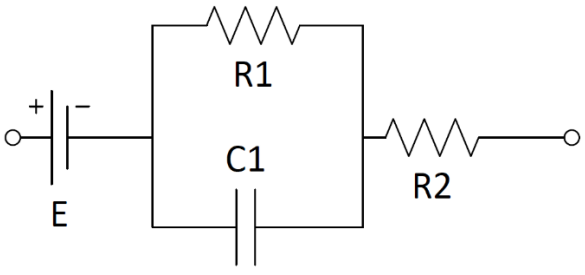

Figure. 4.2: Simple circuit model representation for the skin-electrode interface.

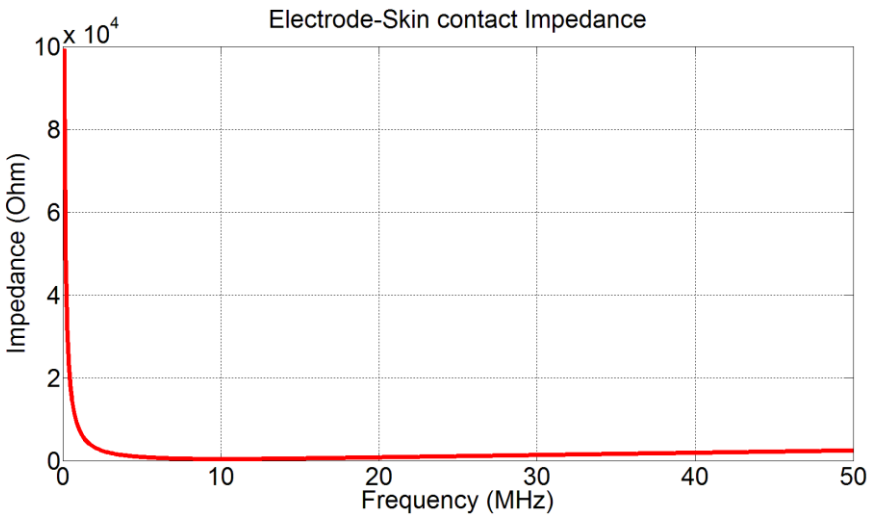

Figure. 4.3: Equivalent Impedance for the first order Electrode-Skin contact model for copper electrodes of radius 5 cm.

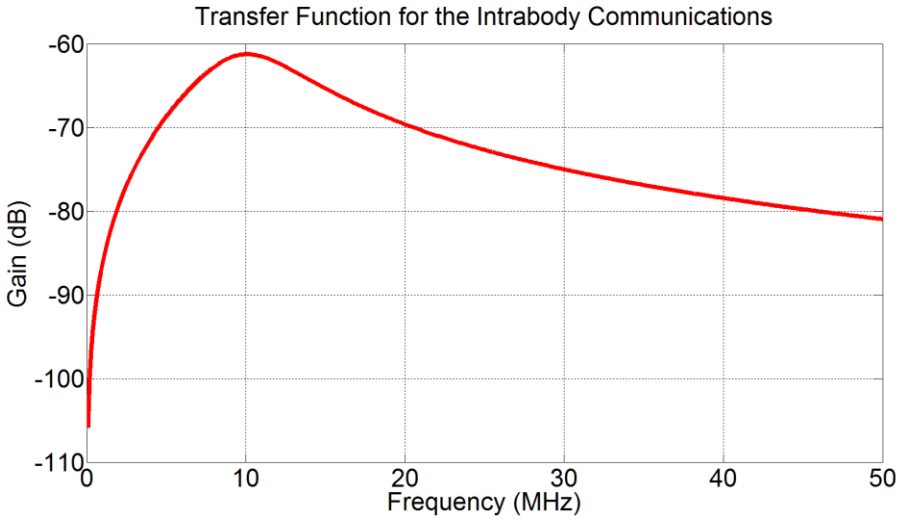

Figure. 4.4: Channel model for galvanic intra-body communications using the first order model for representing the electrodes contact impedance. Gain is plotted from 100 KHz till 50 MHz, distance between transmitter and receiver is 10 cm.

The first order electrode impedance is then integrated into the full channel circuit model that we proposed in the previous chapter to encapsulate all main five layers constituting the human body; skin, fat, muscle, cortical bone and bone marrow. The corresponding channel model (Gain

profile) is shown in Figure 4, where the gain of the channel through a human arm is plotted; the transmitter and receiver are 10 cm apart, electrodes of the same node are 3.5 cm apart, electrode radius is 5 cm and is made from copper.

4.3 Double Order Model

While the single order model is simple and fast in simulations, it lacks the details needed to accurately represent the details shown in Figure 4.1. Thus, a double order model was introduced in [9-10]. The proposed electrode-gel-skin model consists of two main parts; a circuit model representing the electrode – electrolyte (gel) impedance, and another representing the electrolyte-skin impedance, as shown in Figure 4.5. The authors used curve fitting techniques to obtain the values of the circuit elements from experimental data that they conducted.

In order to compare the two approaches, we used the same channel model we proposed in chapter 3. Impedance values (equivalent impedance for each of the two sections solely, then the overall combined electrode-skin impedance) were computed over the range of frequencies of interest, as shown in Figure 4.6. The corresponding channel gain is plotted in Figure 4.7.

It is important to note that the two channel gain profiles are not identical. This fact highlights that the channel gain profile is highly dependent on the electrode modeling approach used and hence a thorough understanding of the parameters affecting the model is needed. In subsequent section, we elaborate on such parameters and their impact on channel gain profiles.

In [11], the authors proposed a more generic model for the second order electrode-human body contact impedance, shown in Figure 4.8, where the model included variables that represent the electrode dimensions and material. In the model, Cd represents the double layer capacitance between the electrode and the electrolyte solution in the body tissue, Ra is the activation

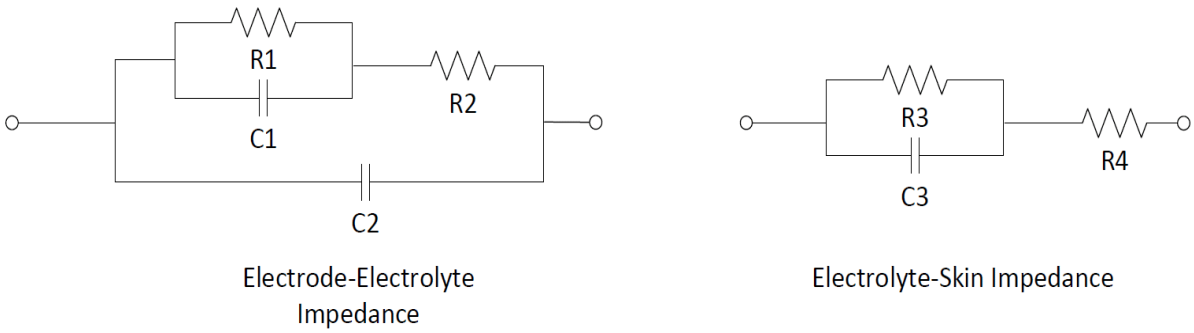

Figure. 4.5: A double order model, consisting of a section modeling the electrode-electrolyte impedance and another modeling the electrolyte-skin impedance.

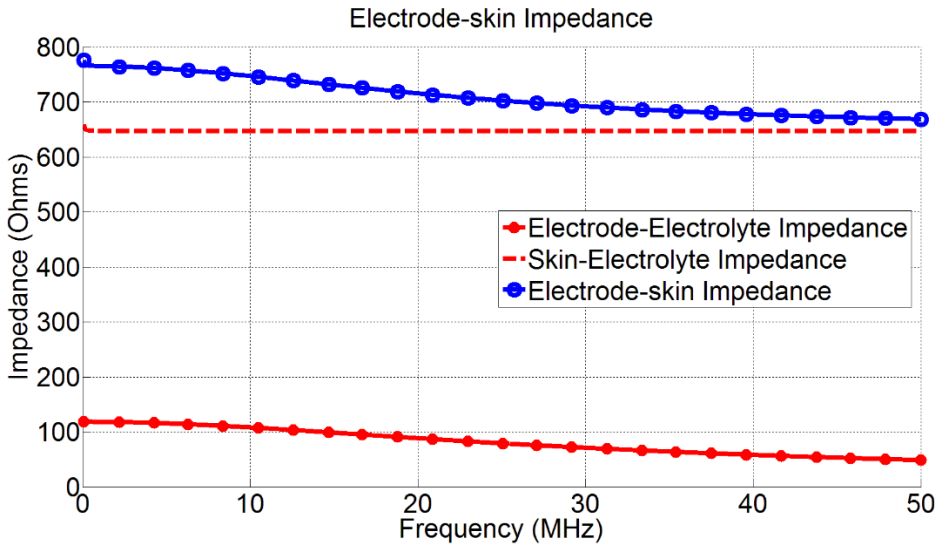

Figure 4.6: Equivalent Impedance of the double order model; electrode-electrolyte impedance, electrolyte-skin impedance and the overall electrode skin impedance.

polarization resistance, Rw and Cw represent the diffusion polarization impedance (Warburg impedance), Z is the reaction impedance and Zt is the impedance of the tissue under the electrode (skin). Using this model, we computed the equivalent impedance for the electrode-skin contact for three different materials; copper, brass and stainless steel over the frequency range of interest, where material dependent parameters are as given in [11].

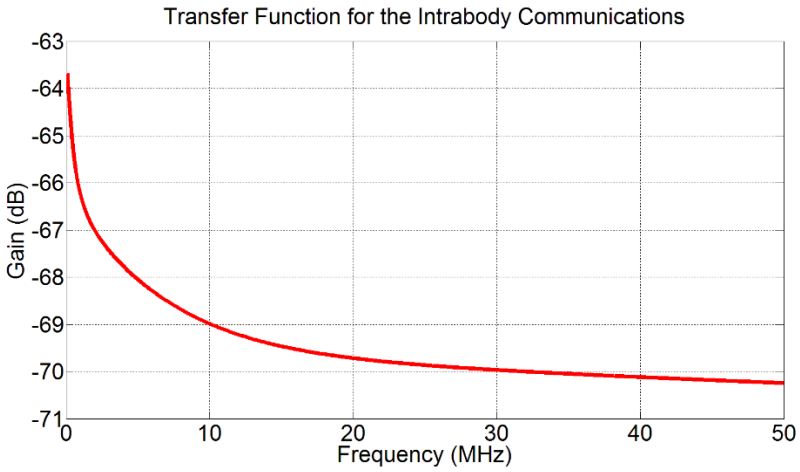

Figure 4.7: Channel model for galvanic intra-body communications using the double order model for representing the electrodes contact impedance.

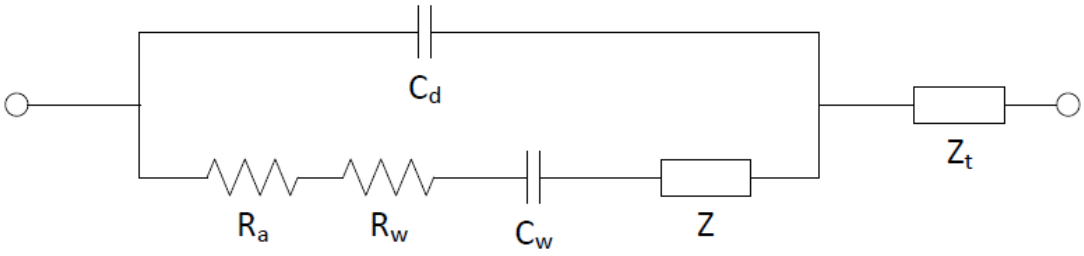

Figure 4.8: Contact impedance circuit model proposed in [11], taking into consideration the activation polarization, diffusion polarization, reaction impedance and the body tissue impedance.

Results are shown in Figure 4.9. The corresponding channel profile using results obtained from this model, for the three electrode materials, are then shown in Figure 4.10, which again show a deviation from the two channel gain profiles presented earlier.

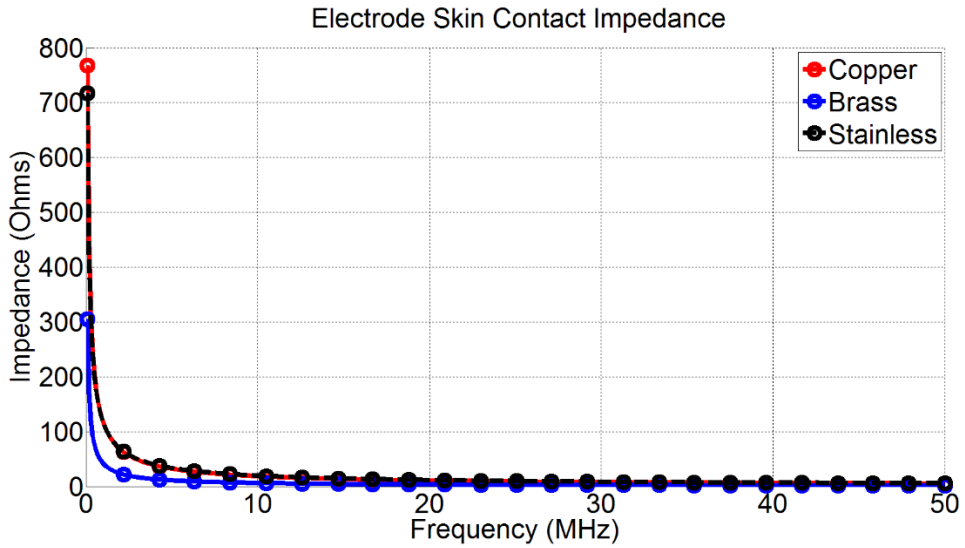

Figure 4.9: Equivalent Impedance using the model suggested in [11], for three different materials; copper, brass and stainless steel, with an electrode area of 100 mm2 each.

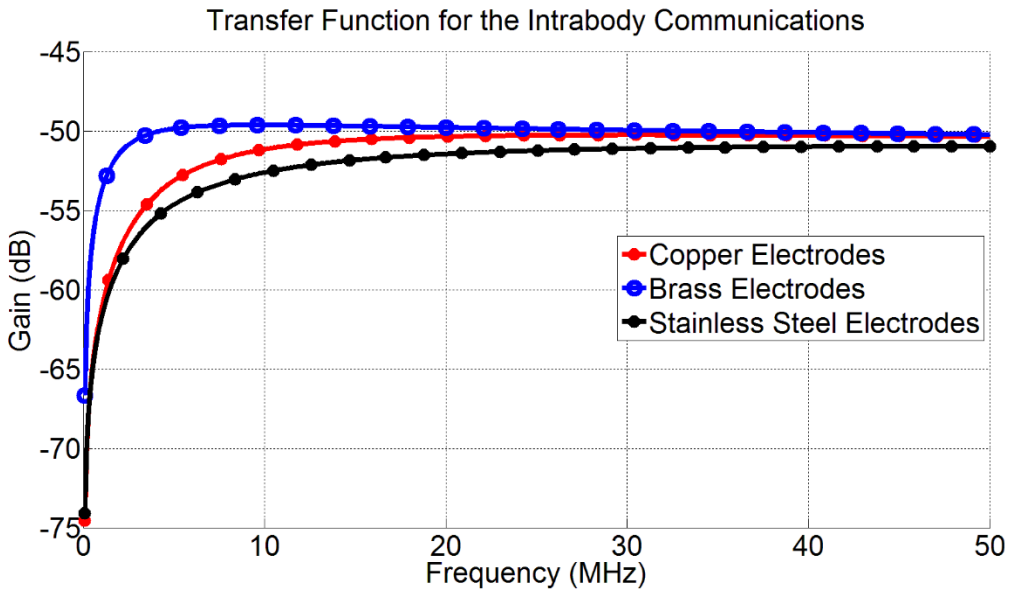

Figure 4.10: Channel model for galvanic intra-body communications for three different electrode materials; copper, brass and stainless steel.

4.4 Channel Model Variation with Respect to Electrodes Parameters

It is now clear how sensitive the channel gain profile is to the adopted electrode skin contact impedance model. It is thus imperative to choose a model that captures as many of the biological processes as possible. The model presented in [11] considers the activation polarization, diffusion polarization, reaction impedance and the body tissue impedance. In the remainder of the paper, we use this circuit model to gain further insight in the impact of various parameters on the channel model.

Effect of distance between the transmitter node and the receiver node electrodes: In Figure 4.11, the electrode area is fixed at 1 cm^2, the separation between each pair of electrodes at the same node is 6 cm. The distance between the two nodes is varied (10, 30 and 50 cm).

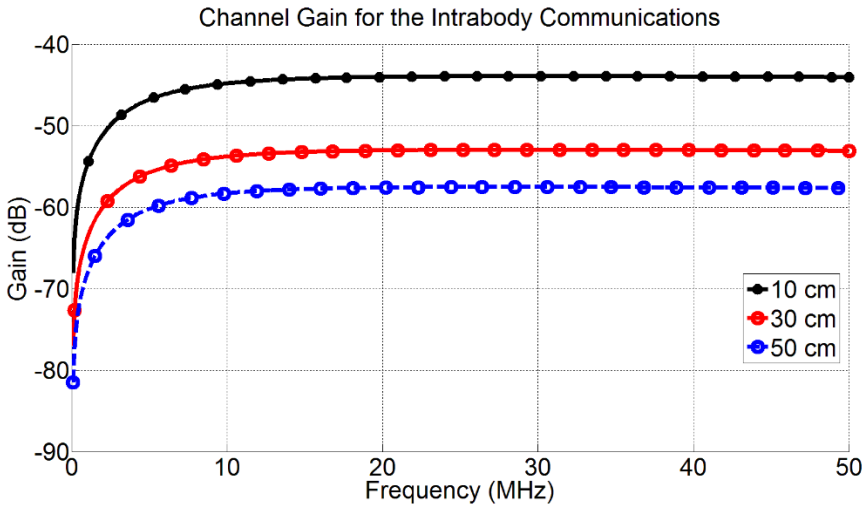

Figure 4.11: Effect of the distance between the transmitter electrodes and the receiver on the channel gain profile, where the distance is varied, while the electrode area and the separation between each pair of electrodes are kept constant at 1 cm2 and 6 cm respectively.

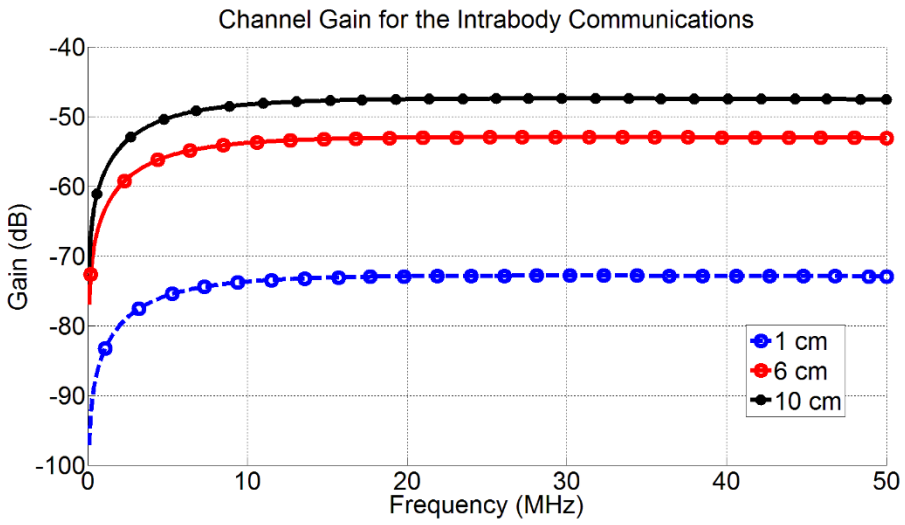

Figure 4.12: Varying the separation between electrodes of each node; 1cm, 6cm and 10 cm, while both the electrode area and distance between the transmitter and the receiver are kept fixed at 1 cm2 and 30 cm respectively.

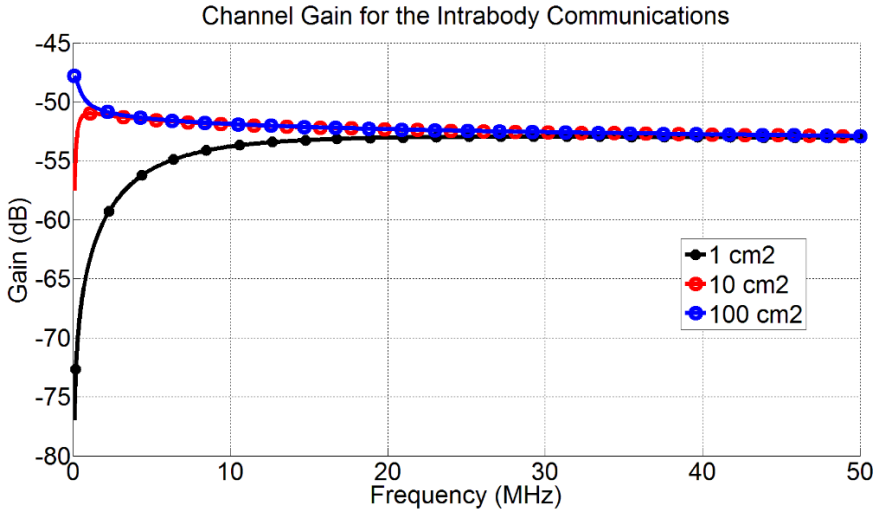

Figure 4.13: Changing the electrode area; 1 cm2, 10 cm2 and 100 cm2 while distance between nodes and separation between pair of each nodes are kept constant at 30 cm and 6 cm respectively

As expected, the results show that as the distance between the transmitter and the receiver increases, the channel gain drops (more attenuation).

Effect of node specific parameters: In Figure 4.12, the separation between electrodes of each node is varied; 1cm, 6cm and 10cm, while the electrode area and distance between the

transmitter and the receiver are kept fixed at 1 cm^2 and 30 cm respectively. In Figure 4.13, the electrode area is varied; 1 cm^2, 10 $cm^2$and 100 cm^2, while the distance between the nodes and separation between pair of each nodes are kept constant at 30 cm and 6 cm respectively. From the results, one can infer that as the area of the electrode increases, the impact its impedance has on the overall channel gain profile decreases, especially at the high frequencies (above 30 MHz). To further illustrate this point, consider the results shown in Figures 4.14 and 4.15 where the electrode area is kept constant at 100 cm^2 and the distance between the transmitter and the receiver as well as the separation between each electrode pairs is varied. Although the same relations deduced earlier stays the same, the channel profile, especially at lower frequencies, follows a different trend.

Electrode Contact Impedance vs. Body Impedance: In order to better understand the change in channel gain profiles for different electrode areas, it is important to understand the regions in which certain impedances dominate; namely the electrode contact impedance and the body impedance (input impedance seen between the two terminals of the node).

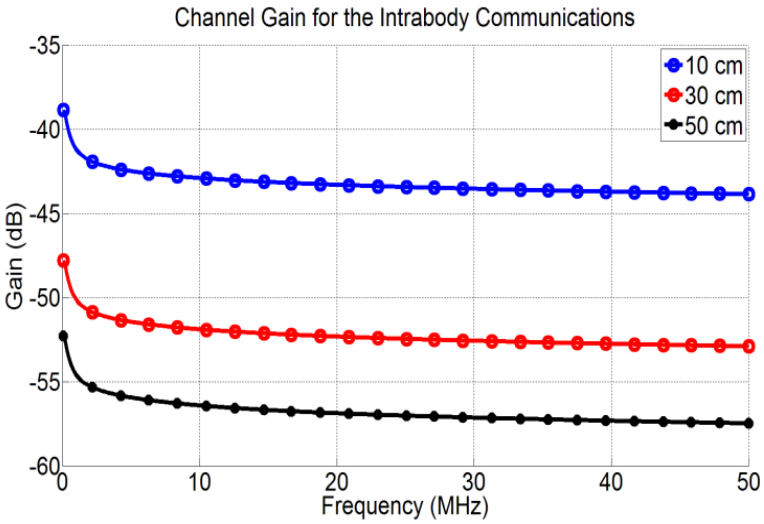

Figure 4.14: Gain vs. distance for electrode area of at 100 cm2 and separation between each pair of electrodes of 6 cm.

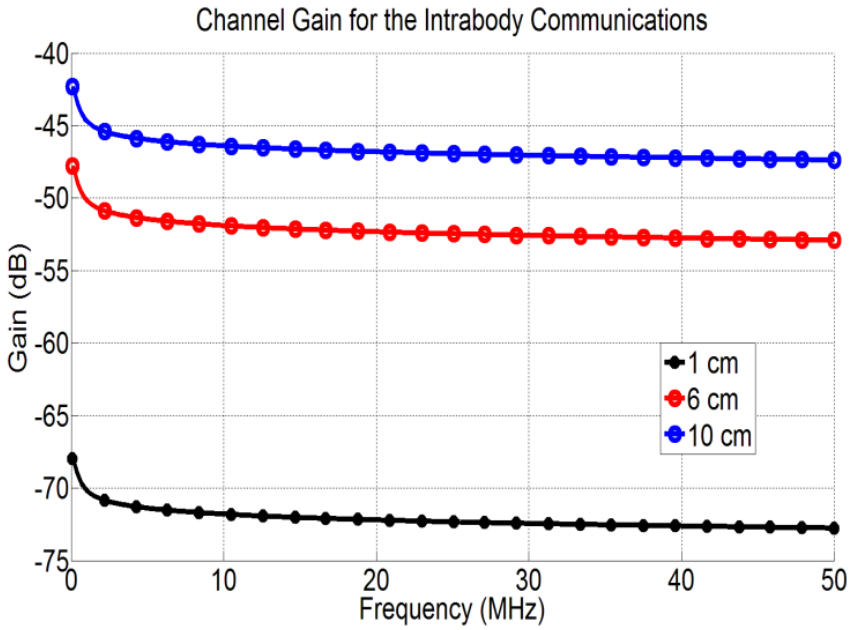

Figure 4.15: Gain vs. separation between electrode pairs of the same node, for electrode area of at 100 cm2 and distance between transmitter and receiver of 30 cm.

To better understand the impact of electrode area, a simulation was run, where two extremes for the electrode area were used; namely 1 cm^2 and 100 cm^2. The magnitude of the equivalent impedances is plotted in Figures 4.16 and 4.17 respectively. From the figures, we notice that for smaller area electrodes, the electrode contact impedance is dominant over the body input impedance, which means the contact impedance has higher impact on the channel gain profile. As the electrode area increases, its impedance drops till the body input impedance becomes dominant over it, thus the body input impedance will have the higher impact on the channel profile. This also explains the results shown in Figure 4.13, as the electrode area increases its impact on the channel gain profile, especially at higher frequencies, becomes negligible. Moreover, changing the separation between the electrode pairs at each node, changes the input impedance seen between these two electrodes according to the model we proposed in the previous chapter, thus the final channel gain will be determined according to the relation

between the various impedances (input impedance, electrode impedance, transmission path impedance …etc.).

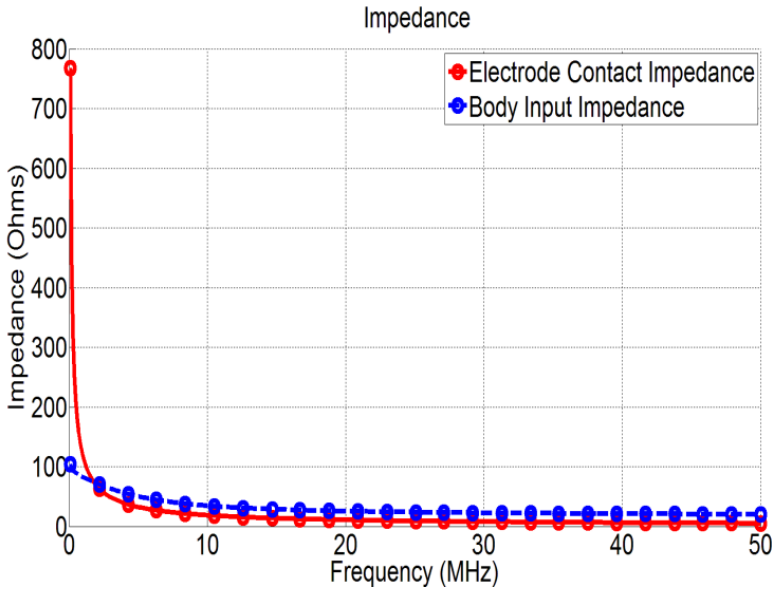

Figure 4.16. Magnitude of the electrode contact impedance as well as the body input impedance seen between the two electrodes of each node, for electrode area of 1cm2.

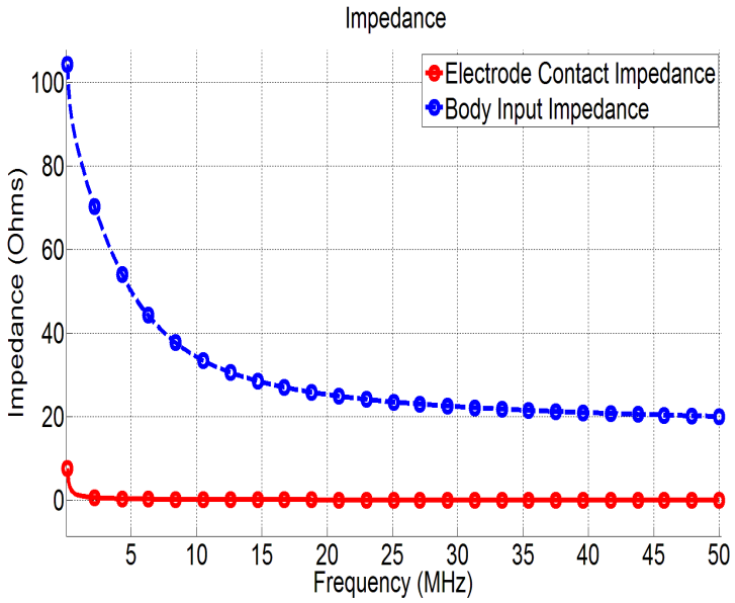

Figure 4.17. Magnitude of the electrode contact impedance and the body input impedance for electrode area of 100 cm2 .

4.5 Conclusion

In this chapter, we investigated various methods used to model the electrical circuit representation of the electrode-body contact. The impact of adopting each of these models on the characteristics of the galvanic intra-body communication channel, using the channel model that we proposed in chapter 3 is presented. We then studied the impact of varying different parameters, related to the electrodes as the electrode area, distance between the transmitter and the receiver nodes and the separation between each pair of electrodes on the characteristics of the channel gain/attenuation profile. It is clear that the gain drops with increasing the distance between the two nodes, yet it increases with increasing the separation between the electrodes of the same node. To further understand the obtained results, we studied the relation between the basic impedances forming our channel model; mainly the electrode contact impedance and the body input impedance. Through observing the values of each for different electrodes dimensions, it became clear the role and impact of each one of them on the channel gain characteristics, and how the relation between both of them dictates the behavior of the channel profile. Results are published in [12]

References

[1] Marc Simon Wegmueller, Andreas Kuhn, Juerg Froehlich, Michael Oberle, Norbert Felber, Niels Kuster, and Wolfgang Fichtner. An attempt to model the human body as a communication channel. IEEE transactions on Biomedical Engineering, 54(10):1851-1857, 2007.

[2] Marc Simon Wegmueller, Michael Oberle, Norbert Felber, Niels Kuster, and Wolfgang Fichtner. Signal transmission by galvanic coupling through the human body. IEEE Transactions on Instrumentation and Measurement, 59(4):963-969, 2010.

[3] R. Xu et al.: Electric-field intrabody communication channel modeling with finite-element method. IEEE Trans. Bio-Med. Eng. 58, 3, pp. 705-–712 (March 2011).

[4] Cho et al.: The human body characteristics as a signal transmission medium for intrabody communication. IEEE Trans. Microw. Theory Techn. 55, 5, pp. 1080–1085. (2007)

[5] Callej´on, M. A. *et al.*: Distributed circuit modeling of galvanic and capacitive coupling for intrabody communication," *IEEE Trans. Bio-Med. Eng.* 59, 11, pp. 3263-–3269. (November 2012).

[6] Kibret, B. *et al.* 2014. Investigation of galvanic-coupled intrabody communication using the human body circuit model. *IEEE J. Biomedi. Health Informat.* 18, 4(July 2014), 1196–1206.

[7] Park, J., Garudadri, H. and Mercier, P.P.: Channel modeling of miniaturized battery-powered capacitive human body communication systems. *IEEE Transactions on Biomedical Engineering*, 64(2), pp. 452-462.

[8] Neuman, M. R.: Biopotential Electrodes.The Biomedical Engineering Handbook: Second Edition, Ed. Joseph D. Bronzino, Boca Raton: CRC Press LLC.(2000)

[9] Saadi, H. and Attari, M.: Electrode-gel-skin interface characterization and modeling for surface biopotential recording: Impedance measurements and noise. 2*nd International Conference on Advances in Biomedical Engineering (ICABME)*, pp. 49--52. (September 2013).

[10] Assambo, C., Baba, A., Dozio, R. and Burke, M.J.: Determination of the parameters of the skin-electrode impedance model for ECG measurement. In *Proceedings of the 6th WSEAS international conference on electronics, hardware, wireless and optical communications, Corfu Island, Greece*, pp. 90--95. (February 2007).

[11] Kanai, H., Chatterjee, I. and Gandhi, O.P.: Human body impedance for electromagnetic hazard analysis in the VLF to MF band. *IEEE transactions on microwave theory and techniques*, *32*(8), pp. 763--772. (1984)

[12] Khorshid, Ahmed E., Ibrahim N. Alquaydheb, and Ahmed M. Eltawil. Electrode impedance modeling for channel characterization for intra-body communication. In *Advances in Body Area Networks I*, pp. 253-266. Springer, Cham, 2019.

Chapter 5

Physical Multi-Layer Phantom Models

5.1 Introduction

As seen in the previous chapters, initial work in the IBC field focused on evaluating the suitability of the human body as a communication medium. Research efforts were first directed towards modeling the gain/attenuation profile of the body channel versus frequency and simulating its behavior using different software tools. The goal of this characterization was to identify the optimum frequency range for IBC as well as the frequency range at which the body's attenuation to the signal propagation would be minimal, thus minimizing the power needed for transmission. Factors affecting such profile were also considered, such as, type, shape and size of the electrodes used, distance between the transmitter and the receiver, biological parameters of the human body and the environmental conditions [1-9]. However, simulation results alone are not sufficient and must be verified through comparison with experimental data from measurements that are carried out on real subjects. Carrying out experiments on real subjects is a tedious process that requires long and complicated procedures, mainly to ensure the safety of the subjects under test, especially for emerging technologies. The above facts, together with the urgent need for experimental data for verifying the proposed channel models, encouraged researchers to adopt the idea of using including thermal, physical and electrical characteristics, in their experimental routines. Phantoms are widely used in the medical and biological studies as substitutes for animals in experiments, lending themselves readily for BAN research.

In this chapter we will focus on two main topics:

1) Describing a methodology to create multilayer phantoms that mimic the electrical properties of the body tissues for low frequency applications such as the IBC, while capturing the effect of the multiple layers in the human body, namely, skin, fat, muscle, cortical-bone and bone-marrow.

2) Providing experimental measurement results for different prepared samples over the frequency range from 100 KHz till 100 MHz.

Key features that should be captured by phantoms are presented and discussed. Next, phantoms are introduced, and two different methods for preparing phantoms suitable for IBC applications are presented. Experimental procedures and setup for preparing different materials constituting the phantom are detailed. Measurement results are then discussed, and properties of the prepared samples are compared with those of the tissues of concern. Composite models are then proposed, wherein results for the experimental measurements are shown proving the efficacy of the methodology in producing multilayer phantoms.

5.2 Phantoms

Phantoms are physical models that simulate certain characteristics of the biological tissues they represent. Phantoms have been used extensively in the medical field [10]. Historically known imaging phantoms were first introduced as objects for evaluating the performance of imaging devices. Phantoms then underwent various improvements, mimicking biological characteristics more accurately, where they proved to be useful solutions for experimentation at the early investigative stages prior to working with living subjects or cadavers. There are various classifications for phantoms, the most commonly used is according to the final state of the

phantom; solid (dry or wet), gel or liquid [11-19]. Finally, phantoms provide a stable and more controllable experimental setup/platform that is hard to realize using living subjects.

Several trials were reported in literature for the use of phantoms for IBC applications as a stable and easy to control, yet accurate experimental setup [20], [21]. Liquid phantoms were usually adopted in these trials, being the easiest to prepare. In [22], the authors used an insulator (polyvinyl chloride bag) containing conductive liquid (salt water) to model the human arm as a cylinder. In [23], the authors used a liquid phantom as well that consists of 0.45% NaCl and 2 gallons of water filled in a plastic container, yielding a solution of conductivity ~ 0.52 S/m at 13MHz and ~1S/m at approximately 900MHz. In [24], the authors used a phantom that is a gel material with a conductivity of 0.59 S/m at 6.75 MHz and packed by a plastic sheet. In [25], the authors constructed a circular phantom consisting of two homo-centric sections each filled with a different substance; water with a given sodium concentration and agar. Agar was used to emulate the skin and a saline solution accounted for the interstitial fluid and muscle. In [26], a semi-cylindrical container was proposed formed by two homo-centric layers composed of different chemical compounds emulating the skin and muscle. In [27], the authors proposed a solid phantom in the form of a rectangular parallelepiped with a relative permittivity of 81 and a conductivity of 0.062 S/m. Wegmueller et al. showed in [28], an ellipsoidal phantom for the simulation of a cross-section of the torso, filled with a muscle simulating fluid that emulates the conductivity of muscle at 27MHz.

A main drawback for the above mentioned trials is that the proposed phantoms all considered the arm as one homogeneous layer; using a single material to represent the whole arm. Such approach results in:

1) Neglecting the biological and physical nature of the arm, mainly the dielectric properties of each of the main five tissues, and over the whole range of frequencies of interest (instead of just reporting such values at one or two discrete frequencies).

2) Considering the arm as one single layer also neglects the interaction between one layer (tissue) and the other, which accordingly neglects and eliminates other important facts of how the signal would diffuse from one layer to the other, propagation of the signal in different layers, etc.

3) Inaccurate representation of the arm's geometry; dimensions of the arm and thickness of each layer (which has a considerable impact on the overall results and performance for IBC) are almost totally neglected.

For the above reasons, it became clear that if phantoms are to serve as stable, controllable, accurate and reliable testing setup for IBC, then more elaborate and detailed phantoms need to be used. In chapter 3, we proposed an accurate circuit model of the human arm as an IBC channel. Since the gain profile obtained using the model showed very good match with experimental results previously reported in the literature, we opted to follow the same approach in constructing the proposed phantom. Two different methods were studied to construct the samples that would satisfy our goal.

5.3 Oil Phantoms

In [29], equivalent anthropomorphic breast phantoms were constructed for use in ultrasound elastography and magnetic resonance (MR) elastography. The proposed method seemed to possess a potential for yielding materials with dielectric properties that can be varied through varying the ratios of the elements used in the preparation of each sample. The main

elements/components used for preparing the materials are shown, with the order at which each element is added throughout the preparation process for each material as shown in Figure 5.1. The liquid aqueous gelatin and the safflower oil are the main two components of the mixture. By varying the ratios of these two components each time, a new material with different dielectric properties is generated. Each resultant sample is identified by the percentage of oil to the total final sample weight; for instance, a 50% sample has safflower oil at 50% of the weight of the final product. The main steps for preparing each sample are as follows [29]:

1. In a beaker, prepare a room temperature solution of propylene glycol and 18 megohm-cm doubly de-ionized water.

2. Slowly add, while stirring, 200 bloom calf-skin gelatin so that no clumping occurs and a uniform "slurry" results.

3. Cover the beaker with a plastic food wrap held in place with a rubber band. Punch a small hole or slit in the plastic wrap so that the gas pressure above the slurry during heating remains at atmospheric pressure.

4. Place the beaker in a larger container of hot water so that the level of the hot water is at or above the top of the gelatin slurry in the beaker.

5. Heat the water until the gelatin temperature rises to about 90° C and becomes transparent. Remove any bubbles at the meniscus. The transparent hot gelatin is referred to below as molten gelatin.

6. Remove the beaker of molten gelatin from the hot water bath and immerse it partially in a cold water bath. Cool the molten gelatin, while stirring, to 50° C and remove it from the cold water bath.

7. While cooling the molten gelatin in step 6, heat the safflower oil to 50° C.

8. Add the molten gelatin to the 50° C safflower oil and mix vigorously with a tablespoon that is bent at right angles near the bowl of the spoon. During mixing, keep the bowl of the spoon beneath the surface and moving about a horizontal axis, thus minimizing disturbance to the surface of the mixture.

9. Add the liquid surfactant and continue the stirring motion until the emulsion is nearly white and a separation of oil does not occur when stirring is stopped.

10. Cool in the cold water bath to 40° C and slowly add with stirring formalin.

11. Continue cooling the emulsion to about 34° C and pour into molds.

12. Allow at least 8 hours for cross-linking of the gelatin by formaldehyde to occur before removing the phantom component from its mold.

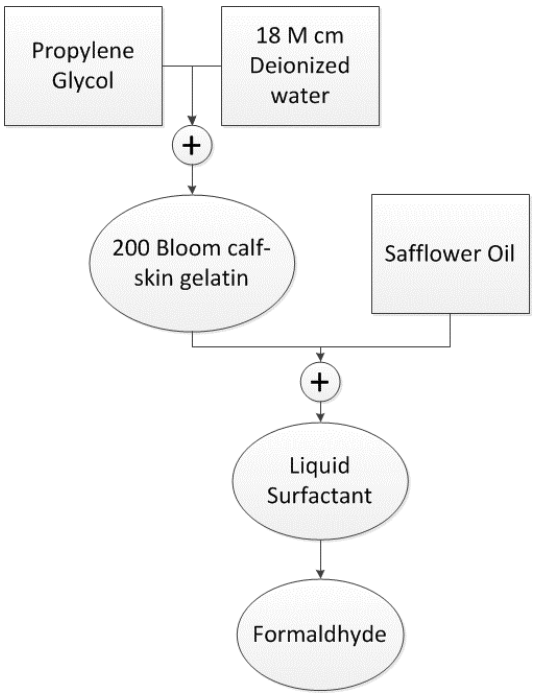

Figure 5.1: Elements used in preparing the oil samples [29].

5.4 Oil-Kerosene Phantoms

In [30], tissues mimicking phantom materials were proposed for microwave applications, where satisfactory results were reported for different samples, yet for a higher frequency range than the one we are interested in. To be able to use these materials within the frequency range of interest for IBC applications (100 KHz till 100 MHz), some modifications were applied. The main elements used in preparing the samples are shown in Figure 5.2. The main difference between this method and the previous one is that the oil solution in this case would be an equal mix of kerosene and safflower oil. The preparation steps for these materials are very similar to those of the Oil Phantom mentioned earlier, and can be found in more details in [30]. Another important advantage to the two methods being adopted for preparing the phantom materials is that they can be employed in a heterogeneous configuration (samples with different concentrations being constructed side by side) without change in geometry or dielectric properties of any of them, a feature that is needed to construct a multi-layer phantom structure.

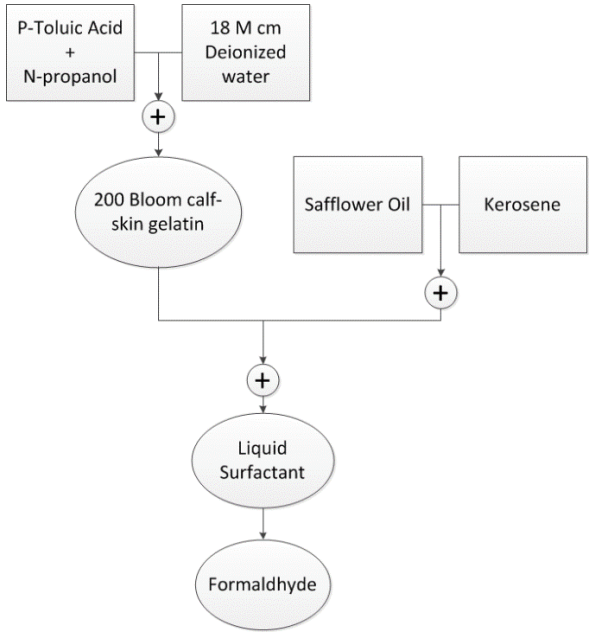

Figure 5.2: Elements used in preparing the oil-kerosene samples [30].

5.5 Experimental Setup

To investigate the potential of both methods - i.e. prepare samples that would have the closest dielectric properties to those of the five body tissues we are trying to mimic- nine different samples of each method were prepared, where the oil (or oil-kerosene solution) percentage was varied from 10% of the sample weight to 90%, with a 10% step each time. The exact weights and percentages of the elements used in preparing the samples are given in Table 5.1 for the oil phantoms and Table 5.2 for the oil-kerosene ones.

After pouring the prepared samples in their molds and allowing time to mature (at least for 5 days for the formalde-hyde cross-linking of gelatin to be completed [30]), the dielectric properties were measured. An HP Agilent 4291B [31] impedance analyzer was used to perform the measurements. Both the real part and the imaginary part of the complex permittivity are measured using the device. Results are then processed using MATLAB software to compute both the permittivity and conductivity of each sample and compare them with those of the five body tissues. The 16453A dielectric material test fixture was attached to the 4291B impedance analyzer, where the function of this fixture is to obtain accurate dielectric constant and loss tangent measurements through employing the parallel plate method, which sandwiches the material between two electrodes to form a capacitor. To be able to use this fixture, the thickness of the sample to be tested should not exceed 3 mm. For each prepared material, at least three different test samples from different locations across each mold were used to make sure that the results are not affected by the position of the sample in the mold. Results are then averaged over the collected readings to compute the dielectric properties for each prepared material. To investigate the properties of the prepared materials over time, measurements were repeated after 8 weeks to study the change in the properties of the material over time.

TABLE 5.1. Weight of Elements Used in Preparing the Oil Phantom Samples

Material\ Sample Percentage	**10%**	**20%**	**30%**	**40%**	**50%**	**60%**	**70%**	**80%**	**90%**
Propylene Glycol(units)	10.5	10.5	10.5	10.5	10.5	10.5	10.5	10.5	10.5
De-ionized water(units)	169	169	169	169	169	169	169	169	169
Gelatin(units)	26.95	26.95	26.95	26.95	26.95	26.95	26.95	26.95	26.95
Safflower Oil(units)	19.4	43.75	75	116.7	175	262.5	408.3	700	1575
Ultra Ivory(units)	0.2314	0.48125	0.825	1.2837	1.925	2.8875	4.4913	7.7	17.325
Formalin(units)	1.323	1.323	1.323	1.323	1.323	1.323	1.323	1.323	1.323

TABLE 5.2. Weight of Elements Used in Preparing the Oil-Kerosene Phantom Samples

Material\ Sample Percentage	**10%**	**20%**	**30%**	**40%**	**50%**	**60%**	**70%**	**80%**	**90%**
P-Toluic acid (g)	0.2	0.2	0.2	0.2	0.2	0.2	0.2	0.2	0.2
De-ionized water (ml)	190	190	190	190	190	190	190	190	190
N-Propanol (ml)	10	10	10	10	10	10	10	10	10
Gelatin (g)	34	34	34	34	34	34	34	34	34
Oil-kerosene (ml)	22.2	50	85	133.3	200	300	466	800	1800
Ultra Ivory (g)	1.26	2.8	4.76	7.46	11.2	13	15	17	20
Formalin (g)	2.16	2.16	2.16	2.16	2.16	2.16	2.16	2.16	2.16

5.6 Experimental Results

Using the experimental measurements provided in [32], [33], the dielectric properties (conductivity and permittivity) for the main five tissues skin, muscle, fat, cortical bone and bone marrow, are determined, as followed in the previous chapters.

The dielectric properties of the samples are plotted in Figure 5.3 (for oil only samples) and Figure 5.4 (for oil and kerosene samples). The figures show that as the oil or oil-kerosene concentration increase, both the conductivity and permittivity of the prepared sample decrease, which is expected as oil in general has more of an insulator properties (weak electrical

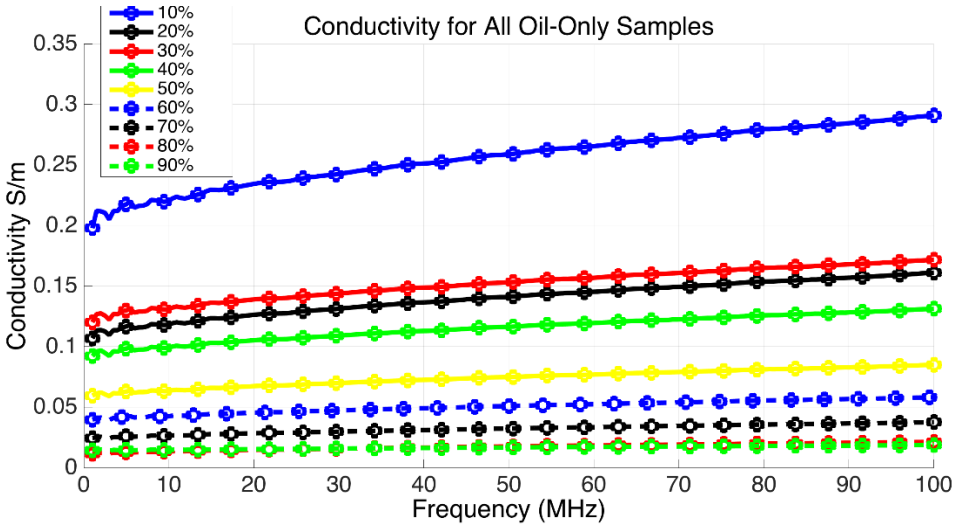

(a)

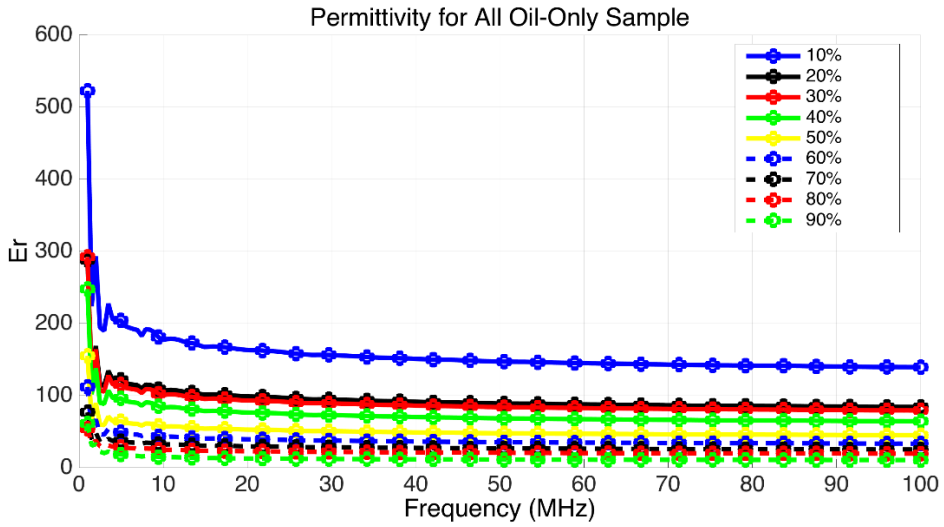

(b)

Figure 5.3: (a) Measured conductivity for the Oil-only samples for the different Oil concentrations. (b) Measured permittivity.

conductivity, yet better heat conductivity). Comparing such results, with the tissue properties plotted in Figures 3.5 and 3.6, it can be observed that both follow the same behavior with respect to frequency; conductivity increases with frequency, while permittivity experiences a sharp fall at lower frequencies and then almost saturates at higher frequency values. Comparing the

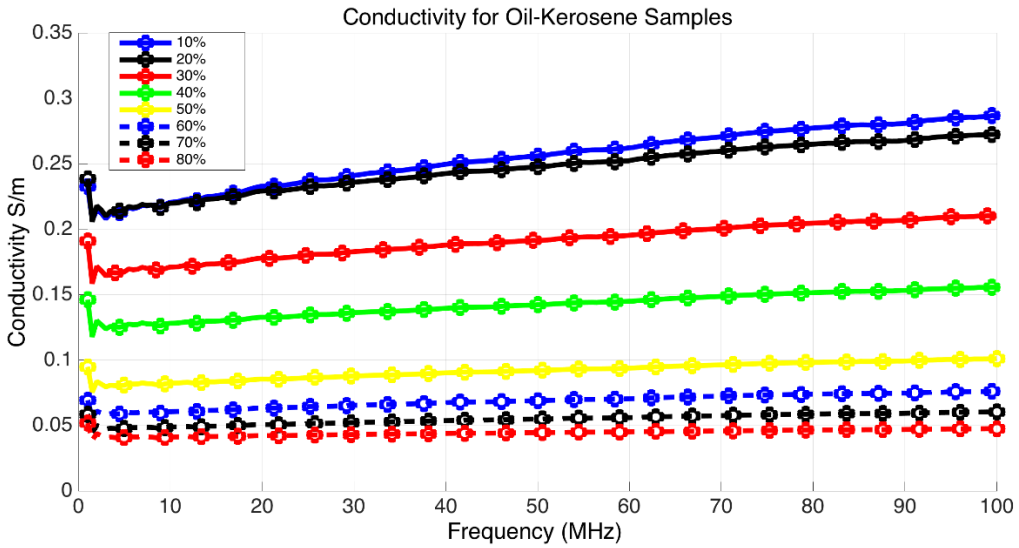

(a)

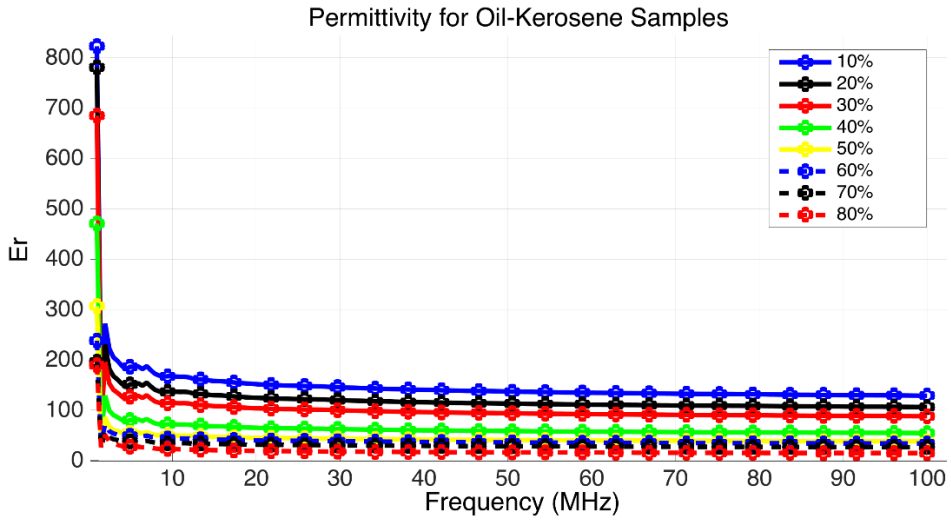

(b)

Figure 5.4: (a) Measured conductivity for the Oil-kerosene samples for different Oil-kerosene to the gelatin solution concentrations. (b) Measured permittivity.

electrical properties plotted in Figure 3.5 and 3.6 with those plotted for the different samples in Figure 5.3 and 5.4, the accurate oil percentage can thus be selected depending upon which specific tissue needs to be mimicked, as well as which electrical property is of more concern

(conductivity or permittivity), and the frequency range of interest. For instance, samples with low oil solution concentration can be utilized for mimicking tissue with high dielectric permittivity, while samples with high oil solution concentration can be used to mimic tissues with low conductivity like cortical bone, as shown in Figures 5.5 and 5.6, where the 80% oil-kerosene solution sample perfectly mimics the permittivity characteristics of the cortical bone, especially for the frequency range between 30 MHz to 100 MHz.

As shown in Figures 5.5 and 5.6, the electrical properties of different tissues can be matched with samples of certain formulations and concentrations, depending on the electrical property of interest (whether conductivity or permittivity is more of concern), and the range of frequency in which the IBC application will operate within. It is important to note that most IBC applications utilize less than 1 MHz of bandwidth [20], due to the nature of medical applications, that typically require low bit rates. A summary of such results; best matching samples (samples that shows less than 10 % matching error) with respect to different tissues, regarding conductivity and permittivity, for different frequency ranges (Fmin is the minimum frequency and Fmax is the maximum frequency in MHz defining the band over which the matching error is below 10%) within the IBC application band, is provided in Table 5.3.

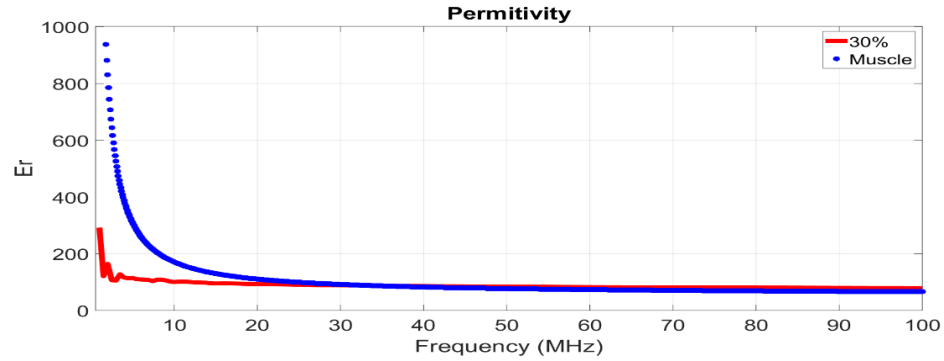

(a)

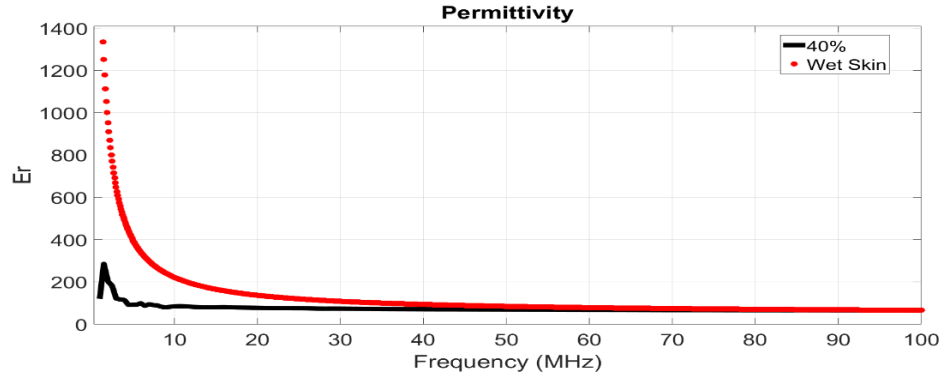

(b)

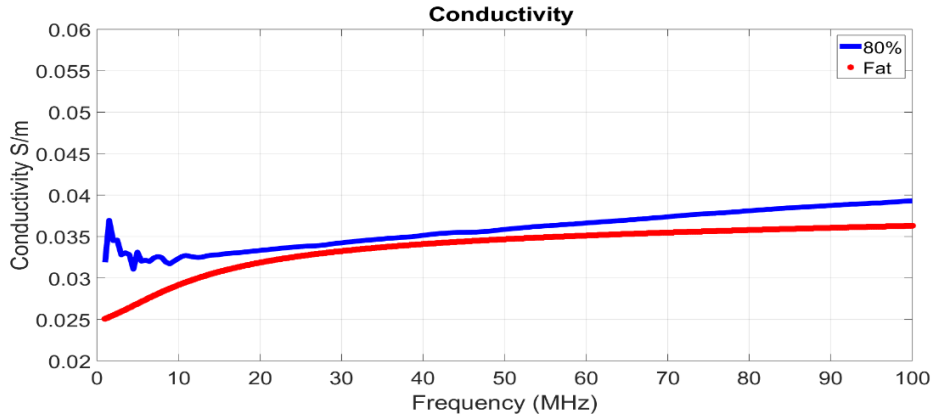

(c)

Figure 5.5: An example for matching the samples with certain solution concentration with the tissue of concern within certain frequency bands: (a) 30% oil-kerosene solution shows accurate match with the muscle tissue, from the permittivity point of view, for frequencies above 30 MHz, (b) 40% oil-only solution for the skin (wet) tissue, regarding the permittivity, for frequencies above 40 MHz, (c) 80% oil-kerosene solution shows accurate match with fat tissue, from the conductivity point of view, for frequencies above 10 MHz

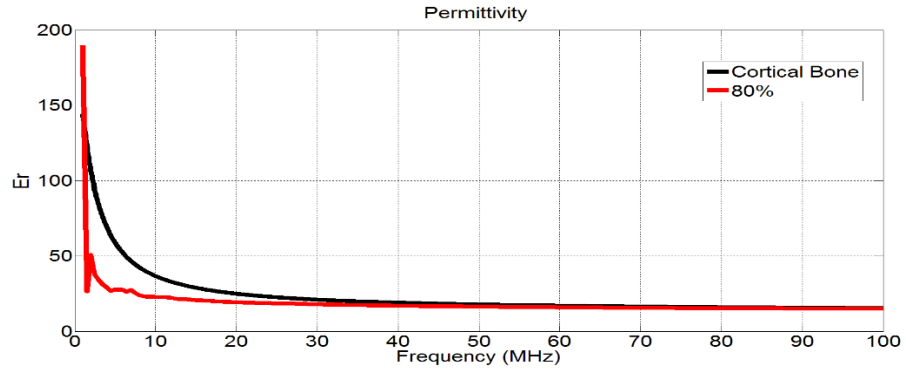

(a)

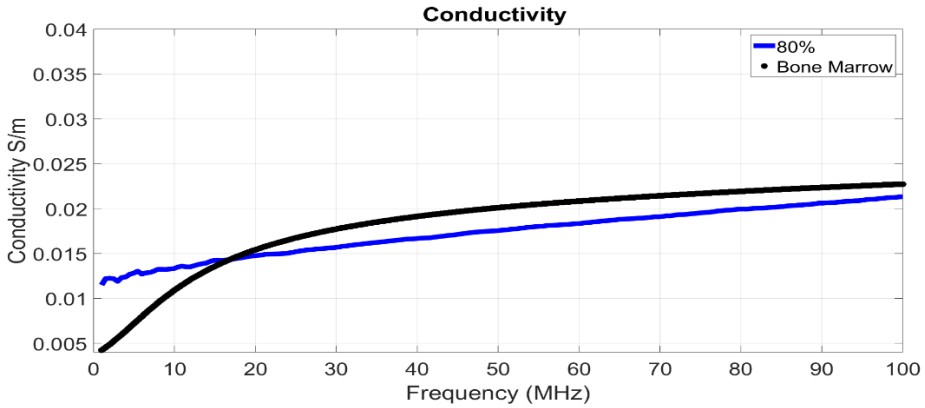

(b)

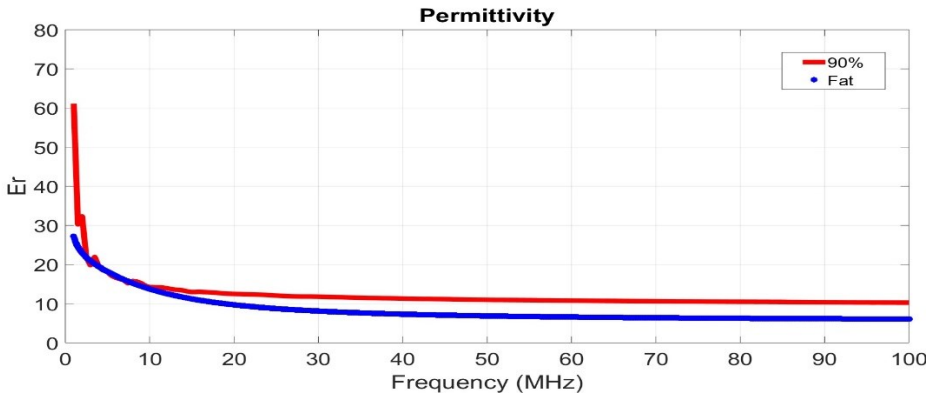

(c)

Figure 5.6: Matching tissues with different samples that show good accuracy within certain frequency ranges; (a) 80% oil-kerosene with the cortical bone, from the permittivity point of view, and specially for frequencies greater than 30 MHz, (b) 80% oil-only solution with the bone marrow, from the conductivity point of view, within the frequency range 12 MHz till 100 MHz, (c) (b) 80% oil-only solution for the Fat tissue, from the permittivity point of view, especially for low frequencies.

Table 5.3 Matching Tissues with Samples of Best Accuracy (less than 10% matching error) for Different Frequency Ranges

Tissue	Electrical Property					
	Conductivity			Permittivity		
	Sample Concentration	Fmin (MHz)	Fmax(MHz)	Sample Concentration	Fmin (MHz)	Fmax(MHz)
Cortical Bone	70% (Oil-Kerosene)	4.2	11	60% (Oil-Kerosene)	1.8	7
	60% (Oil Only)	5.9	100	70% (Oil-Kerosene)	11.8	20
	-	-	-	80% (Oil-Kerosene)	30	100
Bone Marrow	80% (Oil Only)	12.8	100	90% (Oil Only)	1.8	25
Dry Skin	30% (Oil Only)	7	9	10% (Oil Only)	25	33.7
	20% (Oil Only)	10	14.5	10% (Oil Only)	42	58
	-	-	-	20% (Oil Only)	58.4	90
	-	-	-	30% (Oil Only)	93	100
Wet Skin	-	-	-	10% (Oil Only)	11.9	16.8
	-	-	-	20% (Oil-Kerosene)	24	38
	-	-	-	30% (Oil Only)	38	71
	-	-	-	40% (Oil Only)	73	100
Fat	80% (Oil-Kerosene)	11	100	90% (Oil Only)	2.3	11.5
Muscle	-	-	-	30% (Oil Only)	24	54
	-	-	-	30% (Oil-Kerosene)	39	100

5.7 Composite Sample

Building a composite sample that spans multiple layers is essential to observe the behavior of the electric signal and how it diffuses from the skin into other layers while propagating from one node to the other. Towards that goal, a composite oil-kerosene sample was prepared. First, an oil-kerosene sample with 20% oil solution concentration was prepared, and then left it in the mold for two days, to allow the sample to solidify and the chemical reactions to conclude. The sample was then placed in a bigger mold, where a 60% oil-kerosene sample was prepared and poured in the same mold, forming a composite sample in the form of two concentric cylinders, with the 20% sample enclosed by the 60% one, as shown in Figure 5.7. The composite sample was then kept at room temperature for another two days, before experimental measurements were executed. Samples were then taken from three different positions to measure the electrical properties, as shown in Figure 5.7; samples were first taken from position 1 which is deeply in the 60% concentration sample section, others taken from position 2 which is in the middle of the

20% concentration sample, and finally the last samples were taken from position 3 which is at the interface between both samples. Results were averaged over the samples taken at each position and plotted in Figure 5.8. It is clear that the permittivity for both concentrations remained almost the same; however, the 60% sample was a more affected at the interface than the 20% one. Similarly, the conductivities for the same samples are plotted in Figure 9 (b). The conductivity values at the interface were more affected by depositing two different concentrations side by side compared to the permittivity ones. However, both curves, when compared with the results in Figure 3.5 and 3.6, show that the electrical properties at the core of each sample is almost unchanged, which proves the capability of these materials in the preparation of a composite multi-layered phantom models, for an accurate mimicking of the human body, from the electrical properties point of view.

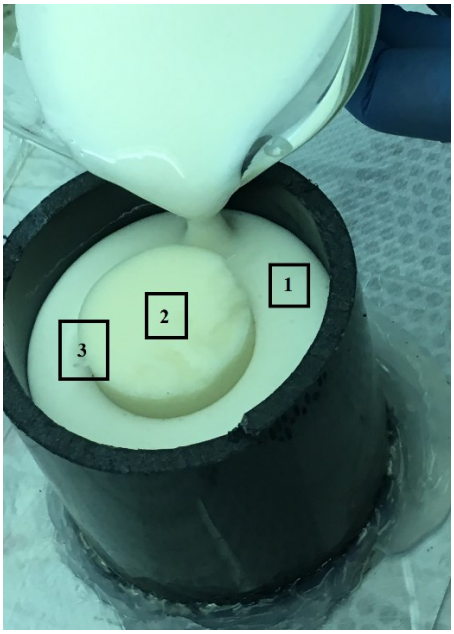

Figure 5.7: The oil-kerosene composite sample being prepared, where the 60% concentration sample is being poured into a mold containing an already semi-solid 20% concentration sample. Inscribe are the positions where samples were taken for experimental testing; 1-from the 60% sample,2- from the 20% sample and finally 3 is take from the interface at both samples.

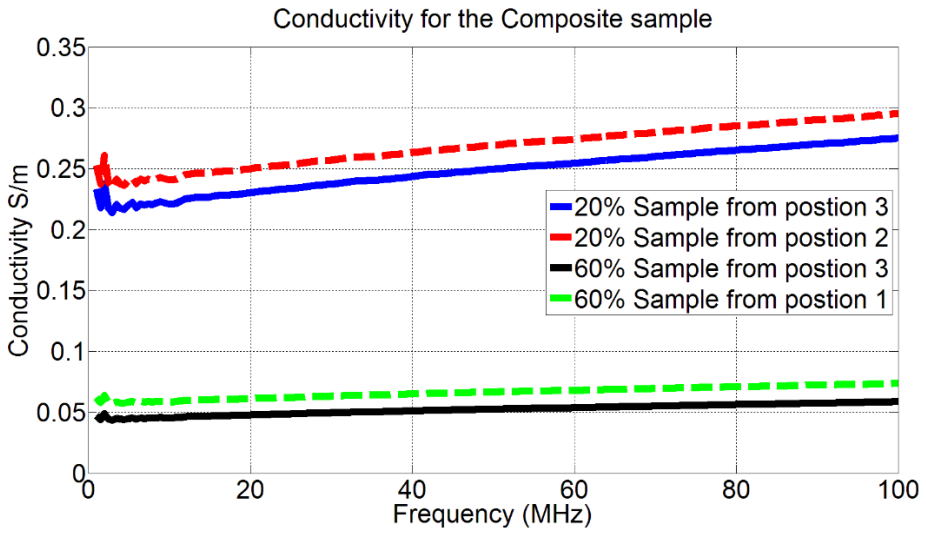

(a)

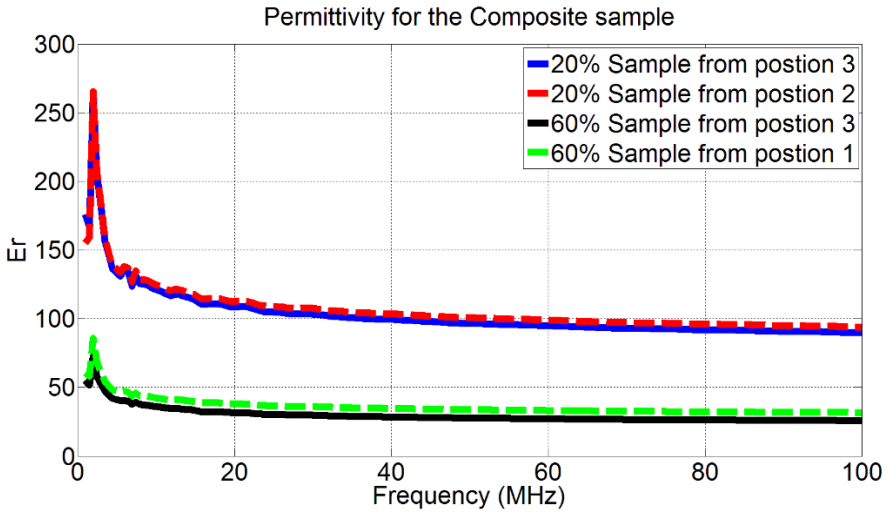

(b)

Figure 5.8: (a) Measured permittivity for samples taken from positions 1, 2 and 3 as indicated in Fig.6, (b) Measured conductivity for the same samples.

5.8 IBC Channel Sensitivity Analysis

As was shown in Table 5.3, sometimes for the same tissue, it's possible to realize one electrical property through the preparation of a material with a certain oil solution concentration, yet the same final material would not be the best for realizing the other electrical property. An example for that would be the muscle tissue; the 30% Oil-Kerosene solutions accurately mimics the permittivity of the tissue with the frequency range 39 – 100 MHz, yet the error in the resultant conductivity is greater than 10%. To solve this issue, a decision need to be taken on which electrical property is more of concern; more critical for the application at hand. In our case, for IBC applications, the IBC channel profile (gain/attenuation) is the major concern, since that's one of the primary goals for preparing these phantom models in the first place. To decide on which material is best for mimicking the electrical properties of tissues of concern, a sensitivity analysis was performed to study the impact of both the conductivity and permittivity of each of the five tissues on the IBC channel profile. The analysis was performed using the circuit model that we proposed in chapter 3, where the electrical properties of each tissue is varied between -20 % to +20% from its nominal values (experimental values published in [32-33]), then the final IBC channel profile is computed as well as the error - deviation of the channel profile from the nominal (0% deviation) case- is computed and shown in Table 5.4 where the maximum error percentage is reported for each case. As shown from the results, the IBC channel characteristics are much more sensitive to the conductivity of the tissues over the permittivity, since the conductivity mainly accounts for the signal transmission capability through a certain medium. This finding is crucial for applications like phantoms design, for manufacturing more accurate tissue mimicking materials. From a tissue perspective, muscle, skin and fat layers tend to affect the characteristics of the IBC channel more than cortical bone and bone marrow, this is due to:

Table 5.4: Maximum error percentages for the deviation in the IBC channel gain when varying the Electrical properties of the Tissues

Tissue	Conductivity				Permittivity			
	-20%	*-10%*	*10%*	*20%*	*-20%*	*-10%*	*10%*	*20%*
Skin	0.1013%	0.05008%	0.04923%	0.09785%	0.04311%	0.02162%	0.02162%	0.04311%
Fat	0.5278%	0.259%	0.2497%	0.4906%	0.03%	0.01506%	0.01525%	0.03069%
Muscle	2.194%	1.053%	0.9776%	1.891%	0.1624%	0.08082%	0.08011%	0.1595%
Cortical Bone	0.004617%	0.002302%	0.002302%	0.004617%	0.001275%	0.000637%	0.000637%	0.001275%
Bone Marrow	0.0014%	0.000697%	0.000697%	0.0014%	0.000524%	0.000262%	0.000262%	0.000524%

a) the better conductive properties of the first three tissues, b) the fact that only a tiny portion of the signal will travel through the bones (since most of the signal is transmitted through the skin, then muscles, as shown in [9]).

5.9 Muscle Tissue Mimicking Materials (Al/TX-150)

It's now clear how conductivity of the tissues impacts the performance of the IBC channel more than their permittivity, thus more attention should be given to conductivity when designing the phantom's materials. Moreover, variations in muscle tissue's conductivity impacts the channel performance significantly, which is expected due to the high conductive properties of the muscle tissue which forces a significant portion of the electrical signal to propagate through the muscle. For these reason, it was necessary to find an alternative method for preparing a phantom material that can mimic the conductivity of the muscle tissue more accurately than the two proposed methods, since none of them provided a sample with acceptable error. After a thorough search was performed in the literature, findings shown in [34] presented promising results. The proposed method uses mainly TX-150, aluminum powder and NaCl to realize the conductivity of the muscle tissue for multiple frequency ranges, including our range of interest, through varying

the percentages of these components with respect to the final mixture. The basic ingredients are: TX-150, Aluminum powder, water and NaCl. The steps for preparing the mixture, as outlined in Figure 5.9, are as follows:

1) Weigh all ingredients and determine percentages by weight, as suggested in Table 5.5.
2) Mix aluminum powder and TX150 and pour in 14-20 "C water and mix with a 10-cm shear stirrer rotating at 1,200 rpm for 45-120 seconds on a drill press
3) If the stirring time is not sufficient, the aluminum powder will sink (Since air bubbles are easily formed in this mixture, it is necessary to rotate the mixing bucket constantly and move it up and down to ensure proper mixing.)
4) When the mixture turns thick, slow down the drill press to about 800 rpm to avoid generation of air bubbles. (If stirred too long, the mixture will become too hard to pour)
5) Pour the mixture slowly into mold to allow the escape of air bubbles from the mixture.

After preparing different samples with the weights shown in Table II, the dielectric properties of the resultant samples were measured using the HP Agilent 4291B impedance analyzer. Both the real part and the imaginary part of the complex permittivity are measured using the device. Results are then processed using MATLAB software to compute both the permittivity and conductivity of each sample and compare them with those of the five body tissues, as done for the previous oil and oil-kerosene samples. From comparing the results obtained with the properties of the muscle tissues, it was clear that if a single sample to be used over the whole frequency range of the IBC, the sample with 10 grams of Aluminum powder gave the best matching results (error less than 10%). Results are plotted in Figure 5.10. Results show that using the sample that contained 10

Table 5.5 Composition of Phantom muscle tissue for different frequencies

Frequency (MHz)	TX-150 (g)	Aluminum Powder (g)	H_2O (mL)	NaCl (g)
100	34	7.4	307	1.7
70	36	9.5	303	1.4
40.68	34	32.2	283	1
27.12	34	31.7	283	0.9
13.56	34	32	283	1

grams of Aluminum powder, it is possible to accurately mimic the dielectric properties of the muscle tissue, with low error (less than 10% for both properties) over almost the entire range for IBC. Table 5.6 then presents a final summary of the best matching samples (samples with less than 10% matching error) using all the three preparation methods (Oil phantoms, Oil-Kerosene phantoms and Muscle phantoms) with respect to different tissues, regarding conductivity and permittivity, for different frequency ranges.

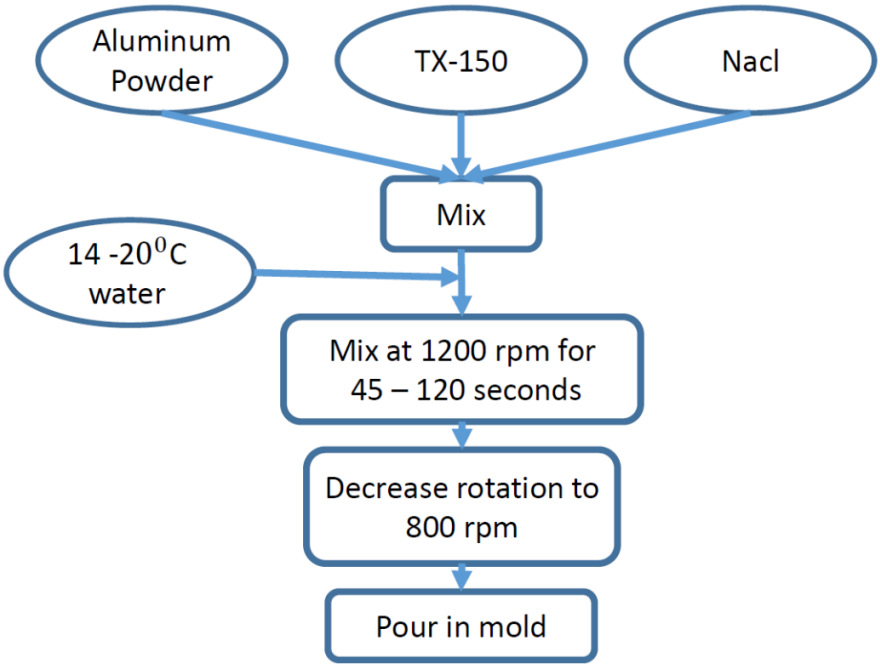

Figure 5.9: Steps and components for preparing the muscle tissue mimicking material [34]

Table 5.6 Final Summary for Matching Tissues with Samples of Best Accuracy (less than 10% matching error) for Different Frequency Ranges Prepared using the three different preparation methods

Tissue	**Electrical Property**					
	Conductivity			**Permittivity**		
	Sample Concentration	**Fmin (MHz)**	**Fmax(MHz)**	**Sample Concentration**	**Fmin (MHz)**	**Fmax(MHz)**
Cortical Bone	70% (Oil-Kerosene)	4.2	11	60% (Oil-Kerosene)	1.8	7
	60% (Oil Only)	5.9	100	70% (Oil-Kerosene)	11.8	20
	-	-	-	80% (Oil-Kerosene)	30	100
Bone Marrow	80% (Oil Only)	12.8	100	90% (Oil Only)	1.8	25
Dry Skin	30% (Oil Only)	7	9	10% (Oil Only)	25	33.7
	20% (Oil Only)	10	14.5	10% (Oil Only)	42	58
	-	-	-	20% (Oil Only)	58.4	90
	-	-	-	30% (Oil Only)	93	100
Wet Skin	-	-	-	10% (Oil Only)	11.9	16.8
	-	-	-	20% (Oil-Kerosene)	24	38
	-	-	-	30% (Oil Only)	38	71
	-	-	-	40% (Oil Only)	73	100
Fat	80% (Oil-Kerosene)	11	100	90% (Oil Only)	2.3	11.5
Muscle	10 grams of Aluminum Powder (Al/Tx-150 method)	4.5	100	10 grams of Aluminum Powder (Al/Tx-150 method)	15.8	100
	-	-	-	30% (Oil Only)	24	54
	-	-	-	30% (Oil-Kerosene)	39	100

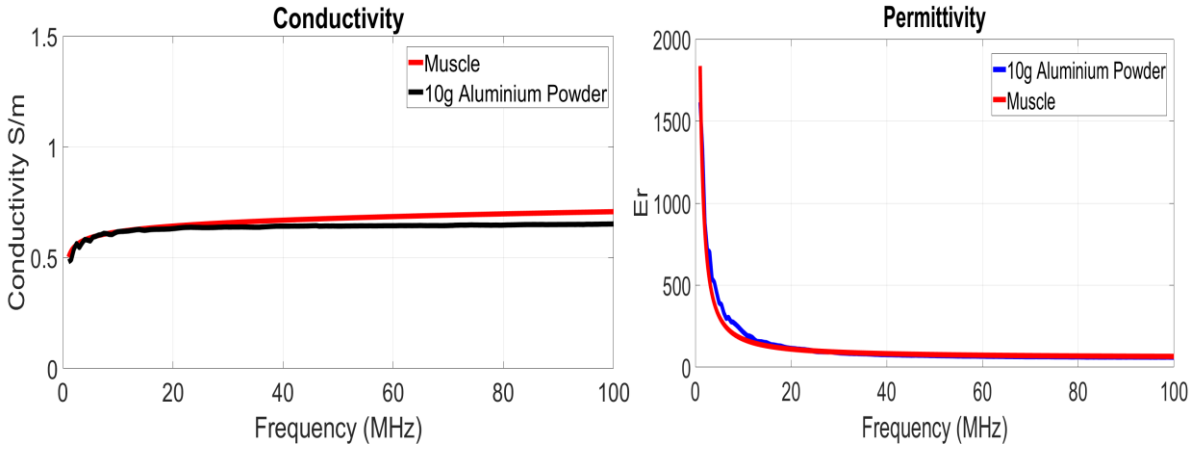

(a) (b)

Figure 5.10: Matching the sample, prepared by the authors, that included the 10 grams of Aluminum powder with the muscle tissue (experimental values obtained from testing on actual muscle tissues reported in [32-33]): (a) conductivity of the prepared sample shows accurate match almost over the entire range of interest, (b) the permittivity of the prepared samples shows accurate match with that of the muscle tissue.

5.10 Composite Sample II

From Table 5.6, it's obvious that if a multilayer tissue mimicking material phantom model is to be constructed, the muscle tissue mimicking material will be placed in between other two materials prepared using one of the first two methods (Oil only or Oil and Kerosene). To insure that the final composite sample will still maintain the same dielectric properties that the samples are designed for, we prepared a composite sample as shown in Figure 5.11., where an Oil sample with 60 % Oil concentration was prepared then left to solidify for two days, allowing the chemical reactions to conclude. The sample was then placed in a bigger mold and a muscle mimicking material sample (Al/TX-150 method) with 10 grams of Aluminum powder concentration was prepared and poured into the mold, forming a composite sample in the form of two concentric cylinders. The composite sample was then left at room temperature for another two days, before starting the experimental measurements.

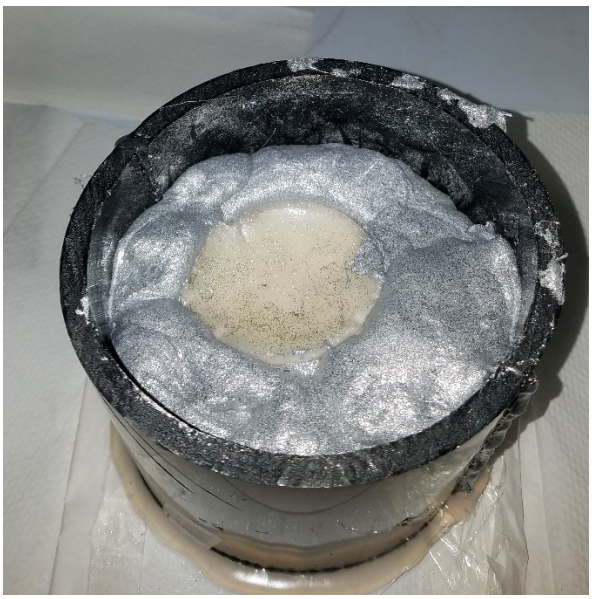

Figure 5.11.: The composite sample where a 60% Oil concentration sample is surrounded by a Al/TX-150 sample with 10 grams of Aluminum powder. Samples for measurement were taken from the middle of the Al/TX-150 sample, from the middle of the Oil Sample and finally from the interface between both samples.

Samples were then taken from three different positions to measure the electrical properties, a) from the middle of the Al/TX-150 sample, b) from the middle of the Oil Sample, c) from the interface between both samples. Results were averaged over the samples taken at each position and plotted in Figure 5.12. From the results, it's shown that results are almost the same at the center for each of the two samples, however properties slightly change for samples close to the interface between the two phantom layers. Moreover, results show that the conductivity of the aluminum powder phantom slightly changes at the interface, with a margin greater than that by which the conductivity of the Oil phantom does. These results are expected due to the interaction between both phantoms, specially the diffusion of some of the Oil solution into the aluminum powder phantom, however as shown from Figure 5.12 and Figure 5.10, the electrical properties of the core of the phantom remains almost unchanged, thus multilayer phantoms that include tissue mimicking materials prepared through any of the three explained methods can be prepared

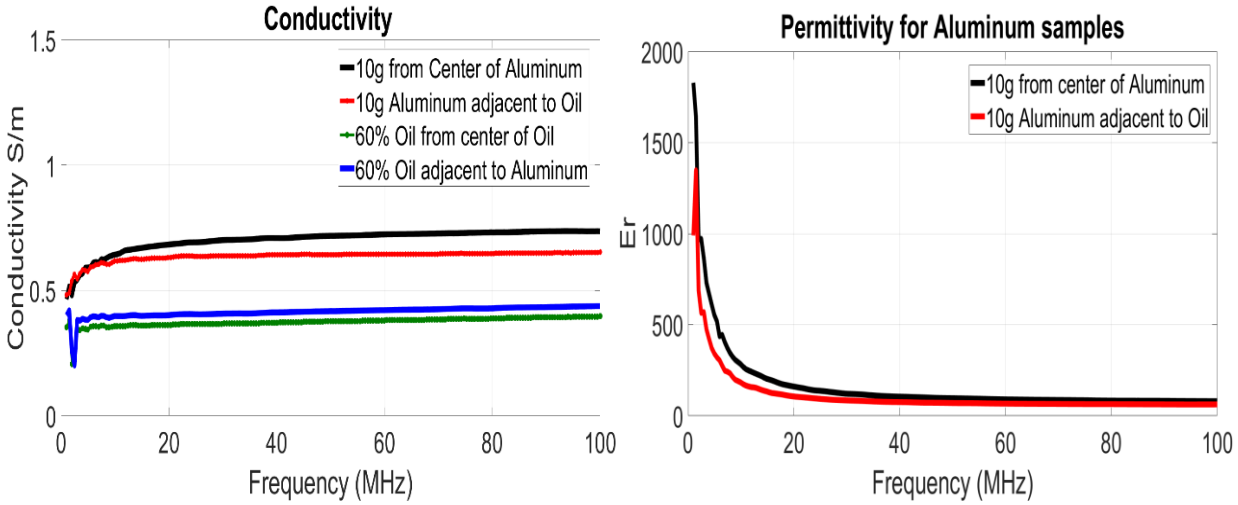

(a) (b)

Figure 5.12: a) Measured conductivity for samples taken from various locations across the composite material. B) Measured permittivity for samples from the aluminum powder phantom in the composite sample.

side by side (deposited adjacent to each other) without altering the dielectric properties of any of these materials in a significant way. These findings then permit the preparation of a multilayer arm phantom model, that consists of five different tissue mimicking materials to represent the five main body tissue layers, with a very high accuracy in terms of the dielectric properties of these tissues; conductivity and permittivity.

5.11 IBC five-layer Arm Phantom Model (IBCFAP)

5.11.1 Construction of the Phantom

Using results shown in Table 5.6, an IBC five-layer Arm Phantom Model (IBCFAP) will be constructed. To build an arm model that would cover the whole range from 100 kHz till 100 MHz, with the least possible error over the whole frequency range for all the five layers, we decided to construct the phantom model with the mixture samples shown in Table 5.7. The IBCFAP will be constructed in the form of concentric cylinders, where each cylinder will represent one of the arm tissue layers, with the inside–out order as follows: bone marrow, cortical bone, muscle, fat and finally skin. As shown earlier, layers of tissue mimicking materials prepared using any of the three methods can be prepared adjacent to each other without altering their dielectric properties. Several trials were performed to find the best methodology for preparing the whole IBCFAP in the most efficient way; to make sure that all the prepared layers are deposited efficiently adjacent to each other, eliminating any vacuum or air bubbles in between the different layers to ensure the smooth and accurate continuity at the interfaces between the different layers for the final phantom. For this reason, and to prepare inner or middle layers with certain thicknesses, phantom material molds were used as an intermediate mold. The phantom material mold used will be one of the Oil-only phantom materials, and will contain Oil-

Table 5.7. Composition of the Five Layer Arm Phantom Model

Tissue	Method Used	Concentration
Skin	Oil Only	20% Oil Solution
Fat	Oil Kerosene	80% Oil Solution
Muscle	Al/Tx-150	10 grams Al powder
Cortical Bone	Oil Only	60% Oil Solution
Bone Marrow	Oil Only	80% Oil Solution

solution concentration close to that of layer that it will be used in preparing, for the following reasons:

a) Avoid using another chemical material that might interact with the components of our prepared tissue mimicking materials, thus changing their dielectric properties in an undesired way.

b) We studied earlier in section 5.4, the effect of preparing two adjacent layers using the first two phantom preparation methods, and it showed how the dielectric properties at the core of each sample remains almost the same.

c) The Oil-only samples tend to be more solid than samples prepared through the other two methods, thus will serve better as a mold for preparing other layers.

Another difficulty we faced was getting the very thin layers out of the molds, or removing the molds off the prepared samples, in case the outermost constructed layer is very thin/delicate. For this reason, fake layers were prepared to help preserving the shape and volume for that layer, then outer layers would be constructed, then the fake layer would be removed (usually it's geometry would be distorted at this phase) and then the final layer would be poured in a molten

form in the preserved volume, to take the right shape, volume and positon in the final phantom model. Throughout the construction of the IBCFAP, only a single layer was prepared per day (being it a final layer in the arm phantom, a layer to be used as a mold for other layers and then will be discarded, or a fake layer for volume and position preservation). The length of the prepared IBCFAP is 20 cm. The ratio for thicknesses of each layer, using the standards followed in the literature [35-36] for an arm of radius 50 mm are as follows: 1.5 (skin), 8.5 (fat), 27.5 (muscle), 6 (cortical bone), and 6.5 mm (radius, bone marrow layers).

The following are the final steps for the preparation of the IBCFAP:

1- Since the bone marrow layer is delicate, a fake bone marrow tissue mimicking layer is prepared.

2- Muscle tissue mimicking material will be prepared using the Al/Tx-150, which has the weakest solid mechanical properties, so it will be prepared first then the surrounding layers will be deposited adjacent to it to fill any empty space between the layers.

3- Prepare a solid mold with the outer diameter as that of the cortical bone layer.

4- Construct the muscle tissue mimicking material (Al/Tx-150 method with 10 grams of Aluminum powder) around that mold.

5- Prepare a mold with a fake skin tissue mimicking layer (as the skin layer thickness is very thin, so the final real layer has to be poured at the end)

6- Insert the previously prepared muscle tissue mimicking material inside the mold that contains the fake skin layer, then pour in the fat tissue mimicking material in between to fill the volume in between them.

7- Remove the cortical bone mold around which the muscle tissue mimicking material was prepared, insert the fake bone marrow layer in the center, then pour the final cortical bone tissue mimicking layer (60% Oil-only sample), to fill the space between the fake bone marrow layer and the muscle layer.

8- Remove the fake bone marrow layer and pour in the final bone marrow tissue mimicking layer (80% Oil-only sample).

9- Remove the fake skin layer and pour in the final skin tissue mimicking layer (20% Oil-only sample)

10- Leave the final phantom for at least twenty-four hours for the cross linking of different mixture components.

5.11.2 Results

To test how accurate the constructed arm phantom is in mimicking the dielectric properties of the body tissues, in other words how successful is the phantom in modeling the IBC channel performance, the next step was measuring the gain / attenuation profile of the constructed arm model and comparing the results with those obtained from real subjects for validation. To carryout experimental measurements, a vector network analyzer (miniVNA Pro [37]) was used to measure the gain/attenuation profile of the constructed phantom. The experimental setup is shown in Figure 5.13, where Ag/AgCl electrodes (30 mm x 24 mm, with sensing area of 80 mm^2 [38]) were used to be compatible with the measurements performed on the real subjects. Measurements were done for a distance of 14cm between the transmitter electrodes and the receiver ones, while the separation between the electrodes at each node were varied between 5 cm and 8cm. Results for the two cases are shown in Figure 5.14, showing the gain of the arm

model phantom channel over the frequency range 100 kHz till 100 MHz. Results agree with results in shown in the previous chapter, in which it was shown that as the inter-electrode distance (separation between electrodes of the same node) increases, the overall channel gain increases due to the matching between the input impedance of the body and that of the electrodes. Yet, to validate the behavior of the channel gain/attenuation profile, the same experiment was carried out on three different real subjects, where the same experimental setup was used to obtain the channel gain/attenuation profile for the arm. Results obtained from the three subjects, together with those obtained using the phantom are plotted in Figure 5.15. As shown in the figure, results obtained using the phantom matches with those obtained from testing on real subjects. The results show how accurately the phantom models the IBC channel performance; in other words, how accurately the phantom mimics the dielectric properties of the body tissues.

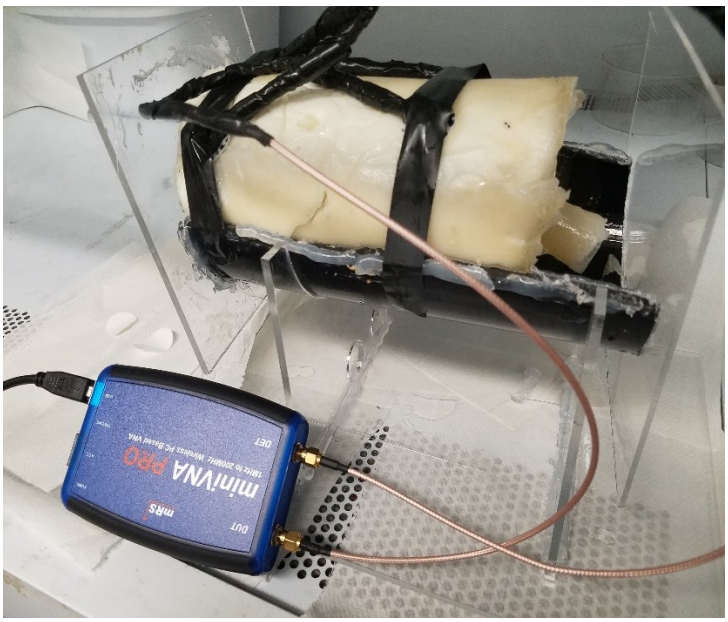

Figure 5.13. Experimental test setup for evaluating the performance of the constructed arm phantom model. A portable VNA is used to measure the gain/attenuation profile of the constructed phantom to test if it can accurately model the body communication channel characteristics, over the frequency range of interest; 100 kHz till 100MHz.

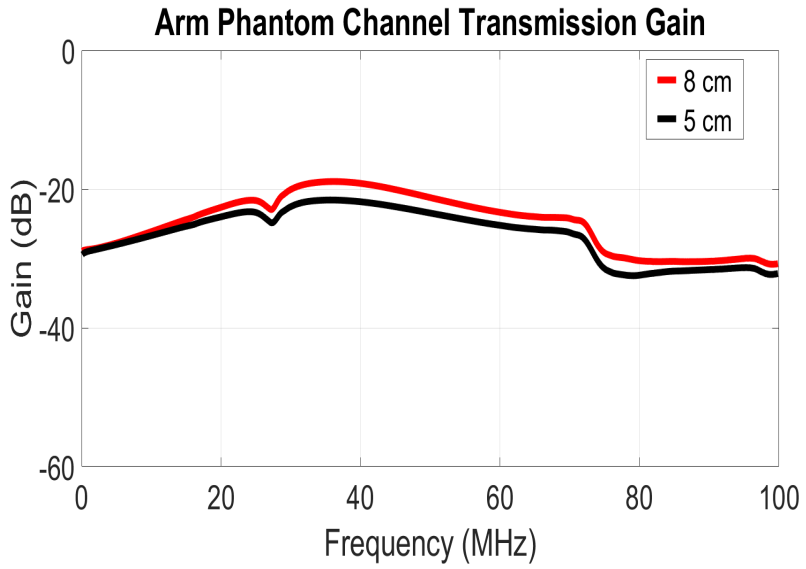

Figure 5.14. Experimental results for the channel Gain for the constructed arm phantom model measured using the miniVNA Pro, with Ag/AgCl electrodes, with the distance between the transmitting and receiving node 14cm, for two different separation distances between the electrodes of each node; 8 cm and 5cm, over the frequency range for IBC; 100 kHz till 100MHz.

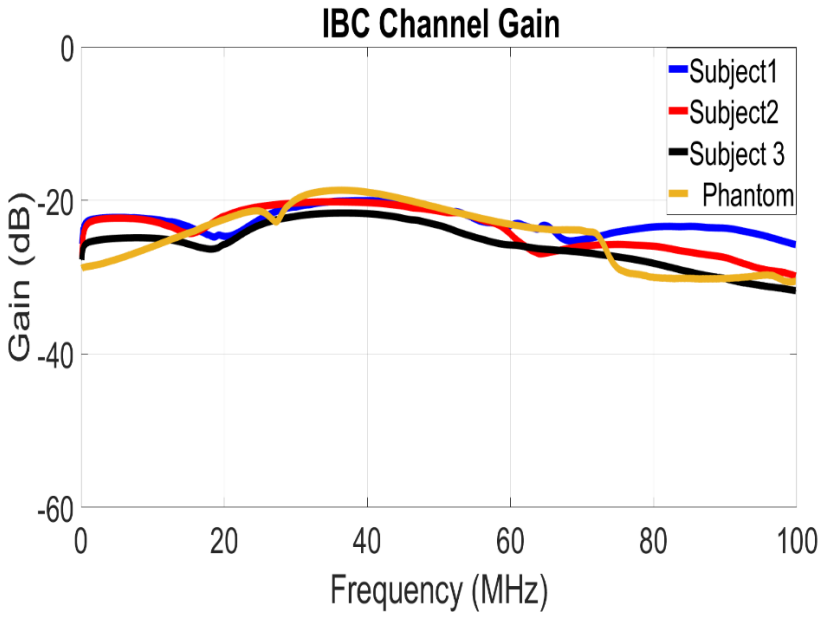

Figure 5.15 IBC channel gain results obtained from carrying out the experiment on three different subject, compared to the results obtained from the phantom, showing how accurate the phantom is in modeling the IBC channel behavior (gain/attenuation profile) over the frequency range of interest (100 kHz till 100 MHz).

Overall channel behavior is almost the same, yet the absolute values might vary from one subject to the other, which is expected due to the biological and geometric difference from one subject to the other (weight, body frame, age …etc. To the authors knowledge, the constructed phantom is the most accurate physical model designed and tested for IBC applications specifically, and body area networks applications in general.

5.12 Conclusion

Throughout this chapter, a five-layer tissue mimicking material arm phantom model was designed, fabricated and tested, to serve as a reliable and accurate test platform for intra-body communication applications, and can also be easily extended to other body area/sensors networks applications. Tissue mimicking materials were first investigated to decide on the materials that can most accurately mimic the dielectric properties of the main body tissues; skin, fat, muscle, cortical bone and bone marrow. Sensitivity of the IBC channel performance, gain/attenuation profile, to the variation of the dielectric properties of the body tissues were studied to find the best formation for a multilayer phantom that would possess the least error in modeling the IBC channel. A different method is proposed to construct the muscle tissue mimicking material, to reach accurate conductivity values, thus improving the accuracy of the whole phantom channel modeling performance. Using that knowledge, a five-layer arm phantom model was constructed [39]. The final model constructed phantom was then tested and the channel behavior (gain/attenuation profile) was measured and compared with results obtained from testing on real subjects. Results show unprecedented accuracy in modeling the human body communication channel using a physical phantom, which would pave the way for numerous possibilities in the body area networks field. With the accuracy of the phantom validated through comparison with results from real subject, the phantom can now be used for rigorous testing for

understanding more about the nature of the IBC channel, its potential, and performance in various situation/working conditions. Moreover, it offers a safe testing platform, for testing the performance of systems designed for IBC; testing power levels, radiations, communication system metrics … etc. before carrying out testing on real subjects, to improve and accelerates the system design process and guarantee safety of the human subjects at the same time. To date, this is the first accurate physical five-layer phantom arm model fabricated for intra-body communication applications covering this frequency range and with such high accuracy.

References

[1] Takashi Handa, Shuichi Shoji, Shinichi Ike, Sunao Takeda, and Tetsushi Sekiguchi. A very low-power consumption wireless ecg monitoring system using body as a signal transmission medium. In Solid State Sensors and Actuators, 1997. TRANSDUCERS'97 Chicago., 1997 International Conference on, volume 2, pages 1003-1006. IEEE, 1997.

[2] J.A. Ruiz, J. Xu, and S. Shimamoto. "Propagation characteristics of intra-body communications for body area networks." In Consumer Communications and Networking Conference, 2006. CCNC 2006. 3rd IEEE, volume 1, pages 509–513. IEEE, 2006.

[3] Keisuke Hachisuka, Yusuke Terauchi, Yoshinori Kishi, Ken Sasaki, Terunao Hirota, Hiroshi Hosaka, Katsuyuki Fujii, Masaharu Takahashi, and Koichi Ito. Simpli_ed circuit modeling and fabrication of intrabody communication devices. Sensors and actuators A: physical, 130:322-330, 2006..

[4] Marc Simon Wegmueller, Andreas Kuhn, Juerg Froehlich, Michael Oberle, Norbert Felber, Niels Kuster, and Wolfgang Fichtner. An attempt to model the human body as a communication channel. IEEE transactions on Biomedical Engineering, 54(10):1851-1857, 2007.

[5] Marc Simon Wegmueller, Michael Oberle, Norbert Felber, Niels Kuster, and Wolfgang Fichtner. Signal transmission by galvanic coupling through the human body. IEEE Transactions on Instrumentation and Measurement, 59(4):963-969, 2010.

[6] N. Cho, J. Yoo, S. Song, J. Lee, S. Jeon, and H. Yoo. "The human body characteristics as a signal transmission medium for intrabody communication." IEEE transactions on microwave theory and techniques, 55(5):1080– 1086, 2007.

[7] M. A. Callejon, D. Naranjo-Hernandez, J. Reina-Tosina, and L. M. Roa. "Distributed circuit modeling of galvanic and capacitive coupling for intrabody communication." IEEE Transactions on Biomedical Engineering, 59(11):3263–3269, 2012.

[8] Behailu Kibret, MirHojjat Seyedi, Daniel TH Lai, and Micheal Faulkner. Investigation of galvanic-coupled intrabody communication using the human body circuit model. IEEE journal of biomedical and health informatics, 18(4):1196-1206, 2014.

[9] J. Mao, H. Yang, Y. Lian and B. Zhaoi. "A Five-Tissue-Layer Human Body Communication Circuit Model Tunable to Individual Characteristics" In IEEE Transactions on Biomedical Circuits and Systems, 12(2):303-312, April 2018

[10] Ahmed T.Mobashsher and Amin M. Abbosh. Artificial human phantoms: human proxy in testing microwave apparatuses that have electromagnetic interaction with the human body." In IEEE Microwave Magazine , 16(6):42-62, 2015

[11] Garrett, John, and Elise Fear "Stable and flexible materials to mimic the dielectric properties of human soft tissues." In IEEE Antennas and Wireless Propagation Letters , 13:599-602, 2014

[12] Roelens, Laurens, et al. "Characterization of scattering parameters near a flat phantom for wireless body area networks." In IEEE Transactions on Electromagnetic Compatibility , 50(1):185-193, 2008

[13] R. Augustine. "Electromagnetic modelling of human tissues and its application on the interaction between antenna and human body in the BAN context." PhD thesis, Université Paris-Est, 2009.

[14] A. Guy. "Analyses of electromagnetic fields induced in biological tissues by thermographic studies on= equivalent phantom models." IEEE Transactions on microwave theory and techniques, 16(2):205–214, 1971.

[15] K. Ito et al. "Development and characteristics of a biological tissueequivalent phantom for microwaves." Electronics and Communications in Japan (Part I: Communications), 84(4):67–77, 2001.

[16] T. Kobayashi et al. "Dry phantom composed of ceramics and its application to sar estimation." IEEE transactions on Microwave Theory and Techniques, 41(1):136–140, 1993.

[17] H. Tamura et al. "A dry phantom material composed of ceramic and graphite powder." IEEE Transactions on Electromagnetic Compatibility, 39(2):132–137, 1997.

[18] Y. Nikawa, M. Chino, and K. Kikuchi. "Soft and dry phantom modeling material using silicone rubber with carbon fiber." IEEE transactions on microwave theory and techniques, 44(10):1949–1953, 1996.

[19] J. T. Chang et al. " A conductive plastic for simulating biological tissue at microwave frequencies." IEEE transactions on electromagnetic compatibility, 42(1):76–81, 2000.

[20] Naranjo-HernÃa¸ndez, David, et al "Past Results, Present Trends, and Future Challenges in Intrabody Communication." Wireless Communications and Mobile Computing , 2018.

[21] Ullah, Sana, et al. "A comprehensive survey of wireless body area networks." In ." Journal of medical systems , 36(3):1065-1094, 2012

[22] K. Hachisuka et al. "Intra-body data transmission for the personal area network." Microsystem Technologies, 11(8-10):1020–1027, 2005.

[23] C. Tang and R. Bashirullah. "Channel characterization for galvanic coupled in vivo biomedical devices." In Circuits and Systems (ISCAS), 2011 IEEE International Symposium on, pages 921–924. IEEE, 2011.

[24] M. Ishida et al. "Signal propagation characteristics between transceivers on human body for mhz-band near-field coupling communication." In Proceedings of the 8th International Conference on Body Area Networks, pages 453–456. ICST (Institute for Computer Sciences, Social-Informatics and Telecommunications Engineering), 2013.

[25] Y.M. Gao, S. H. Pun, M. Du, M. I. Vai, and P. U. Mak, "A Preliminary two dimensional model for Intra-body communication of body sensor networks." In ." Proceedings of the 2008 International Conference on Intelligent Sensors, Sensor Networks and Information Processing, ISSNIP , 273â˘A ¸S278, December 2008.

[26] S. H. Pun, Y. M. Gao, P.Mak, M. I. Vai, and M.Du "Quasi-static modeling of human limb for intra-body communications with experiments." In ."IEEE Transactions on Information Technology in Biomedicine , 15(6):870-876,2011.

[27] K. Fujii, M. Takahashi, and K. Ito, "Galvanic coupling enabling wireless implant communications." In ."IEEE Transactions on Instrumentation and Measurement, 58(8):2618-2625,2009.

[28] M. S. Wegmueller, S. Huclova, J. Froehlich et al, "Electric field distributions of wearable devices using the human body as a transmission channel." In ."IEEE Transactions on Antennas and Propagation, 55(7):2080-2087,2007.

[29] E. L. Madsen et al, Timothy J Hall, Tomy Varghese, Marvin M Doyley, and John B Weaver. "Anthropomorphic breast phantoms for testing elastography systems." Ultrasound in Medicine and Biology, 32(6):857– 874, 2006.

[30] M. Y. Kanda et al. "Formulation and characterization of tissue equivalent liquids used for rf densitometry and dosimetry measurements." IEEE Transactions on microwave theory and techniques, 52(8):2046–2056, 2004.

[31] Keysight Technologies [Online]. Available: https://www.keysight.com/en/pd-1000000857%3Aepsg%3Apro-pn-4291B /rf-impedance-material-analyzer?cc=US&lc=eng.

[32] S. Gabriel, R. Lau, and C. Gabriel. "The dielectric properties of biological tissues: Ii. measurements in the frequency range 10 hz to 20 ghz." Physics in medicine & biology, 41(11):2251, 1996.

[33] S. Gabriel, R. Lau, and C. Gabriel. "The dielectric properties of biological tissues: III. Parametric models for the dielectric spectrum of tissues." In Physics in Medicine & Biology , 41(11):2271, 1996.

[34] Chung-Kwang Chou, Gang-Wu Chen, Arthur W Guy, and Kenneth H Luk. Formulas for preparing phantom muscle tissue at various radiofrequencies. Bioelectromagnetics, 5(4):435{441, 1984.

[35] M. S. Wegmueller, “Intra-body communication for biomedical sensor networks,” Ph.D. dissertation, ETH Zurich, Zurich, Switzerland, 2007.

[36] Yong Song; Qun Hao; Kai Zhang; Ming Wang; Yifang Chu; Bangzhi Kang, "The Simulation Method of the Galvanic Coupling Intrabody Communication With Different Signal Transmission Paths," IEEE Transactions on Instrumentation and Measurement, vol.60, no.4, pp.1257,1266, April 2011.

[37] miniVNA PRO [Online]: http://miniradiosolutions.com/minivna-pro/

[38] Bio-medical: Kendall [Online]: https://bio-medical.com/covidien-kendall-disposable-surface-emg-ecg-ekg-electrodes-1-24mm-50pkg.html

[39] Khorshid, Ahmed E., Ibrahim N. Alquaydheb, Ahmed M. Eltawil, and Fadi J. Kurdahi. Physical Multi-Layer Phantoms for Intra-Body Communications. *IEEE Access* 6 (2018): 42812-42821.

Chapter 6

Applications Based on IBC

6.1 Introduction

In the previous chapters, we studied the nature of the IBC channel, modeled it through an accurate circuit model, then validated and compared the model to a FEM simulation model as well. We then prepared a reliable testing platform for IBC and body area networks in general, through the multilayer physical phantom proposed in chapter 5, to facilitate the research effort in this field, through providing a reliable and accurate test setup for carrying out extensive measurements that would aid in further understanding the nature of the channel as well as system design constraints. It also provides a safe test platform, as a step to validate the designed system safety, before taking it to testing on real subjects. Finally, the physical model was validated through comparing the obtained results with those obtained from tests on real subjects. In this chapter, we provide more insight regarding the nature of the IBC channel, through providing the experimental results for testing on the IBC channel in different testing scenarios. These results are then used in a number of applications, including the stress profile analysis, obtaining a statistical model for the channel, for use by other applications and last but not least, biometric identity, demonstrating a prove for the tremendous and unique potential that this novel technology possess in different fields of applications.

6.2 Experimental Setup

As mentioned in chapter in chapter 5, testing was performed using the miniVNA Pro [1]. The miniVNA Pro is a handheld, portable Vector Network Analyzer that covers the frequency range of 100 KHz till 200 MHz. In addition to its accuracy, the device has a number of advantages that makes it an appropriate candidate for the experimental setup:

- Covers the whole frequency range of interest
- Portable, allowing the subject under test to move freely, thus more testing scenarios are made possible
- Measures and reports the S-parameters, which we are interested in (especially the S21, which represents the channel gain)
- Maximum RF output power is 0 dBm, thus it adheres to the health safety limits mentioned earlier [2-3]

Testing was performed on five real subjects in addition to two models of the five-layer's arm phantom that we proposed in the previous chapter, and were prepared in our lab. Testing was done after getting approval from the UC Irvine Institutional Review Board (UCI IRB) for our human subjects research protocol, under the number: HS# 2017-4049. Off the self Ag/Agcl biomedical electrodes were used for the testing. Electrodes were placed on the arm and measurements were carried out for distances between transmitter and receiver of 10 cm, 15 cm and 20 cm. Spacing between electrodes of the same node are kept at 5cm apart from each other. Measurements for each scenario are taken over 50 different instances, where the average is then taken. These different trials will then be used for getting the statistical model for

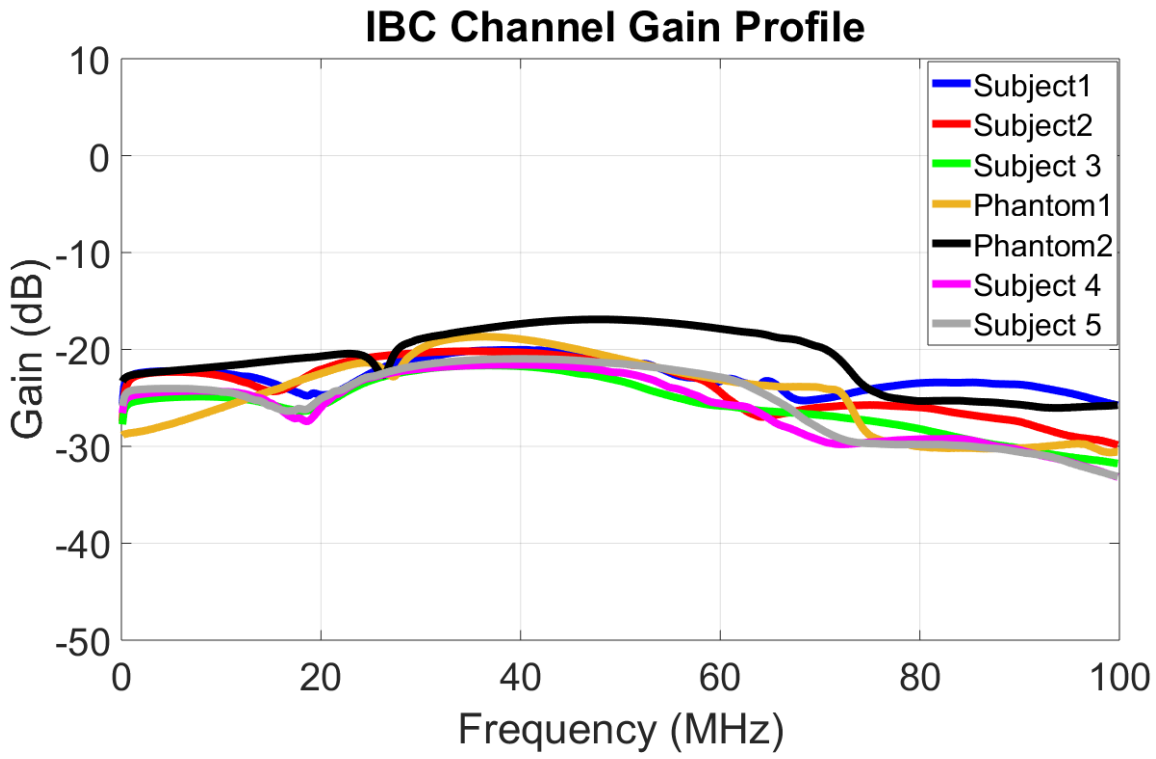

Figure 6.1 IBC channel gain results obtained from carrying out the experiment on seven different subject; five real subjects and two arm phantom models over the frequency range of interest (100 kHz till 100 MHz), for a transmitter – receiver distance of 10 cm and separation between electrodes of 5 cm.

representing the channel. Results for the total seven subjects, for a TX-RX distance of 10 cm is shown in Figure 6.1. As can be seen from the figure, although the channel response seems very similar in behaviors, each subject still has a unique response, due to the biological and geometrical differences as outlined in previous subjects. To study the effect of different parameters, and to validate the deductions and conclusions reached in the previous chapters regarding the nature of the channel and the relation between different parameters, we carry out the measurements in different scenarios. Same behavior is observed over all subjects, so we will show the results for a single subject, although the conclusions hold for all subjects. Also from Figure 6.1, it is clear that the gain drops at higher frequencies, especially around the 60 MHz, due to various reasons, as the impedance values increase, as well as the body antenna effect,

where at the high frequencies, the human body operates as an antenna radiating the signal power into the air; can be considered as leakage/loss power as demonstrated in [4]. In Figure 6.2, we examine the effect of the distance between the transmitter and the receiver (in the miniVNA pro case, by the transmitter and the receiver we mean the two different ports of the VNA, as the IBC channel is considered as a two port network), where the distance was varied between 10, 15 and

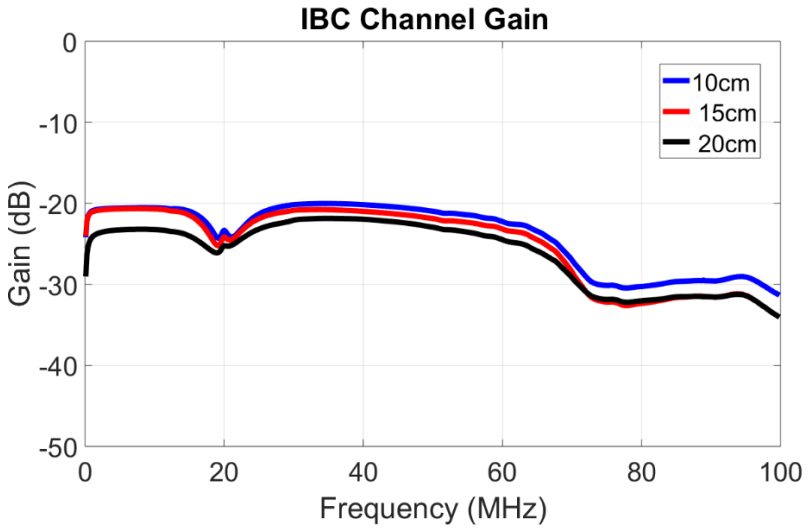

Figure 6.2 IBC channel gain for subject 1 when varying the distance between the transmitter and the receiver to be at 10, 15 and 20 cm and separation between electrodes of each node is 5 cm.

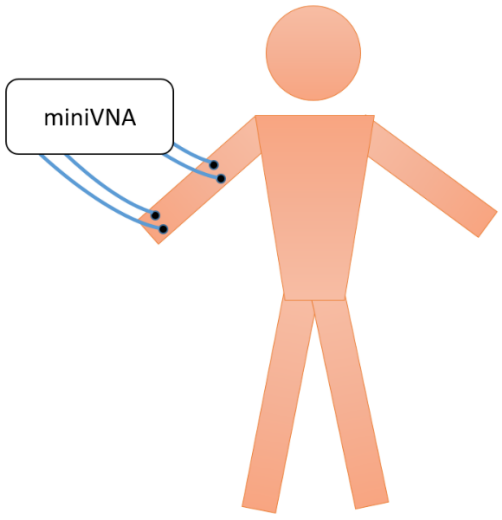

Figure 6.3. Position of the electrodes for the results shown in Figure 6.2

20 cm, while the separation between both electrodes of each node are kept at 5 cm apart, as shown in Figure 6.3.

As expected, the grain drops as the distance between the transmitter and the receiver increases, since the propagation path increase, thus the signal suffers more power loss (dissipation) along the way, thus the channel overall gain drops. In Figure 6.4, we study the effect of varying the separation between transmitter and the receiver for two scenarios; once when the transmitter and receiver are 20 cm apart, yet placed on the same arm, and the other case when the transmitter is placed close to the wrist of one arm and the receiver electrodes at the wrist of the other arm as shown in Figure 6.5.

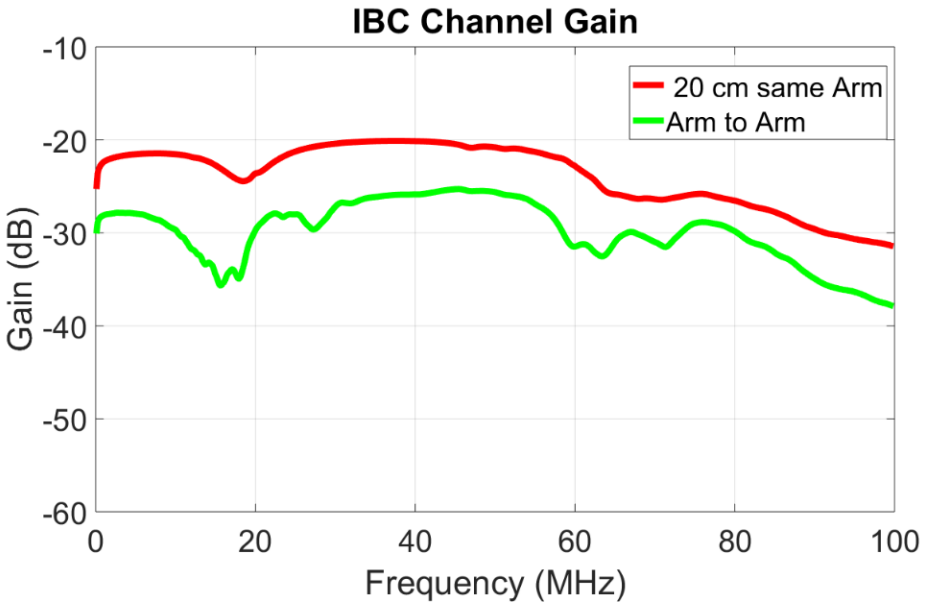

Figure 6.4. Studying the effect of varying the separation between transmitter and the receiver for two scenarios; once when the transmitter and receiver are 20 cm apart, yet placed on the same arm, and the other case when the transmitter is placed close to the wrist of one arm and the receiver electrodes at the wrist of the other arm as shown in Figure 6.4.

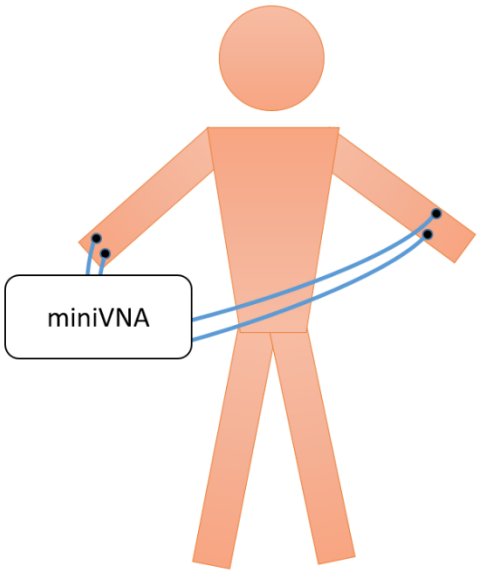

Figure 6.5. Position of the electrodes for the results shown in Figure 6.4, for the arm to arm case

To study the effect of the body posture as well as the movement, we carried out the measurement over one arm, where the transmitter is placed near the wrist while the receiver electrodes are placed just after the joint elbow of the same arm. Measurements were performed for three different scenarios;

a) when the arm is still (no movement) and stretched
b) when the arm is bent at 90 degrees, but still, no movement
c) when the arm is moving between both the first two scenarios (stretched and bent at 90 degrees)

Results are shown in Figure 6.6, and the electrodes positions are shown in Figure 6.7. Although the channel behavior remains the same, bending the arm or moving it, does affect the channel gain value, especially at higher frequencies. This change is also observer in the case when the arm is bend at 90 degrees and stays still as well.

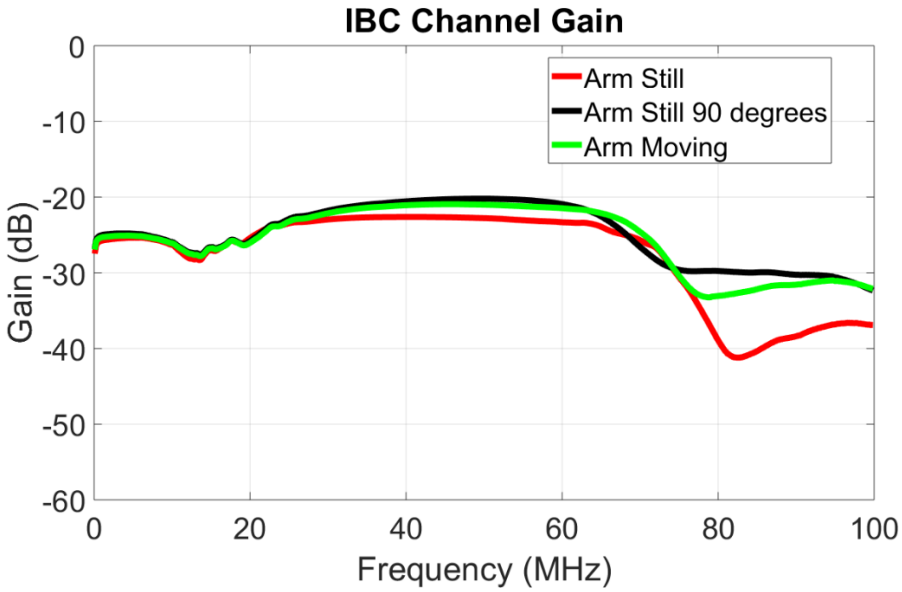

Figure 6.6. Results for when the electrodes are placed at the wrist, and after the elbow of the same arm. The arm is first kept stretched and still, then bent at 90 degrees, then moving between both positions.

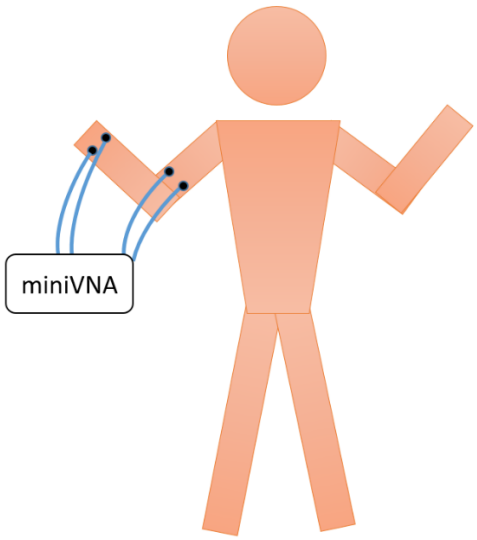

Figure 6.7. Position of the electrodes for the results shown in Figure 6.6, where the arm is bent at an angle of 90 degrees, then the arm is moving between the stretched position and the bend position.

Finally, to cover all the possible positions for the sensors, we compared the results of having the sensors on the same arm (when 20 cm separated), with that when having one node on the wrist, while the other is on the leg (close to the ankle), as shown in Figures 6.8 & 6.9, As expected, there is a drop in the gain for the arm–to-leg case as the propagation path increases.

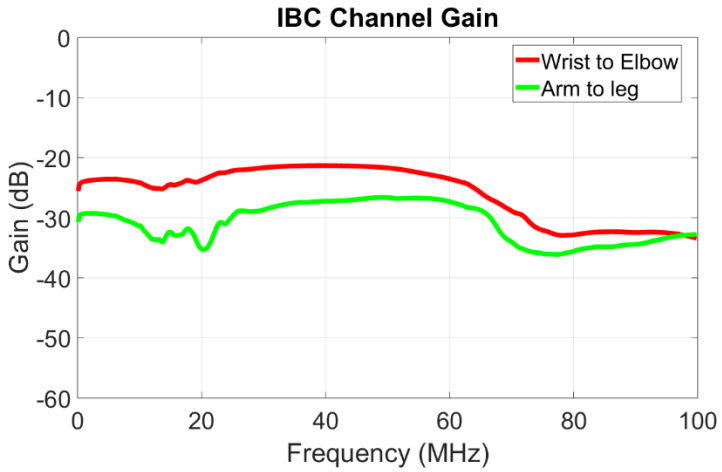

Figure 6.8. Comparison between results for the placing the communicating nodes/sensors/ports on the same arm, with the scenario shown in Figure 6.7, where one node is at the wrist while the other is closer to the ankle.

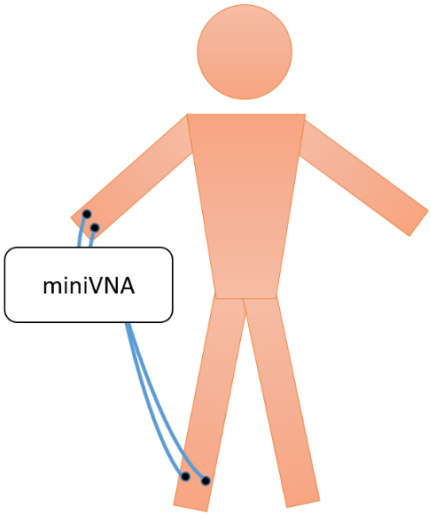

Figure 6.9. Position of the electrodes for the results shown in Figure 6.7, one node is at the wrist while the other is close to the ankle (mimicking a set of accelerometers for motion/fall detection scenario for example)

6.3 Stress Profile Analysis Platform

As mentioned in chapter 1, IBC technology possesses a huge potential for body area networks, especially for the ones that requires a network of distributed sensors for gathering physiological data. IBC body area networks can thus offer much more compact, ultra-low power and a highly secured solution for these applications, that was not really practical earlier with the currently available wireless solutions, since they are bulky, power hungry and security has always been a concern. Among such applications is ***stress profile analysis***. Since human resources are undoubtedly considered to be the most crucial and valuable asset in any organization, ensuring the personal safety and efficiency of the members of the organization is a major concern. Monitoring the performance of vital body functions (body temperature, blood pressure, heart beat, electrocardiogram, stress profile) for personnel that operate in stressful and harsh environments such as firefighters, policemen and workers in mines, is thus a necessity for their safety, and has to be conducted seamlessly without any hindering to their efficiency on the field. Under conditions of stress for example, the sympathetic division of the autonomic nervous system prepares the body for a rapid defense reaction by modulating hemodynamic patterns [5]. Major responses include increased heart rate and contractile force, dilation of blood vessels in skeletal and cardiac muscles, and constriction of blood vessels that supply internal organs. The redistribution of blood flow in superficial vessels causes changes in skin temperature that can be detected through having the appropriate sensing elements distributed over various locations along the body. The personal telemetry biofeedback for assessing the personnel‘s stress profile/status, provided by sensors, can be used by the officers themselves to modulate their response, or monitored remotely at the command and control center to decide on appropriate actions. In addition to the use cases discussed above, stress profile analysis scan also be used for

civilian applications, for ensuring the physical and mental wellbeing of people, and to maintain a healthy and less stressful lifestyle. A comprehensive study was carried out to pin out the most vital body signals and parameters (temperature, blood pressure, heart rate ...etc.) that need to be monitored and would be adequate to accurately identify the personal's mental and physical state, including his/her stress profile [5 -12].

6.3.1 Physiological Signals

Numerous research [5-14] has been done to try and associate the state of stress, when a person starts getting stressed or develop a stressful sensation, and the change in the body's various physiological signals. Research was able to identify certain physiological signal and parameters that show certain behavior when the person develops certain sensations, like stress, fear, joy ...etc. Among the physiological signals that showed behavior correlation with the change in a subject's sensation /mood are: Heart Rate (HR), Heart rate Variability (HRV), Skin Temperature (ST), Galvanic Skin Response (GSR), Respiration rate, Blood Volume Pulse (BVP) and finally the electrical activity of the muscles.

Heart Rate: determines the number of heart beats per minute. An electrocardiogram (ECG) can be used to determine the heart rate, where it records the electrical activity of the heart using electrodes placed upon the body. The ECG signal is usually periodic, as shown in Figure 6.10, consisting of three parts: the P wave, the QRS complex and the T wave. The heart rate is measured using the R waves as the reference; in other words, through the R-R interval.

Heart Rate Variability (HRV) [15-16]: Heart rate variability (HRV) is the temporal variation between sequences of consecutive heart beats. On a standard ECG, the maximum upwards

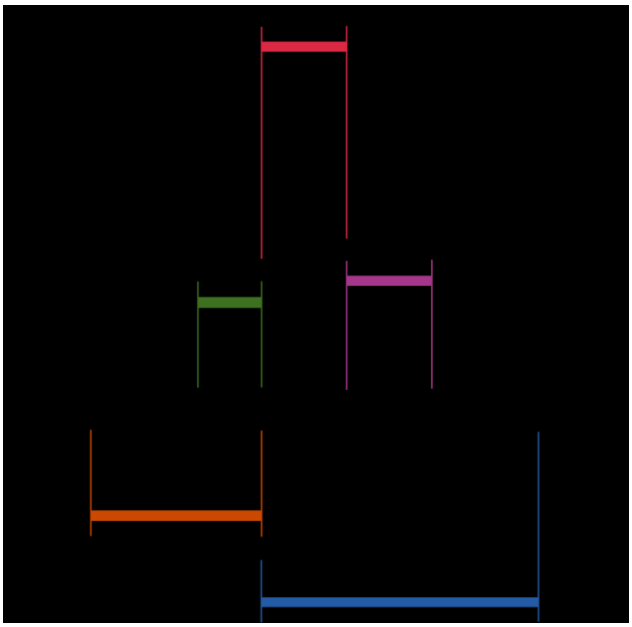

Figure 6.10: ECG signal [17].

deflection of a normal QRS complex is at the peak of the R-wave and the duration between two adjacent R-wave peaks is termed as the R-R interval. The ECG signal requires editing before HRV analysis can be performed, a process requiring the removal of all non-sinus-node originating beats. The resulting period between adjacent QRS complexes resulting from sinus node de-polarizations is termed the N-N (normal-normal) interval. HRV is finally the measurement of the variability of the N-N intervals.

Galvanic Skin Response (GSR): The sweat glands and the skin blood vessel are only connected to the sympathetic nervous system, not the parasympathetic one. Sweat secretion increases the conductance of the skin proportionally, thus the GSR is measured by the conductivity of the skin. The density of sweat glands is highest around the palms of the hands or the feet, so this is usually where it is measured.

Blood Volume Pulse: An alternative method for measuring the heart rate, where Photoplethysmogram (ppg) is used to measure the differences in light caused by the blood

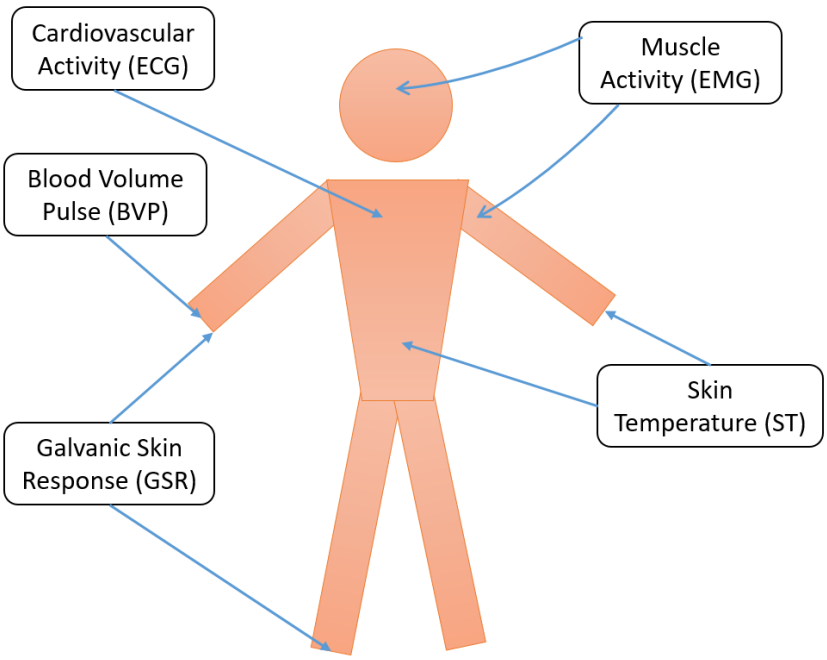

Figure 6.11: Physiological signals of concern, for monitoring a person's stress activity, level and profile, and the potential location on the body where the bio-sensors to monitor such vitals are to be placed.

volume pulsations. Photoplethysmogram can measured by using a pulse oximeter which illuminates the skin and measures changes in light absorption.

Skin Temperature: Under conditions of stress for example, the sympathetic division of the autonomic nervous system prepares the body for a rapid defense reaction by modulating hemodynamic patterns [5]. One of the major responses include the constriction of blood vessels that supply internal organs. The redistribution of blood flow in superficial vessels causes changes in skin temperature in various body locations, including but not limited to, a subject's back as well as the distal phalanx of the thumb.

Electromyogram (EMG) [14]: records the electrical potential generated by skeletal muscle cells. Needle electrodes are used in this purpose, usually placed on an arm, a leg or a shoulder. Facial electromyography is also common, where electrodes are placed upon various facial muscles.

A summary for the potential physiological signals to be monitored for evaluating the subject's stress level/profile, with the potential locations where the sensors would be placed to monitor these signals [5-14], is shown in Figure 6.11.

To determine the stress profile (whether a person is stressed or not), a workflow/methodology is proposed in Figure 6.12. The first step is monitoring certain vital signals, as explained earlier, through having a network of distributed sensors at various locations across the body. Machine learning algorithms would then be used to train models to be able to associate the change in the physiological signals with whether a person is stressed or not. To do so, certain features will be extracted from these physiological signals, as the mean, standard deviation, amplitude, maximum, minimum and others. These features will then be extracted from the measured signals and fed as inputs to the machine learning algorithms to train the models. The output would then be the state of the body; whether the person is stressed or not. A summary for the features that proved to be distinguishable in determining whether a person is stressed or not, as proven in the literature [5-14] is shown in Table 6.1.

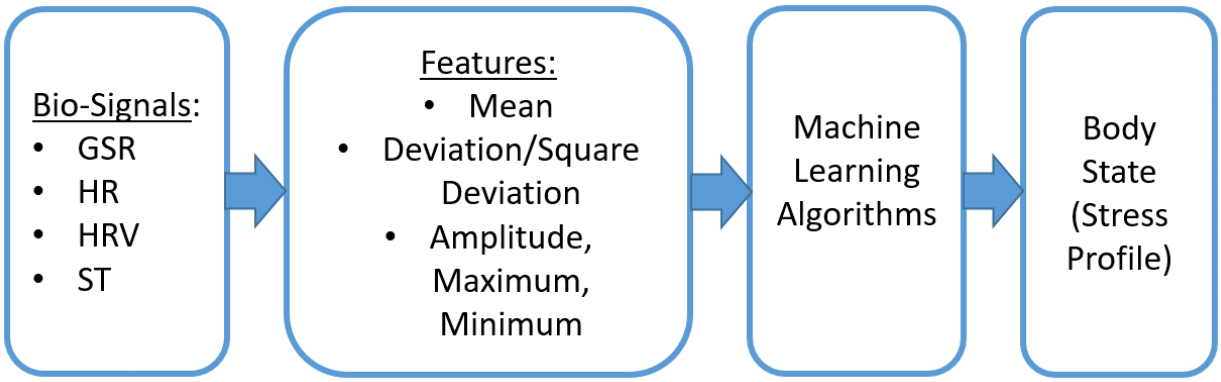

Figure 6.12: Methodology/workflow for determining the body state including; the test that will be applied for stimulating the response, the Bio-signals that will be captured and features to be extracted.

Table. 6.1. Bio-signals to be captured and the features of interest regarding each

Heart Rate (HR)	Hear Rate Variability (HRV)	Galvanic Skin Response (GSR)	Skin Temperature (ST)	EMG
Mean	Global max of peak-to-peak intervals (PPI)	Number of local maxima and minima	Amplitude	Raw Mean
Amplitude	Global min of PPI	Global maximum and minimum	Mean	Rectified RMS
Standard Deviation	Mean of PPI	Difference between max and min	Deviation	----------
Mean of absolute values of first differences	Standard deviation of PPI	Normalized mean	----------	----------
----------	LF/HF ratio	Deviation	----------	

6.3.2 IBC Design Platform

Using the knowledge that we presented throughout the previous chapters, as well as in first part of this chapter, we were able to provide a unique and comprehensive platform for IBC applications design. Since stress profile analysis is a good show case for the potential of the IBC technology, due to its need for a network of distributed sensors, thus minimizing power and area is crucial, we designed a platform with the knowledge that we developed in this field, that would provide the basic foundation for the design of a network of sensors for this application, as well as for other similar applications that would use data gathered from different distributed biosensors across the body. The basic architecture of the platform is shown in Figure 6.13. The main goal of the platform is providing a step by step solution that would provide the basic system design parameters for a certain application that would adopt the IBC technology for the communication between its nodes, being them sensors, actuators, relays, processing units, central hub, or a wireless gateway. The platform would also provide the exact mixture for building the appropriate multilayer phantom, that is designed specifically for the application in hand to ensure

accurate dielectrically properties for the targeted frequency range and to provide a safe testing platform once the system's hardware is designed, before testing it on real subjects.

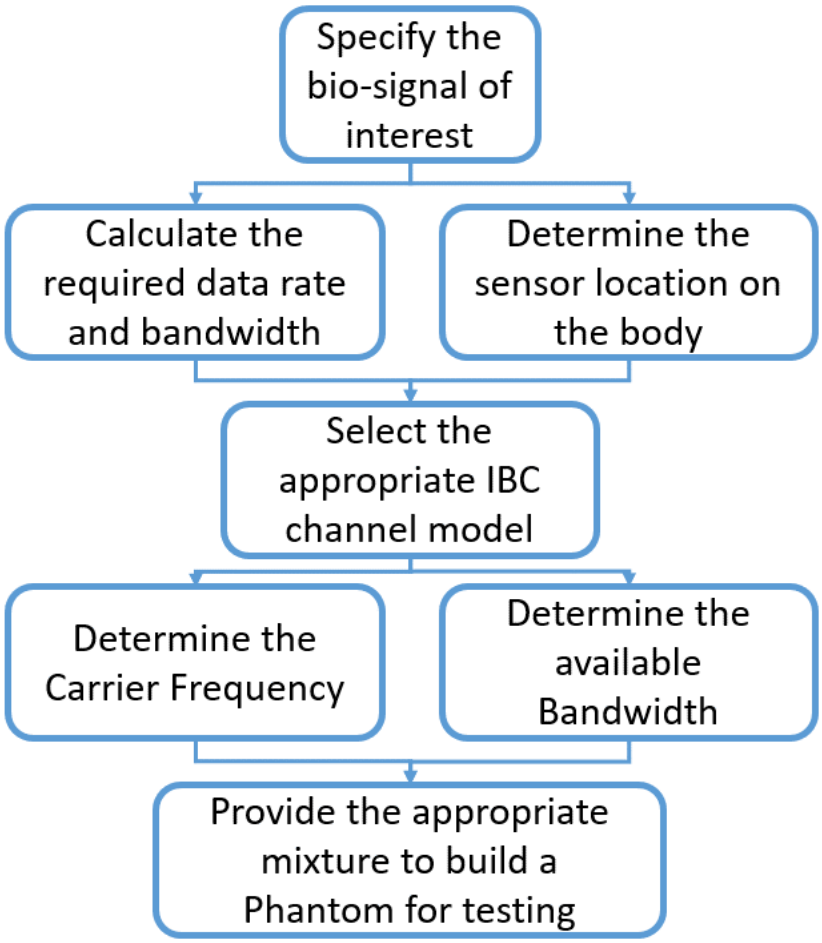

Figure 6.13: The basic flow chart for the proposed IBC platform for designing body area networks, like stress profile analysis system, using the IBC technology.

The basic steps in the platform's workflow are as follows:

1- According to the application, the designer selects the bio-signals of interest that needs to monitored.

2- The platform then calculates accordingly the adequate/standard data rate and bandwidth needed for the correct and accurate transmission of each of these signals, as shown in Table 1.1.

3- The platform also determines the standard location on the body where the sensor should be placed for accurately monitoring the signal of concern, while the user then specifies the distance between each of these sensors and the next node

4- With the knowledge now of the locations of the communicating nodes and the separation between each of them, the model then loads the appropriate IBC channel model, from the experimental results that we provided earlier in this chapter, which covered the basic potential locations where the sensors are expected to be located

5- The platform then uses these channel models, together with the bandwidth requirements determined earlier, to find the best carrier frequency at which gain is maximum, and the available bandwidth sufficient to cover the transmission requirements for the signal.

6- Finally, with the knowledge of the frequency range of interest, the platform then uses the information presented in chapter 5, Table 5.6, to determine the mixture and concentration of constituting materials needed to build a multilayer phantom, that would be designed specifically for this application (mimics the dielectric properties of the body with the highest possible accuracy)

For the ease of usage, we designed a Graphical User Interface (GUI) application, using MATLAB, that automates the whole platform process flow that we just explained. The interface for this GUI application is given in Figure 6.14 (a). The inputs for the platform are simply the application or bio-signal of interest, the number of channels needed (in case of ECG and EMG signals) and the spacing between the communication nodes; the sensor responsible for capturing

the signal, and the following node, that can be another sensor, a repeater or a wireless gateway for example. The application then processes these inputs, and goes through the steps explained earlier to generate the following outputs:

- The suggested carrier frequency, and the associated available bandwidth
- The channel gain/attenuation profile, that depends on both the sensors location on the body as well the separation between them
- The appropriate phantom preparation method, required materials and their concentrations, for constructing the appropriate phantom for that certain frequency range.

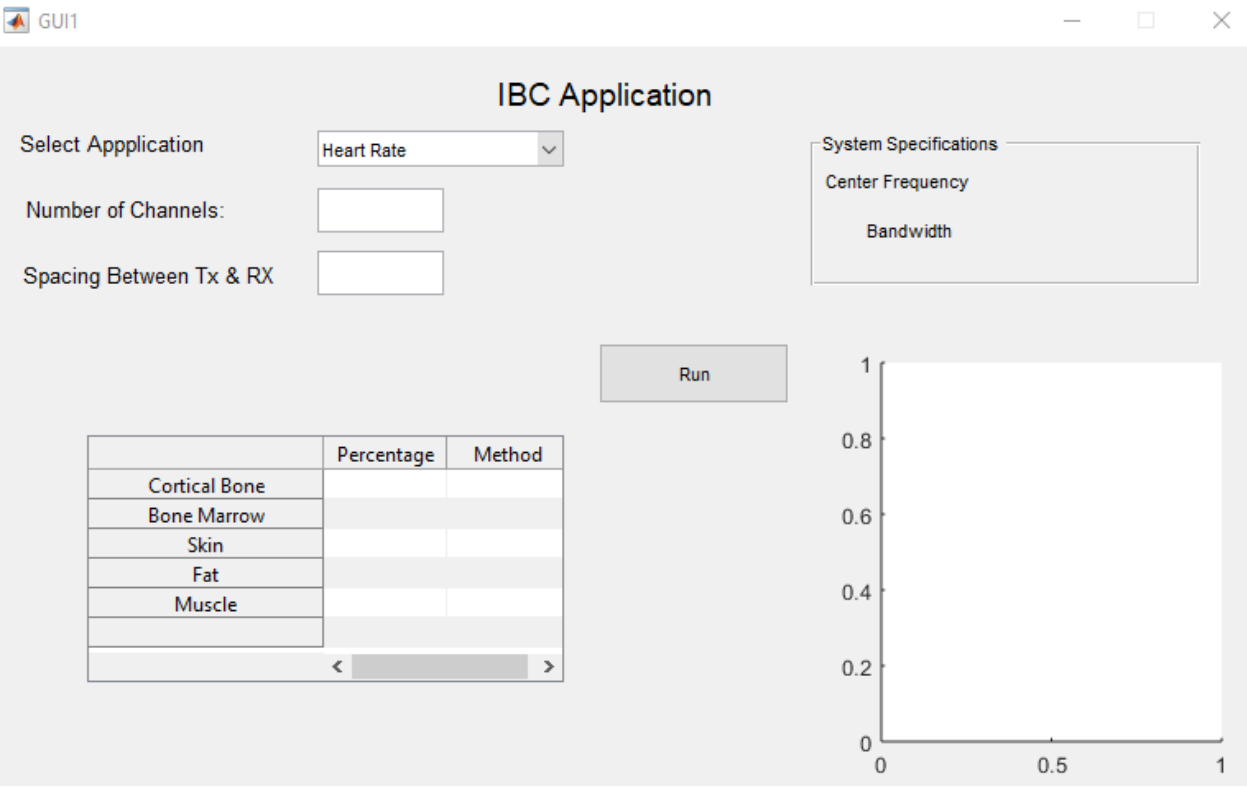

Figure 6.14 (a): The GUI application interface for the proposed IBC platform.

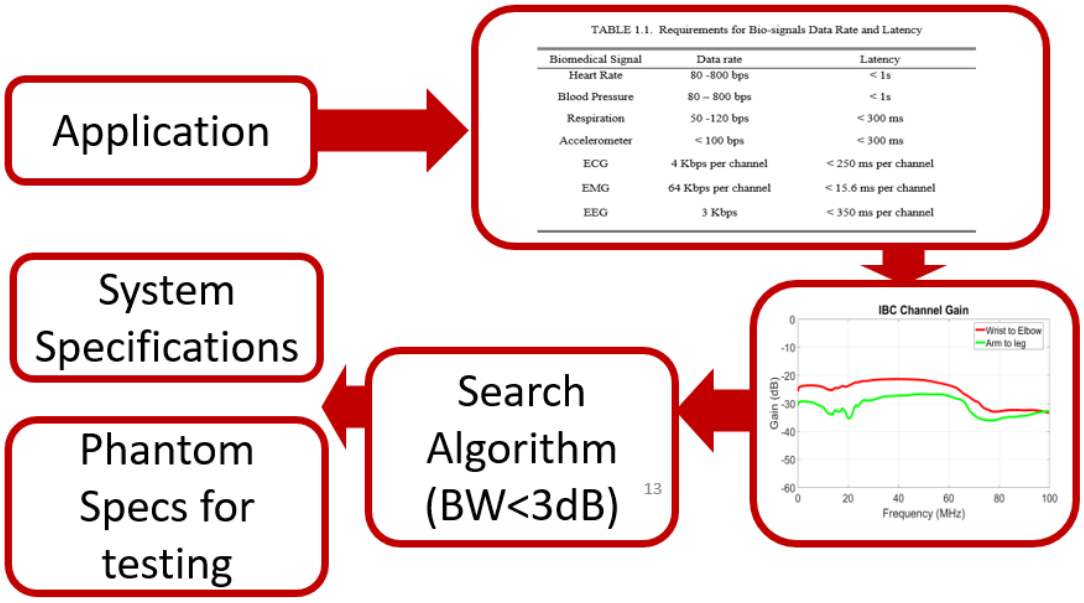

Figure 6.14 (b): The followed process/steps for the proposed automated IBC design platform.

With the targeted signals and sensor locations suggested in Figure 6.11, a prototype for the platform was designed, covering the suggested bio-signals, the shown locations on the body, and the standard data rates determined in Table 1.1, as shown in Figure 6.14 (b). An example for the available options for bio-signal that are incorporated in our platform, is shown in Figure 6.15. An example for the final outputs, for a case when ECG is selected, with only 2 channels and with 20 cm separation between the communication nodes are selected, is shown in Figure 6.16, where the carrier frequency and bandwidth values are given in Hz, and the appropriate experimental channel model is plotted. The final frequency band for that application, with the 3dB bandwidth for this application is plotted in Figure 6.17.

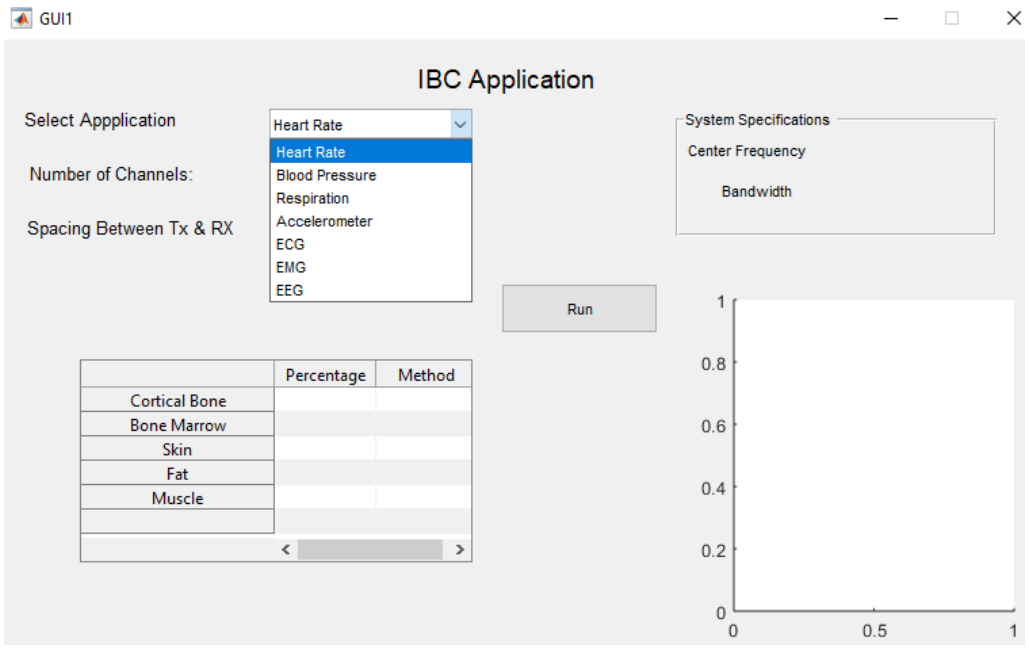

Figure 6.15: An example for the applications/bio-signals incorporated in the platform.

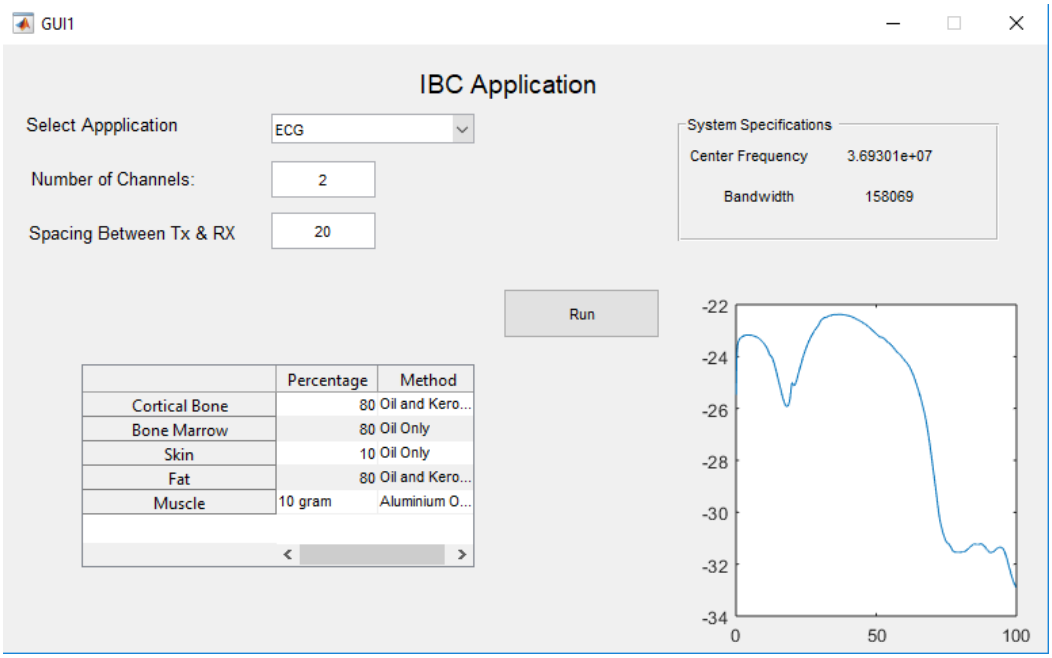

Figure 6.16: Results for an ECG example, with two channels and a separation of 20 cm between the senor and the next communicating node

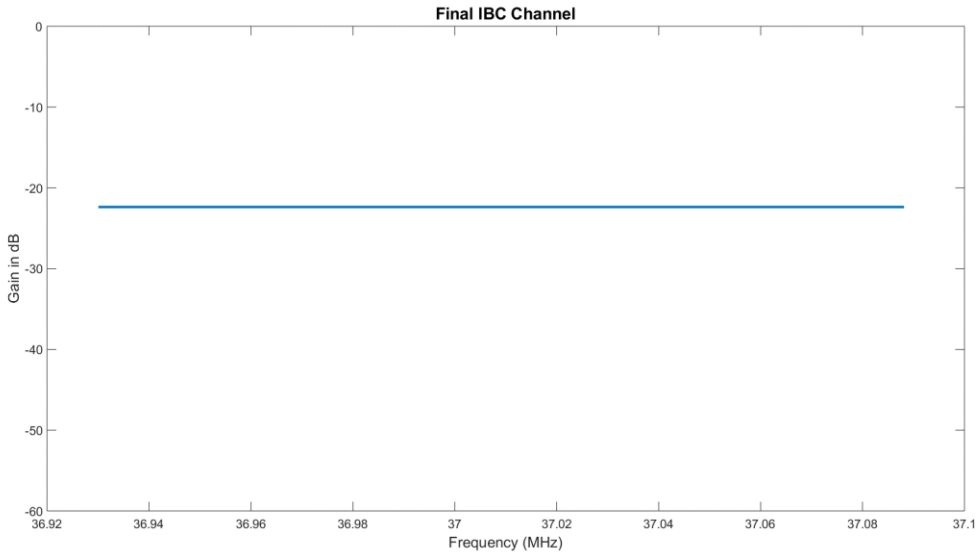

Figure 6.17: The gain available within the bandwidth suggested for communication for the case shown in Figure 6.16.

With the proposed IBC design platform, we combine the knowledge and information that we developed throughout this project, to provide the system designers with a very powerful tool that would provide the basic system design parameters, as well as a safe and accurate testing platform - the phantoms, for a variety of healthcare applications, such as stress profile analysis systems, that would rely on body area networks of sensors, that are communicating together efficiently and securely through the novel IBC technology. The platform is highly flexible and modular, thus can easily be continuously updated to include more applications, more IBC channel models as more data is gathered, as more design rules and constraints, to facilitates the IBC system design process, provide an early prototyping solutions, as well as building safe and accurate testing platforms to ensure the system's safety and functional operation, before carrying out any further testing on human subjects.

6.4 Biometric Identity

Results presented throughput this work shows how the body's behavior as a signal transmission channel, depends on different features, both biological and geometrical, and is thus unique to each person. The characteristics of this channel can therefore be used as a unique identifier for each individual, hence the idea of using the channel characteristic (gain/attenuation profile) as a biometric identity. An advantage for using this proposed biometric over the conventional biometrics currently used, as the fingerprints, is that it can provide periodic and continuous identification/authorization with no required effort from the person; the two nodes can communicate very single period of time for re-authorization while the person is working or doing a normal activity, while in the case of fingerprint for example, the person has to touch the scanner every single instance where authorization is needed. Moreover, some biometrics can be hacked or replicated, yet the biometric used in this invention is extremely hard to replicate, since the signal has to physically travel inside the body first before being picked up by the RX node.

The concept to sue IBC technology was first introduced, yet in a different form, in 2004 [18], through a device called Redtackon. The device was a prototype for a transceiver system that utilizes the Electrostatic (Capacitive) coupling IBC technology for communications. Among the applications intended for Redtackon was authentication, as shown in Figure 6.18, where the IBC channel just acts as s medium for connecting the ID or tool used for authentication with the other end where authentication is required; in other terms, the body just acts a safe communication channel for transporting the identity information, without the actual IBC cannel characteristics being used in the identification process [18-20]. Research then followed, and in 2007 authors in [21] suggested using the IBC galvanic channel characteristics as a metric for identification among different subjects. Using the setup shown in Figure 6.19, testing was performed on five

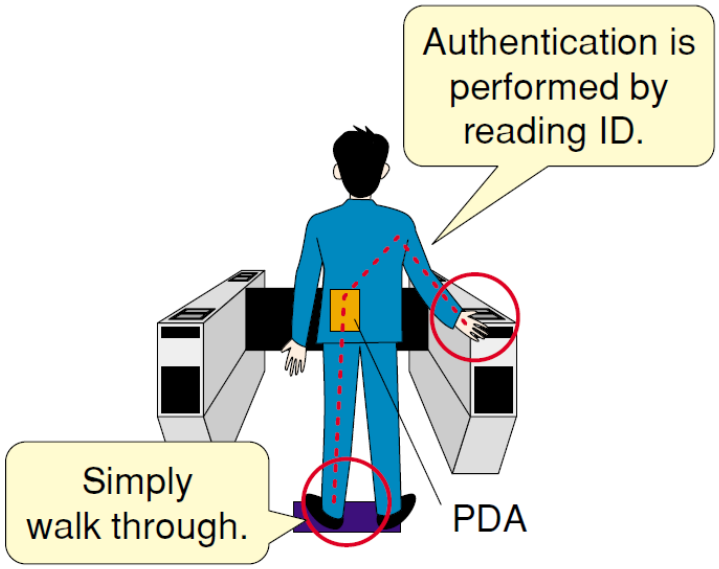

Figure 6.18: Communication from a device on the person, containing the authentication data, to an external embedded system that requires authentication, through the body that closes the circuit for the flow of data to occur (more like wired communications)

subjects, where a technique based on Euclidian distance technique, calculated using the sum of the power spectrums at different frequency bands; 0 -30 MHz, 30 MHz – 60 MHz and finally from 60 MHz till 90 MHz was used to calculate the similarities between certain measured datasets and the different subjects to identify which subject it belongs to. The best verification rate of 58% was obtained in the 30-60MHz sub-band. In [22], the same research group used the galvanic IBC channel response, but this time when the TX and RX are on the palm only, as shown in Figure 6.19. Support Vector Magnitude (SVM) machine learning technique was use, but still an identification error of 25 % (verification accuracy of 75 %) was achieved. In [23] authentication using biometric pulse response was introduced, where the subject under test holds brass cylindrical electrodes in his/her hand for signal flow, then a pulse is transmitted through the body, where the pulse response is recorded using an oscilloscope and is used for verification and authentication purposes.

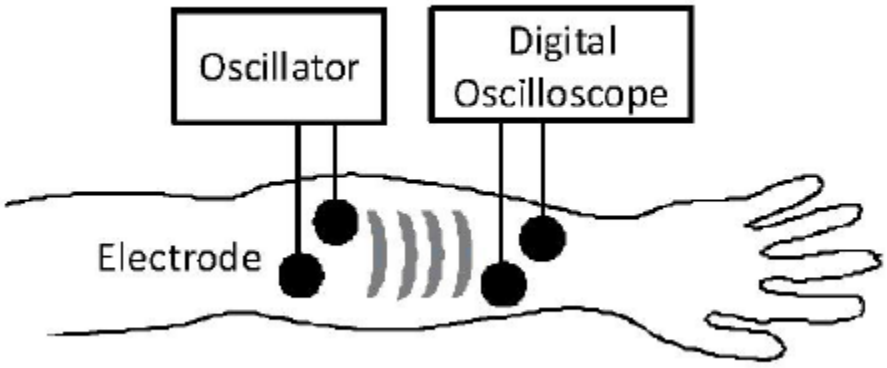

Figure 6.19: The method proposed in [21] for using the galvanic channel response for verification and subject identification, with an accuracy of 57% achieved.

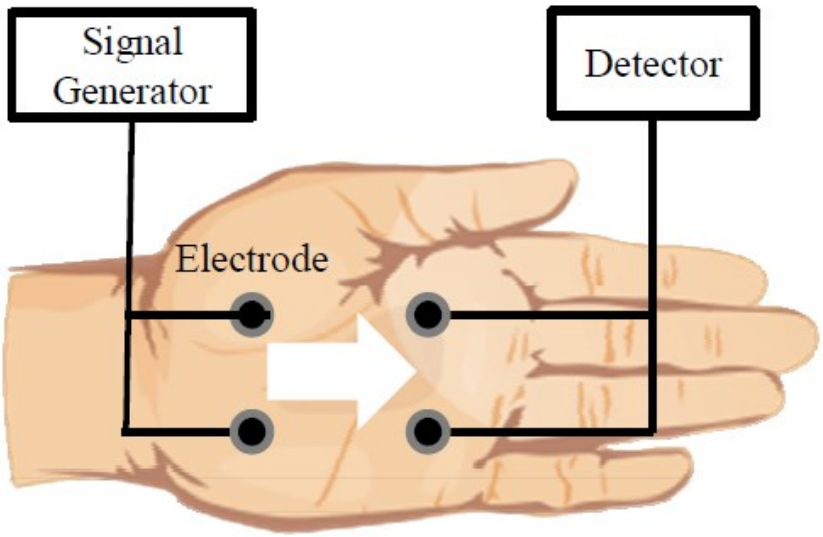

Figure 6.20: Measurement of the intra-palm propagation signal [22]

Although these trials did prove that IBC technology does poses the potential to be used as a biometric identity, verification accuracy results were still not very encouraging, or the setup used is not very practical for a daily life scenario. In order to fill this gap, we proposed a simple yet effective method for using galvanic IBC channel response as a biometric identity for both subject verification and authentication.

6.5 Our Proposed Solution for Biometric Identity

Using the knowledge we developed in the field, as well as the experimental measurements we obtained, an accurate solution for using IBC channel characteristics as a biometric identity is proposed and tested. Our methodology is tested for the purpose of both biometric identification and authentication.

Biometric authentication refers to identify confirmation or verification. When a user claims a certain identity, authentication entails deciding whether the claim is correct or not. The goal of the biometric classifier is to compare the current sample to the known template for that user, as a kind of 1:1 comparison [23].

Biometric identification differs from authentication where the current sample comes from an unknown user, and the job of the biometric classifier is to match it to a known sample, being a 1:n comparison, where n is the number of subjects.

The proposed system follows the methodology described below:

1- An electrical signal is coupled into the body at the transmitter (TX) node, then picked up at the receiver nodes (RX).

2-The received signal would then include information about the channel that it was transmitted through - the body in this case - which is unique for each person and can thus be used as a biometric identifier.

3-The above procedure would be repeated automatically a couple of times (taking few Nano to Micro-seconds) for the calibration of the system, to extract unique features to be able to accurately identify this subject

4-Once the system is calibrated the person's identity will thus be stored, yet still will be unique and relevant to the specific system (hardware) used, adding an extra layer of security.

5-Continuous authentication/identification/authorization can then take place, where a predefined signal is then transmitted from the TX node, every specific time interval.

6-The received signal is picked up at the RX node and further processed through machine learning algorithms to complete the identification process and verify the identity of the subject, after comparing the received signal with previously recorded identifiers that are unique for that subject.

The experimental setup we used is the same as defined earlier in this chapter, where the miniVNA is used to obtain the galvanic IBC channel gain (S21), for different transmitter and receiver positions along the arm

6.5.1 Identification

First step was carrying out the experiment to obtain the best features that can be used a unique identifier for each subjects. We used the results obtained using the miniVNA that defined the channel characteristics, in terms of gain/attenuation profile. We started extensive testing first on four different subjects (two humans and two arm phantoms), to first identify the best identifying features, to be used for training and testing the machine learning algorithms, then we added more subjects to the experiment. Measurements were carried out for three scenarios for each subject; distance between TX and RX were varied between 10, 15 and 20 cm, while the separation between electrodes of the same node are kept constant at 5 cm. For each subject, more than 150 measurement instances were carried out, with 632 measurement point per instance. To study the different features that can used for subject's identification, we explored various approaches:

1- Using the amplitude of the galvanic channel gain at different frequencies directly as the features, over the whole frequency range, at each TX-RX separation distance separately
2- Use the same approach as 1 but when using all the data for the different TX-RX separations, as different cases
3- Same as approach 1, but when combining the measurements for all TX-RX separation measurements, not as test cases, but as features (magnitude at 10 MHz for the 10cm is used as feature, while the magnitude at 10 MHZ for the 15 cm is used as a different feature, thus for each measurement case, the three separations are combined as a single trial)
4- Divide the spectrum into bins of equal sizes (example: 1 MHz bin, 5 MHz bin), compute the total power spectral density for the frequency components within each bin, then use it a single feature.

MATLAB [24] was used for signal processing, and computing the above mentioned features. These features were then imported to WEKA [25-26], a suite of machine learning software written in Java, developed at the University of Waikato, New Zealand and is a free software licensed under the GNU General Public License, for applying different machine learning algorithms for training and testing the data, and obtain performance metrics for comparison between different approaches in features selection as well as comparing between different machine learning algorithms. The machine learning algorithms that we used are: Support Vector Magnitude (SVM), the k-nearest neighbor, J48, Random Forest and the Naïve Bayes classifier.

The Support Vector Magnitude (SVM) is a discriminative classifier formally defined by a separating hyperplane. In other words, given labeled training data (supervised learning), the algorithm outputs an optimal hyperplane which categorizes new examples. In two dimensional

space this hyperplane is a line dividing a plane in two parts where in each class lay in either side [27].

The k-nearest neighbors (KNN) is a non-parametric, lazy learning algorithm. Its purpose is to use a database in which the data points are separated into several classes to predict the classification of a new sample point.

The J-48 is the WEKA implementation of the C4.5 algorithm which builds decision trees from a set of training data using the concept of information entropy. At each node of the tree, C4.5 chooses the attribute of the data that most effectively splits its set of samples into subsets enriched in one class or the other. The splitting criterion is the normalized information gain (difference in entropy). The attribute with the highest normalized information gain is chosen to make the decision. The C4.5 algorithm then recuses on the partitioned sub lists [28].

Naïve Bayes classifiers are a family of simple "probabilistic classifiers" based on applying Bayes' theorem with strong (naive) independence assumptions between the features.

Finally, *Random Forest* classifiers are an ensemble learning method for classification, regression and other tasks that operates by constructing a multitude of decision trees at training time and outputting the class that is the mode of the classes (classification) or mean prediction (regression) of the individual trees [29].

The basic performance metrics that will be used for comparison are: accuracy, precision, recall and F-measure.

Accuracy is simply the percentage of correctly predicted cases, among all the predicted ones; in other terms, how many time the algorithm was correct in its final prediction.

Precision for a class is the *number of true positives* (i.e. the number of items correctly labeled as belonging to the positive class) *divided by the total number of elements labeled as belonging to the positive class* (i.e. the sum of true positives and false positives, which are items incorrectly labeled as belonging to the class).

$$Precision = \frac{True\ Positive}{True\ Positive + false\ Positive}$$

Recall is defined as the *number of true positives divided by the total number of elements that actually belong to the positive class* (i.e. the sum of true positives and false negatives, which are items which were not labeled as belonging to the positive class but should have been) [30].

$$Recall = \frac{True\ Positive}{True\ Positive + false\ Negative}$$

F1-score combines both metrics, for getting a more accurate performance metric as follows:

$$F1 = 2 * \frac{Precision * Recall}{Precision + Recall}$$

6.5.2 Identification performance and Feature Selection

In tables 6.2, 6.3 and 6.4, results for applying different machine learning algorithms, using WEKA, are shown, where the standard performance metrics are reported, for the results when the first approach (the gain at each frequency component is used as a feature), for each of the TX-RX separations of 10, 15 and 20 cm. Total number of features used for each case is 632 feature, and a cross validation of 10 folds' technique is used for training/testing. As can be seen from the results, and is expected as well, when using measurements obtained from the 10 cm separation, results are better, reaching an identification accuracy of 98% ~100%.

Table. 6.2. Performance Metrics for TX-RX of 10cm features (632 features per case)

Classifier	Accuracy	Precision	Recall	F-measure
Naïve Bayes	98.8372%	0.989	0.988	0.988
SVM	95.5%	0.962	0.955	0.955
KNN	100%	1	1	1
Random Forest	96%	0.962	0.960	0.959
J48	92%	0.939	0.920	0.923

Table. 6.3. Performance Metrics for TX-RX of 15cm features (632 features per case)

Classifier	Accuracy	Precision	Recall	F-measure
Naïve Bayes	91.9811%	0.920	0.920	0.920
SVM	90.566%	0.909	0.906	0.907
KNN	91.9811 %	0.921	0.920	0.920
Random Forest	91.9811%	0.921	0.920	0.920
J48	81.6038%	0.827	0.816	0.818

Table. 6.4. Performance Metrics for TX-RX of 20cm features (632 features per case)

Classifier	Accuracy	Precision	Recall	F-measure
Naïve Bayes	71.6102%	0.740	0.716	0.691
SVM	80.5085%	0.838	0.805	0.812
KNN	83.8983 %	0.750	0.581	0.655
Random Forest	79.661%	0.793	0.797	0.782
J48	78.3898%	0.606	0.645	0.625

Yet the accuracy drops, for the same classifiers, when using data for bigger separations (15 cm and 20cm). Once again, such findings are expected, since the signal is most powerful for smaller separation between the communicating nodes, yet as the separation increases, the attenuation increase, thus more channel characteristics are lost. Results for approaches two and three are shown in Tables 6.5 and 6.6 respectively. For approach two, results from all TX-RX separations are used in a single training/test run, meaning that test trials are all used as train/test cases, yet each is considered as a separate case. Total number of features per case stays the same, at 632. For approach three, a case from each TX-RX separation is combined with other separations, to form a combo case, thus number of features per case would be 1896 features. For approach two, it is similar to training the system using the 10 and 15 cm cases, and testing it on the 20 cm cases. In spite of fact that the characteristics and geometry changes, as shown in the previous chapter, the performance would still reach an accuracy of 89% for the KNN classifier, which is still an acceptable result, given that training and testing are performed for different TX-RX separation cases. As for approach three, where each frequency component has three different features (gain at 10 cm, 15 cm and 20 cm), the performance stays at a very good level ~98%, since more features are added to the system. The SVM classifier didn't converge for both cases

Table. 6.5. Performance Metrics for all TX-RX as different cases (632 features per case)

Classifier	Accuracy	Precision	Recall	F-measure
Naïve Bayes	85.9756%	0.844	0.609	0.708
SVM	---	----	----	-----
KNN	89.4817 %	0.894	0.895	0.894
Random Forest	87.0427 %	0.870	0.870	0.868
J48	82.3171%	0.833	0.823	0.826

Table. 6.6. Performance Metrics for all TX-RX as different features (1896 features per case)

Classifier	Accuracy	Precision	Recall	F-measure
Naïve Bayes	97.9695 %	0.981	0.980	0.980
SVM	----	-	-	-
KNN	96.9543 %	0.970	0.970	0.970
Random Forest	97.9695 %	0.981	0.980	0.980
J48	92.3858%	0.941	0.924	0.926

The final approach is to divide the spectrum into power bins of equal sizes (example: 1 MHz bin, 5 MHz bin), compute the total power for the frequency components within each bin, then use it a single feature. This approach is more resilient to noise and system/environment changes, as it computes the feature as the average power within a range of frequencies, not just at a single relative one, thus has higher ability to eliminate noise and irregular changes. In Table 6.7, we show the performance metrics for the case when the spectrum is divided into bins of size 0.5 MHz each.

Table. 6.7. Performance Metrics for the power bin approach (0.5 MHz bin size)

Classifier	Accuracy	Precision	Recall	F-measure
Naïve Bayes	98.8889 %	0.989	0.989	0.989
SVM	96.6667 %	0.971	0.967	0.967
KNN	99.4444 %	0.995	0.994	0.994
Random Forest	81.6667 %	0.849	0.945	0.944
J48	50 %	0.675	0.500	0.484

Results for this approach are better and more reliable, especially for the Naïve Bayes and KNN. Since this approach possess other advantages as we explained earlier, we decided to adopt the power bin approach. The next step would be:

- Determine the exact frequency range of interest for our experiment
- Determining the optimum size for the power bin (how wide the spectrum of each bin should be, which would determine the number of features as well; the wider the bin, the less features used)

For the above shown results, we used the conventional frequency (100 KHz till 100 MHz), yet we observed that the gain drops at higher frequencies (greater than 50 MHz), this occurs due to different reasons; body antenna effect, causing power leakage as well as signal interference, and the attenuation introduced by body tissues. This is also confirmed in [21], where the frequency band of less than 60 MHz showed better results. We then tested our algorithms, for the last approach of the power bins, for the frequency range of 100 KHz till 50 MHz (only half the number of features is now used, compared with the full spectrum case). Results for a bin size of 50 MHz are shown in Table 6.8. As seen from the results, although the number of features is decreased by half, the performance stayed almost the same (only 1% degradation), thus it is much more efficient to use this approach, for a frequency range till 50 MHz only, where performance stays almost the same, while memory needed and processing time are reduced significantly. To finally determine the optimum bin size, we repeated these algorithms and tests for different bin sizes, of 0.5 MHz increment for each trial. Some of the results are shown in Tables 6.9 – 6.13. As can be observed, the identification accuracy drops as the power bin size increases (as the number of features decreases).

Table. 6.8. Performance Metrics for the power bin approach (0.5 MHz bin size, frequency range of 100 KHz till 50 MHz only (instead of 100 MHz))

Classifier	Accuracy	Precision	Recall	F-measure
Naïve Bayes	97.2222 %	0.974	0.972	0.972
SVM	97.22227%	0.975	0.972	0.973
KNN	97.2222 %	0.976	0.972	0.973
Random Forest	84.4444%	0.871	0.844	0.828
J48	50 %	0.675	0.500	0.484

Table. 6.9. Performance Metrics for the power bin approach (1 MHz bin size)

Classifier	Accuracy	Precision	Recall	F-measure
Naïve Bayes	96.1111 %	0.965	0.961	0.961
SVM	96.6667 %	0.971	0.967	0.967
KNN	97.2222 %	0.976	0.972	0.973
Random Forest	77.7778%	0.795	0.778	0.759
J48	40 %	0.668	0.4	0.365

Table. 6.10. Performance Metrics for the power bin approach (1.5 MHz bin size)

Classifier	Accuracy	Precision	Recall	F-measure
Naïve Bayes	95.5556 %	0.959	0.956	0.954
SVM	93.8889 %	0.947	0.939	0.940
KNN	96.1111%	0.963	0.961	0.960
Random Forest	78.8889 %	0.807	0.789	0.763
J48	32.7778 %	0.631	0.328	0.309

Table. 6.11. Performance Metrics for the power bin approach (2 MHz bin size)

Classifier	Accuracy	Precision	Recall	F-measure
Naïve Bayes	93.8889 %	0.949	0.939	0.939
SVM	95 %	0.957	0.950	0.951
KNN	92.2222 %	0.939	0.922	0.922
Random Forest	72.7778%	0.759	0.728	0.708
J48	40.5556 %	0.646	0.406	0.406

Table. 6.12. Performance Metrics for the power bin approach (3 MHz bin size)

Classifier	Accuracy	Precision	Recall	F-measure
Naïve Bayes	90.5556 %	0.911	0.906	0.904
SVM	91.1111 %	0.927	0.911	0.912
KNN	90 %	0.911	0.900	0.900
Random Forest	66.6667 %	0.681	0.667	0.650
J48	36.6667 %	0.635	0.367	0.361

Table. 6.13. Performance Metrics for the power bin approach (4 MHz bin size)

Classifier	Accuracy	Precision	Recall	F-measure
Naïve Bayes	87.7778 %	0.889	0.878	0.875
SVM	87.2222 %	0.901	0.872	0.875
KNN	86.1111 %	0.868	0.861	0.860
Random Forest	63.3333 %	0.628	0.633	0.614
J48	35 %	0.575	0.350	0.338

Results are plotted in Figure 6.21 & 6.22, showing the tradeoff between accuracy and bin size; basically between accuracy and available resources (more features, thus bigger networks, which means more hardware and more processing time needed).

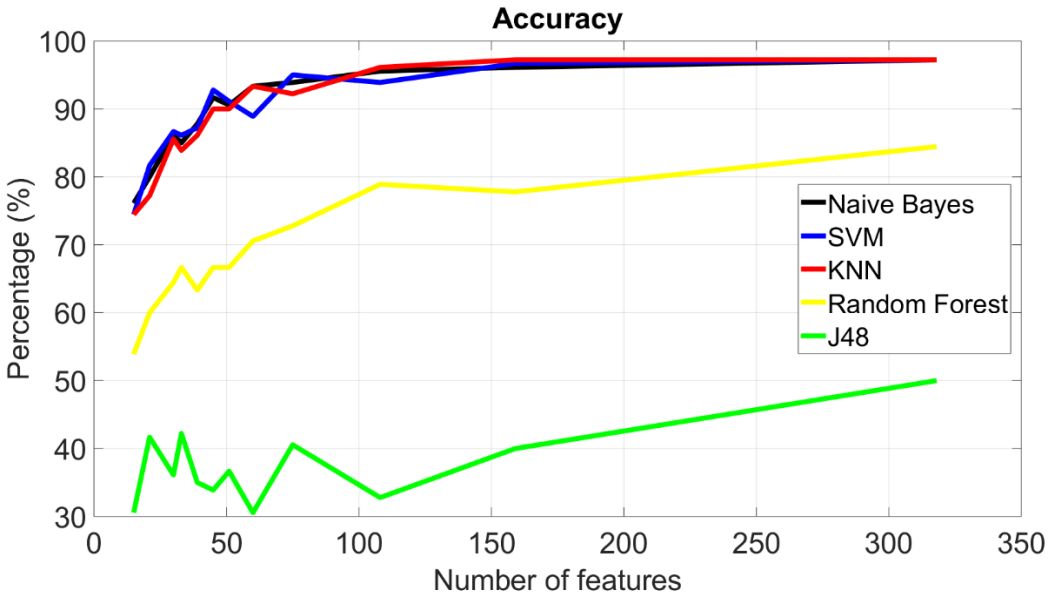

Figure 6.21: Accuracy for different classifiers versus the number of features.

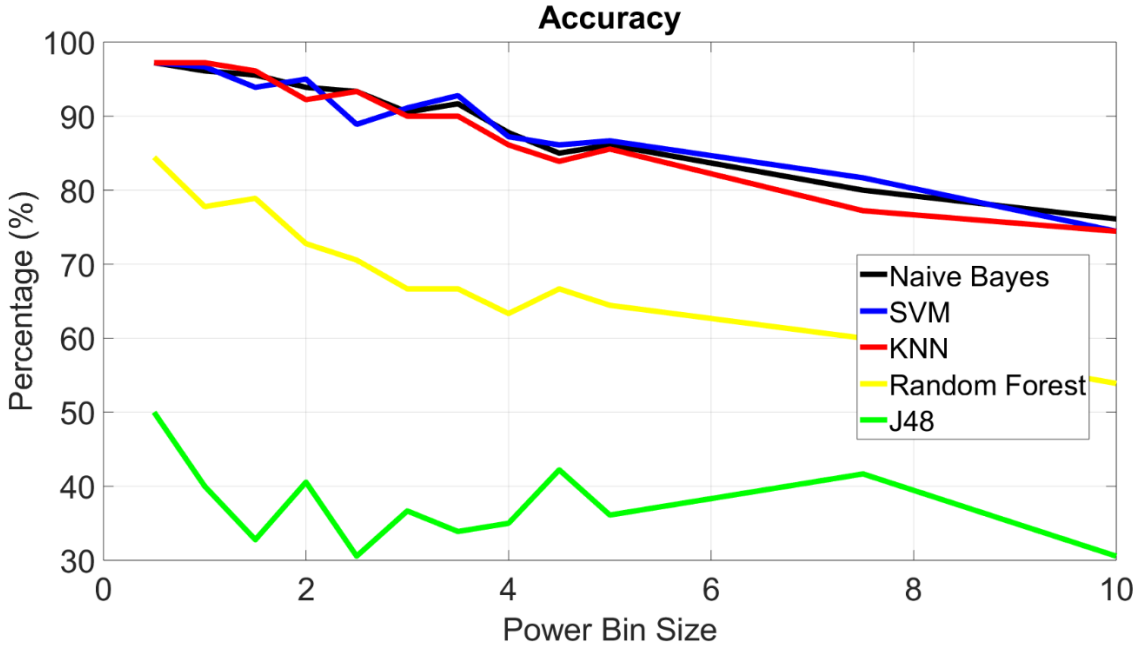

Figure 6.22: Accuracy for different classifiers versus power bin size

Table. 6.14. Performance Metrics for the power bin approach (0.5 MHz bin size)

Classifier	Accuracy	Precision	Recall	F-measure
Naïve Bayes	98.4127 %	0.984	0.984	0.984
SVM	94.9206 %	0.963	0.949	0.952
KNN	97.7778 %	0.978	0.978	0.978
Random Forest	87.619 %	0.892	0.876	0.863
J48	47.9365 %	0.750	0.479	0.512

From the findings we reached after the above trials, we concluded that for best accuracy, with efficient resources, we will use the averaged power bin approach, with bin size of 0.5 MHz, over the frequency range of 100 KHz till 50 MHz only, with either the KNN or Naïve Bayes classifiers, since they are simple yet accurate classifiers in our case. Finally, we use these findings for testing the identification technique on all 7 subjects we have; five human subjects and two arm phantom models. Results are shown in Table 6.14. It's clear how solid the identification algorithm is, where the performance metrics stayed almost the same, even when number of subjects increased. MATLAB Classification learner toolbox was also used for running the machine learning classifiers and obtaining the performance metrics as well. Similar results were obtained, where a sample for these results for the SVM classifier are shown in Figures 6.23 – Figure 6.26. The accuracy obtained was 99.7%, and the confusion matrix, as well as other performance metrics as the true positive rate and the false negative rate …etc. are plotted in Figures 6.23, 6.24 and 6.25.

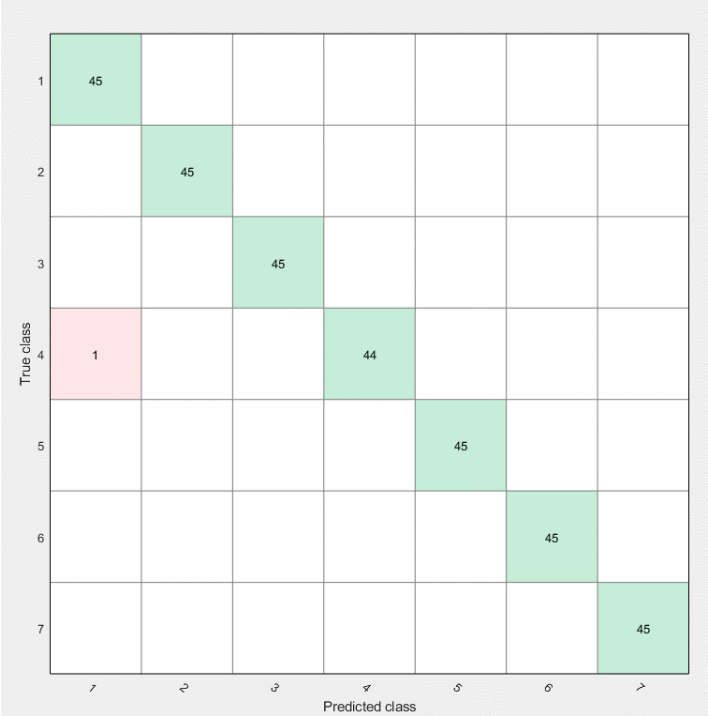

Figure 6.23: Confusion Matrix for the Identification results of using SVM classifier on measurements from 7 subjects

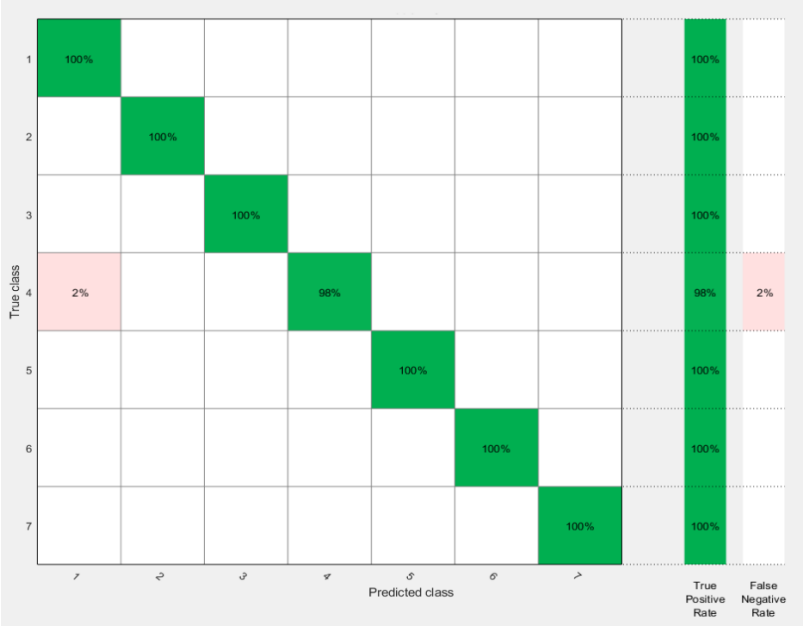

Figure 6.24: Performance Metrics Matrix for the Identification results of using SVM classifier on measurements from 7 subjects.

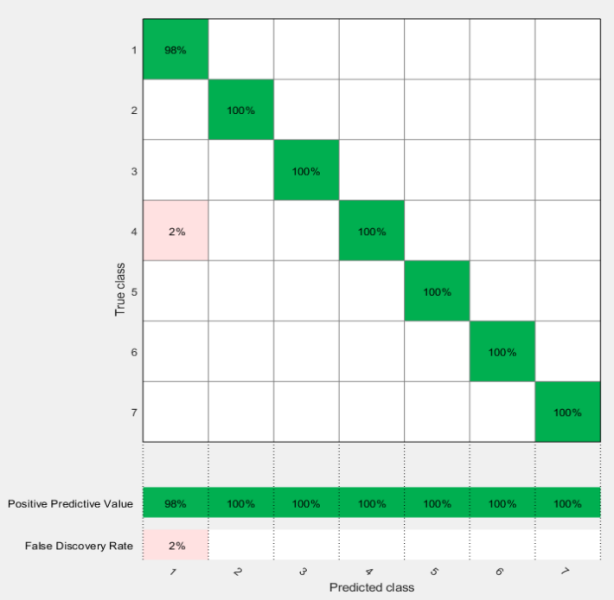

Figure 6.25: Other performance Metrics Matrix for the Identification results of using SVM classifier on measurements from 7 subjects.

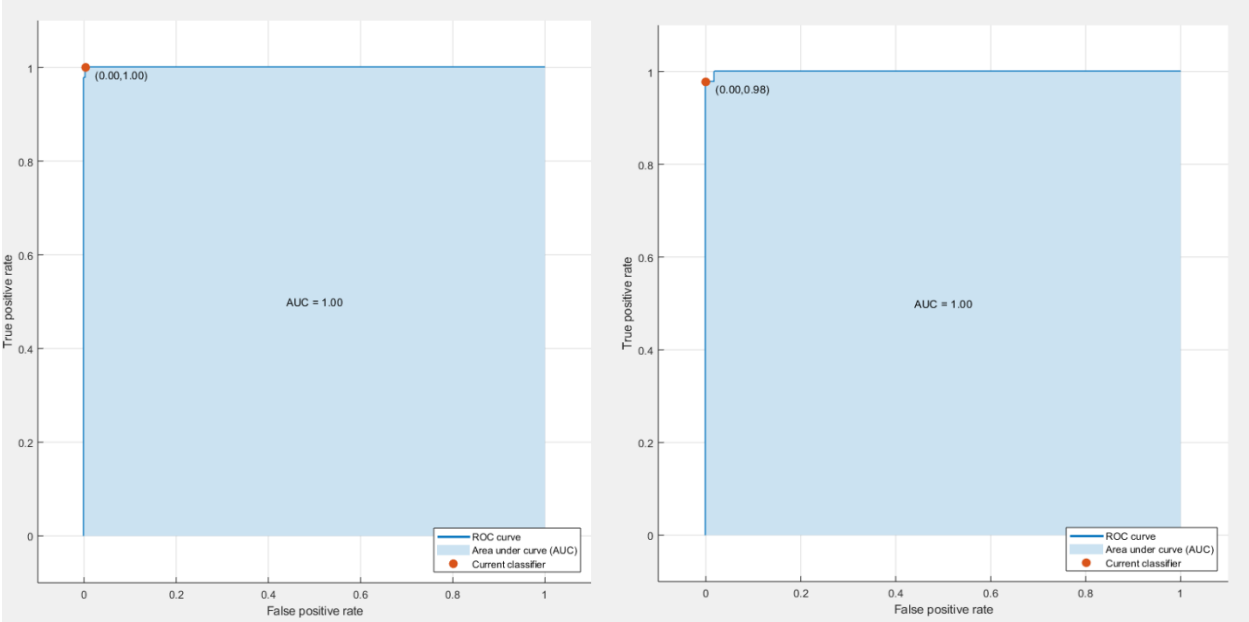

(a) (b)

Figure 6.26: ROC Curves for (a) Subject 1 & (b) Subject 4 for the Identification results of using SVM classifier on measurements from 7 subjects.

Finally, the ROC curves (Receiver Operating Characteristic curves; graphical plots that illustrate the diagnostic ability of a binary classifier system as its discrimination threshold is varied. The ROC curve is created by plotting the true positive rate against the false positive rate at various threshold settings) for the identification performance for a couple of subjects are plotted in Figure 6.26.

6.5.3 Authentication

As mentioned earlier, authentication refers to identify confirmation or verification. That's when a user claims a certain identity, authentication entails deciding whether the claim is correct or not. Training a system for that purpose is thus different from the identification case. First of all, for training purposes, data for only a single subject will be provided. Also the output of the system will be just confirming the identity of the subject; whether he is the person he claims to be or not. For such an application, the model is trained with a set of data that should include both data for the subject of concern; the person whose identity is to be associated with the account/ ID, and outliers: biometric identity data that doesn't belong to this subject, in other terms, fake ID data. A flow chart for the steps followed for the authentication process is shown in Figure 6.27:

1- First the VNA/hardware used is connected to the subject whose identity is to be identified and stored, and experimental testing is carried out to store the subjects' IBC channel characteristic (gain/attenuation profile), where the features explained earlier (power bins of 0.5 MHz wide each, for the frequency range from 100 KHz till 50 MHZ) are processed and stored.
2- A statistical model for the IBC channel is then generated using the subject's data, then used to generate distorted and noisy versions of these characteristics and features (IBC

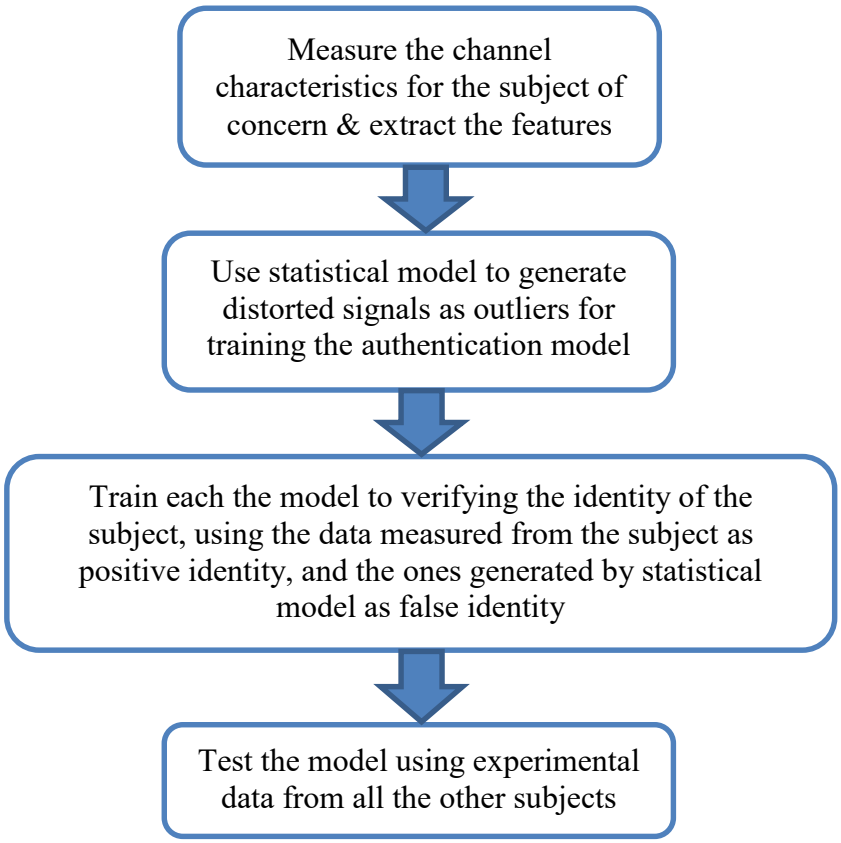

Figure 6.27: Flowchart for the methodology followed for the subject identity authentication process

channel characteristics for fake subjects), as for the authentication process the channel characteristics of other subjects won't be available for the system.

3- Train the classifier using the current dataset which consists of two parts: experimental data set for the subject, used to train the classifier to recognize the subject identity, and outlier cases, generated using the statistical model, to train the classifier to reject any other identity that is not the same as that of the subject's.

4- Finally test the classifier using a dataset that contains: test samples for the subject of concern (yet should be cases that wasn't used in the training process) and real test cases

from other subjects (representing other unauthorized subjects trying to access this subject's device)

Statistical Model: To generate a statistical model for the IBC channel, ifft (inverse fast Fourier transform) is first performed to transfer the IBC channel response to the time domain. An example for the channel response in the time domain is shown in Figure 6.28, where results for 50 different experimental instances are plotted (instances are measurements taken at different time instances, yet for the same subject and for the same experimental setup; same electrodes, electrodes spacing and TX-RX separation). Different statistical models are then compared to see which model best fits and represents the distribution of the channel in the time domain.

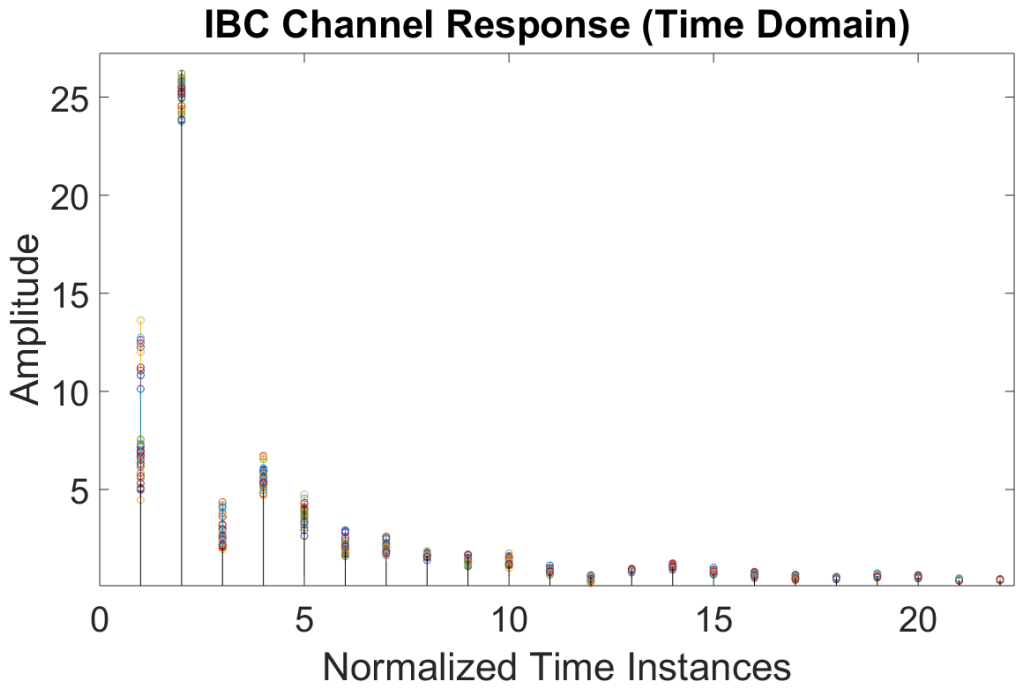

Figure 6.28: Time domain representation for the IBC channel response for fifty different measuring instances.

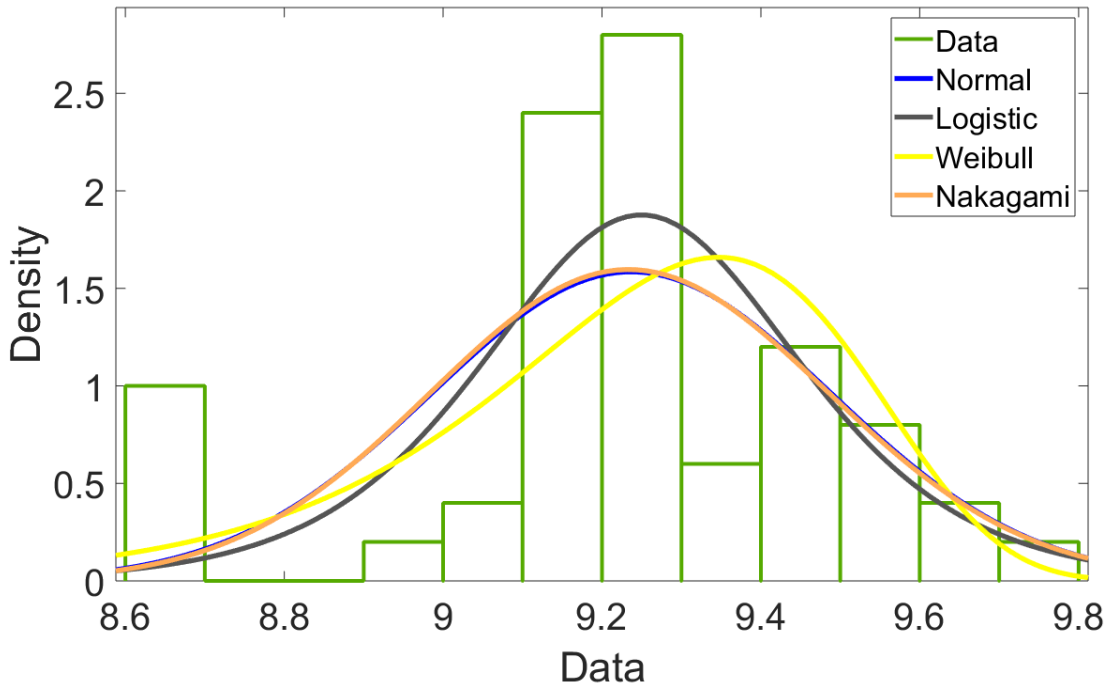

Figure 6.29: Using Different statistical models to fit a single time component for the IBC channel response, for fifty different measurement cases.

An example is shown in Figure 6.29, where Normal, logistic, Weibull and Nakagami models are used to fit the amplitude of the channel response at a certain time component, and for all the 50 experimental instances. Although the difference between the model were very small, Normal distribution seems to best fit the experimental data. Normal distribution was then used to fit the data for different time domain components for the statistical data we had. Model parameters were then saved and later used to generate distorted version of the IBC channel characteristics to represent outliers for training our system.

Finally, following the steps shown in Figure 6.29, we trained different classifiers to test the feasibility of using the IBC channel characteristics as a biometric identity for authentication purposes. Best results we got was using the Naïve Bayes classifiers, as shown in Table 6.15.

Table. 6.15. Performance Metrics for Authentication Using IBC Channel Characteristics, for the Naïve Bayes Classifier Case

	Subject 1	**Subject 2**	**Subject 3**	**Subject 4**	**Subject 5**	**Subject 6**	**Subject 7**
Accuracy	96.46 %	98.80 %	100%	100%	98%	97.21 %	99.2 %
Precision	0.975	0.988	1	1	0.983	0.973	0.992
Recall	0.965	0.988	1	1	0.98	0.972	0.992
F-measure	0.969	0.0987	1	1	0.981	0.967	0.992

As can be inferred from the Table, the classifier shows high accuracy for the authentication applications. The features used for the training are the same that specified in the identification part (power bins, where we integrate the power within a certain frequency range, 0.5 MHz in this case, over the frequency range from 100 KHz till 50 MHz). Results are shown for each subject, where the classifier is trained for each subject, then tested against the when the other six subjects trying to be falsely identified as the subject of concern. These results show that the IBC channel characteristic can be used as an accurate, secure and reliable biometric identity, and for both types of ID biometrics; identification and authentication/verification.

6.6 Conclusion

In this chapter, we first started by extracting the IBC channel characteristics experimentally, identifying the gain/attenuation profile for various body locations and postures. Such information was later then used to verify the feasibility of using the IBC technology in various applications. Two major applications were selected to show the unique potential of the IBC technology, namely; the platform for designing and building a stress profile analysis system and the other is the biometric identity. Identifying the basic physiological signals needed to identify whether a

person is stressed or not, the platform then provides the system specifications needed to physically build such system, using IBC as the mean of communications between the different nodes. Not only did IBC show potential for distributed body area networks, but it was shown that it can be used in another crucial applications as security. Using the IBC channel characteristics, which are found to be unique to each person, as a biometric identity, showed huge potential for both identification and authentication applications, which opens the door for numerous continuous verification and identification applications, that can be even useful for securing the distributed body area networks suggested in the first application.

References:

[1] MiniVNA PRO [Online]: http://miniradiosolutions.com/minivna-pro/ Accessed on April 21st – 2019

[2] International Commission on Non-Ionizing Radiation Protection (ICNIRP), Guidelines for limiting exposure to time-varying electric, magnetic, and electromagnetic fields (up to300GHz), 1997.

[3] IEEE C95.1-2005, IEEE Standard for Safety Levels with Respect to Human Exposure to Radio Frequency Electromagnetic Fields, 3 kHz to 300 GHz, The Institute of Electrical and Electronics Engineers Inc., New York , 2006.

[4] Cho, N., Yoo, J., Song, S. J., Lee, J., Jeon, S., & Yoo, H. J. (2007). The human body characteristics as a signal transmission medium for intrabody communication. *IEEE transactions on microwave theory and techniques*, *55*(5), 1080-1086.

[5] Cross, Carl Brady, "An Investigation of Thermal Imaging to Detect Physiological Indicators of Stress in Humans.", M.S.Egr Thesis., Department of Biomedical, Industrial and Human Factors Engineering, Wright State University, Dayton, OH, 2013.

[6] Ekman, P., Levenson, R. W., & Friesen, W. V. (1983). Autonomic nervous system activity distinguishes among emotions. *Science*, *221*(4616), 1208-1210.

[7] Hamdi, H., Richard, P., Suteau, A., & Allain, P. (2012, June). Emotion assessment for affective computing based on physiological responses. In *2012 IEEE International Conference on Fuzzy Systems* (pp. 1-8). IEEE.

[8] Constantinou, E., Panayiotou, G., & Theodorou, M. (2014). Emotion processing deficits in alexithymia and response to a depth of processing intervention. *Biological psychology*, *103*, 212-222

[9] Valderas, M. T., Bolea, J., Laguna, P., Vallverdú, M., & Bailón, R. (2015, August). Human emotion recognition using heart rate variability analysis with spectral bands based on respiration. In *2015 37th*

Annual International Conference of the IEEE Engineering in Medicine and Biology Society (EMBC) (pp. 6134-6137). IEEE.

[10] Sharma, T., & Kapoor, B. (2014, February). Intelligent data analysis algorithms on biofeedback signals for estimating emotions. In *2014 International Conference on Reliability Optimization and Information Technology (ICROIT)* (pp. 335-340). IEEE.

[11] Haag, A., Goronzy, S., Schaich, P., & Williams, J. (2004, June). Emotion recognition using bio-sensors: First steps towards an automatic system. In *Tutorial and research workshop on affective dialogue systems* (pp. 36-48). Springer, Berlin, Heidelberg.

[12] Lisetti, C. L., & Nasoz, F. (2004). Using noninvasive wearable computers to recognize human emotions from physiological signals. *EURASIP journal on applied signal processing*, *2004*, 1672-1687.

[13] Rahman, M. M., Bari, R., Ali, A. A., Sharmin, M., Raij, A., Hovsepian, K., ... & Preston, K. L. (2014, September). Are we there yet?: Feasibility of continuous stress assessment via wireless physiological sensors. In *Proceedings of the 5th ACM Conference on Bioinformatics, Computational Biology, and Health Informatics* (pp. 479-488). ACM.

[14] Ollander, S. Wearable sensor data fusion for human stress estimation. Thesis. Linköpings universitet, Sweden (2015).

[15] Karim, N., Hasan, J. A., & Ali, S. S. (2011). Heart rate variability-a review. *Journal of Basic & Applied Sciences*, *7*(1).

[16] Reed, M. J., Robertson, C. E., & Addison, P. S. (2005). Heart rate variability measurements and the prediction of ventricular arrhythmias. *Qjm*, *98*(2), 87-95.

[17] [Online]: https://en.wikipedia.org/wiki/Electrocardiography Accessed on April 21st – 2019

[18] Shinagawa, M. (2004). Development of electro-optic sensors for intra-body communications. *NTT Technical Review*, *2*(2), 6-11.

[19] Shinagawa, M., Ochiai, K., Sakamoto, H., & Asahi, T. (2005). Human area networking technology: RedTacton. *NTT Technical Review*, *3*(5), 41-46.

[20] Kado, Y. (2010). Red tacton near-body electric-field communications technology and its applications. *NTT Technical Review*, *8*(3), 1-6.

[21] Nakanishi, I., Yorikane, Y., Itoh, Y., & Fukui, Y. (2007, September). Biometric identity verification using intra-body propagation signal. In *2007 Biometrics Symposium* (pp. 1-6). IEEE.

[22] Nakanishi, I., Inada, T., Sodani, Y., & Li, S. (2013, July). Performance evaluation of intra-palm propagation signals as biometrics. In *2013 International Conference on Biometrics and Kansei Engineering* (pp. 91-94). IEEE.

[23] Rasmussen, K. B., Roeschlin, M., Martinovic, I., & Tsudik, G. (2014). Authentication Using Pulse–Response Biometrics.

[24] MATLAB [Online]: https://www.mathworks.com/products/matlab.html Accessed on April 21st – 2019

[25] Eibe Frank, Mark A. Hall, and Ian H. Witten (2016). The WEKA Workbench. Online Appendix for "Data Mining: Practical Machine Learning Tools and Techniques", Morgan Kaufmann, Fourth Edition, 2016.

[26] Mark Hall, Eibe Frank, Geoffrey Holmes, Bernhard Pfahringer, Peter Reutemann, and Ian H. Witten (2009). The WEKA Data Mining Software: An Update. SIGKDD Explorations, Volume 11, Issue 1.

[27] SVM [Online]: https://medium.com/machine-learning-101/chapter-2-svm-support-vector-machine-theory-f0812effc72 Accessed on April 21st – 2019

[28] C4.5 Algorithm [Online]: https://en.wikipedia.org/wiki/C4.5_algorithm Accessed on April 21st – 2019

[29] Ho, T. K. (1995, August). Random decision forests. In *Proceedings of 3rd international conference on document analysis and recognition* (Vol. 1, pp. 278-282). IEEE.

[30] Precision and Recall [Online]: https://en.wikipedia.org/wiki/Precision_and_recall

Chapter 7

Conclusion & Future Work

Throughout this dissertation, we demonstrated the basic characteristics of the IBC channel. We first started by reviewing the prior work in the literature in this field, and identified the basic two approaches for the IBC technology; capacitive coupling and galvanic coupling. We presented the main efforts published in an attempt to study this novel channel and explore its potential for various applications. We then took one step back to verify if the electromagnetic signals were indeed the optimum data carrier for this emerging technology. We compared the characteristics of the channel for EM waves, with that of ultrasound ones, being a potential for various applications in the biomedical field, However, as demonstrated in chapter two, not only are the EM waves more convenient from the systems and circuits point of view, but it is the optimum data carrier from the body tissues' electrical and signal propagation characteristics. Having verified the optimum data carrier, the next step was modeling this new channel. In chapter three we introduced two different approaches for modeling the IBC channel. We first proposed a simple yet accurate circuit model that takes into consideration various system, geometric and biological variables and parameters into account, thus improving the model's accuracy significantly. Next, a model relying on the FEM approach was introduced as well, and compared with the circuit model, verifying the accuracy of the circuit model as well as its efficiency when it came to the time needed for running both simulation models.

The electrode contact impedance was further investigated in chapter 4, showing the crucial role played by that component in the IBC system, and its major impact on the IBC overall channel

characteristics. The relation between the electrode impedances and the other system component impedances' were investigated as well. In chapter 5, we designed the first multi-layer tissue mimicking phantom for the IBC applications field. We showed how the phantom accurately mimicked the die-electrical properties, the ones shaping the IBC channel characteristics. Experimental measurements, performed on real subjects, confirmed our claims as well, proving that the phantom can be used as an accurate testing platform for body area networks applications in general and IBC applications specifically. Finally, we explored some of the applications that can make use of the potential of the IBC technology, namely distributed sensor networks for healthcare monitoring – stress profile analysis in our example- as well biometric identity, where IBC channel characteristics showed unique potential to be used for identifying subjects using their own channel characteristics as a unique biometric identity.

Throughout the dissertation, we laid the foundation for setting up an accurate and reliable platform for the design of systems built upon utilizing the IBC technology. Telecommunications and networking research can use our circuit model for exploring the modulation schemes, network topologies and other parameters that would suit different body area networks applications. Circuits designers can use our physical phantoms for rigorous testing for their system specifications, such as the output power levels, field distribution and intensity as well as adherence to the safety limits for electric and magnetic fields exposure, before doing any testing on real subjects. System designers can also use our IBC design platform application for determining the basic system parameters and specifications, needed to design a senor network using the IBC technology.

Further research is still necessary in the circuits and electronic design field, to be able to harness the potential of the IBC technology. Designing a compact, ultra-low power circuit, that is

uniquely and solely designed to operate using the IBC technology should be the next step in the IBC research efforts, since the basic characteristics and features of the IBC channel have been identified, in this work and in prior research available in the literature. New design techniques should be considered as well, such as using flexible electronics for designing IBC circuits and sensor nodes. Research into an efficient and optimum solution for powering IBC circuits and systems is crucial, to preserve and maintain the advantages of the IBC technology and to further expand the horizon for the applications that can make use of this emerging technology. And last but not least, safety standards for the operation of this technology should be more thoroughly explored and clearly determined, to ensure the safety of such systems. After all, the basic motivation behind this technology and this research is designing systems and technologies for sustaining a safe and healthy life for the human being.